**NASA TECHNICAL MEMORANDUM**

**NASA TM X-62,419**



NASA TM X-62,419

# WIND TUNNEL INVESTIGATION OF A LARGE-SCALE UPPER SURFACE BLOWN-FLAP MODEL HAVING FOUR ENGINES

Kiyoshi Aoyagi, Michael D. Falarski and David G. Koenig

Ames Research Center
and
U. S. Army Air Mobility R&D Laboratory
Moffett Field, Calif. 94035

July 1975

## SYMBOLS

| | |
|---|---|
| $b$ | wing span, m (ft) |
| BLC | boundary layer control |
| $c$ | wing chord measured parallel to the plane of symmetry, m (ft) |
| $C_p$ | pressure coefficient, $P_l - P_s/q_\infty$ |
| $c_t$ | horizontal tail chord measured parallel to the plane of symmetry, m (ft) |
| $\bar{c}$ | mean aerodynamic chord of wing, $2/S \int_o^{b/2} c^2 dy$, m (ft) |
| $C_D$ | drag coefficient, drag/$q_\infty S$ |
| $C_{D_{ram}}$ | ram drag coefficient, $WV/gq_\infty S$ |
| $C_J$ | jet momentum coefficient, $F_g/q_\infty S$ |
| $C_L$ | lift coefficient, lift/$q_\infty S$ |
| $C_l$ | rolling-moment coefficient about stability axis, rolling moment/$q_\infty Sb$ |
| $C_m$ | pitching-moment coefficient about 0.40 c, pitching moment/$q_\infty S\bar{c}$ |
| $C_n$ | yawing-moment coefficient about stability axis, yawing moment/$q_\infty Sb$ |
| $C_\mu$ | momentum coefficient $WV/gq_\infty S$ |
| $C_y$ | side-force coefficient about stability axis, side force/$q_\infty S$ |
| $F_A$ | static (wind off) incremental axial force due to flap deflection with power on, N (lb) |
| $F_g$ | gross thrust with engine alone, N (lb) (obtained statically) |
| $F_N$ | static (wind off) incremental normal force due to flap deflection with power on, N (lb) |
| $F_h$ | resultant force $\sqrt{F_A^2 + F_N^2}$, N (lb) |
| $g$ | acceleration of gravity, 9.81 m/sec$^2$ (32.2 ft/sec$^2$) |
| $i_t$ | horizontal tail incidence, deg |
| LE | leading edge |
| $P_l$ | local static pressure, N/m$^2$ (lb/sq ft) |

$P_s$ free-stream static pressure, $N/m^2$ (lb/sq ft)

$q_\infty$ free-stream dynamic pressure, $N/m^2$ (lb/sq ft)

S wing area, $m^2$ (sq ft)

V free-stream air velocity, m/sec (ft/sec) or velocity based on isentropic expansion

W engine inlet weight rate of flow, kg/sec (lb/sec) or weight rate of flow at blowing nozzle

WCP wing chord plane

x chordwise distance from wing leading edge, cm

y spanwise distance perpendicular to the plane of symmetry, m (ft)

$y_L$ lower surface distance from WCP, cm

$y_U$ upper surface distance from WCP, cm

$\alpha$ angle of attack of fuselage, deg

$\beta$ sideslip, deg

$\delta_{ail}$ aileron deflection, deg

$\delta_f$ deflection of Coanda plate trailing edge measured parallel to the plane of symmetry, deg (see fig. 2(f))

$\delta_{f_2}$ trailing-edge second flap deflection measured parallel to the plane of symmetry, deg (see fig. 2(f))

$\delta_j$ jet exhaust deflection angle wing off, $\tan^{-1} F_N/F_A$, deg (average value)

$\delta_s$ slat deflection, measured parallel to the plane of symmetry, deg

$\eta$ spanwise extent, $y/(b/2)$

$\eta_f$ flap system static turning efficiency, $F_R/F_g$ (average value)

$\Lambda_{LE}$ wing leading edge sweep, deg

Subscripts:

| | |
|---|---|
| ail | aileron |
| NAC | nacelle |
| LE | leading edge |
| u | uncorrected |

# WIND TUNNEL INVESTIGATION OF A LARGE-SCALE UPPER SURFACE BLOWN-FLAP MODEL HAVING FOUR ENGINES

Kiyoshi Aoyagi*, Michael D. Falarski**, and David G. Koenig*

*Ames Research Center
and
**U. S. Army Air Mobility R&D Laboratory

## SUMMARY

Investigations were conducted in the Ames 40- by 80-Foot Wind Tunnel to determine the aerodynamic characteristics of a large-scale subsonic jet transport model with an upper surface blown flap system. The model had a 25° swept wing of aspect ratio 7.28 and four turbofan engines. The lift of the flap system was augmented by turning the turbofan exhaust over the Coanda surface. Results were obtained for several flap deflections with several wing leading-edge configurations at jet momentum coefficients from 0 to 4.0.

Three-component longitudinal data are presented with four engines operating. In addition, longitudinal and lateral data are presented with an engine out.

The maximum lift and stall angle of the four engine model were lower than those obtained with a two engine model that was previously investigated. The addition of the outboard nacelles had an adverse effect on these values. Efforts to improve these values were successful. A maximum lift of 8.8 at an angle-of-attack of 27° was obtained with a jet thrust coefficient of 2 for the landing flap configuration.

## INTRODUCTION

Lift augmentation by the upper surface blown-flap (USB) concept is currently being considered in some powered-lift transport designs. An important factor for this consideration is the noise reduction due to wing shielding to a ground observer during the takeoff and landing operation of an upper surface blowing aircraft.

A wind tunnel investigation of this concept with a large-scale 25° swept-wing transport model having two engines has been reported in references 1 and 2 for aerodynamic and noise characteristics, respectively.

In order to determine the effects of four engines and increased spanwise extent of the Coanda surface on the aerodynamic characteristics of a large-scale USB transport model, two nacelles were added outboard of the existing

nacelles on the model reported in reference 1. The resulting four engine configuration was investigated in the Ames 40- by 80-Foot Wind Tunnel. Aerodynamic and noise characteristics of the model were obtained with several flap deflections and leading-edge configurations at jet momentum coefficients from 0 to 4.0. Only the aerodynamic characteristics of the model will be presented in this report.

This report presents basic data of two wind tunnel investigations. The first investigation determined the aerodynamic characteristics of the model with the wing leading edge completely swept and then unswept from the outboard nacelle to the fuselage. This modification was made to improve the maximum lift and the stall angle of the model. The second investigation was made to determine the aerodynamic characteristics of the model with improved leading-edge devices and with BLC along the unswept leading-edge section and along the sides of the nacelles. The data with the horizontal tail on were obtained only during this investigation. The data of both investigations were obtained at Reynolds numbers from $2.1 \times 10^6$ to $3.0 \times 10^6$, based on a mean aerodynamic chord of 1.69 m (5.56 ft) and at dynamic pressures from 239 to 479 $N/m^2$ (5 to 10psf), respectively.

## MODEL AND APPARATUS

Two wind tunnel investigations were undertaken with the model. For the first investigation (Test 434), the wing leading edge was swept as shown in figure 1(a). Later, during the same investigation, the wing leading edge was unswept to 0° between the nacelles and between the inboard nacelle and the fuselage as shown in figure 1(b). For the second investigation (Test 441), BLC nozzles were added to the unswept leading edge and along the sides of the nacelles. In addition, highly cambered slats were installed at these sections.

Pertinent dimensions of the model are given in figure 2(a). This model has the same geometry as that reported in reference 1 except as follows: the wing airfoil sections were altered from a NACA 63 series to a modified supercritical section, and the wing thicknesses were increased from 0.14c to 0.15c and 0.11c to 0.12c at the root and tip respectively; the aileron was extended inboard from $\eta$ = 0.75 to 0.70; the outboard nacelles were installed at $\eta$ = 0.48; and the Coanda surface was extended out to the aileron.

### Wing

The wing had a quarter chord sweep of 25°, an aspect ratio of 7.28, and an incidence of 0°. The airfoil had a modified supercritical section that was .15c thick at the root and .12c thick at the tip. The ordinates of these sections are given in Table I. The wing tapered linearly in thickness between these two sections.

For the first wind tunnel investigation, the entire wing leading edge was swept. Later, the wing leading edge was unswept to 0° for the wing

extending from $\eta$ = 0.087 to 0.190 and from $\eta$ = 0.321 to 0.413 because of the leading edge flow separation problem at these sections. This was accomplished by adding a chord extension to the existing swept wing leading edge as shown in figure 2(b).

## Leading-edge devices

Figure 2(c) shows the leading edge configurations used during the first wind tunnel investigation. When the wing leading edge was fully swept during the first wind tunnel investigation, a 0.15c slat was deflected 60° with a 0.015c gap from $\eta$ = 0.087 to 0.190 and $\eta$ = 0.326 to 0.413, and a 0.25c slat was deflected 52° from $\eta$ = 0.546 to 1.00. The 0.15c slat was also used as a Krueger flap deflected 68°. When the wing leading edge was unswept from $\eta$ = 0.087 to 0.190 and $\eta$ = 0.326 to 0.413, a constant 0.2410 m (.79 ft) slat was deflected 70° over these spanwise extents. For the wing leading edge section from $\eta$ = 0.546 to 1.00, the slat was the same as the fully swept case.

Figure 2(d) shows the leading edge configurations used during the second wind tunnel investigation. Highly cambered slats with increased chords of 0.3397 m (1.114 ft) and 0.3086 m (1.013 ft) were installed at the unswept leading-edge sections. These slats could be deflected either 60° or 70° with a 0.015c gap. In addition, these slats were used as Krueger flaps that could be deflected either 70° or 80°. For the wing leading edge section from $\eta$ = 0.546 to 1.00, the slat used during the first investigation was modified to give more camber at its trailing edge and was relocated to give a 0.015c gap with respect to the modified wing leading edge. A slat deflection of 65° was used during the investigation.

The leading edge configurations used during the investigations are summarized in Table II.

## Leading-edge BLC system

Figure 2(e) shows the leading-edge BLC system and nozzle arrangement used during both wind tunnel investigations.

Air for the blowing BLC nozzles was supplied by a centrifugal compressor located at the forward portion of the fuselage. This compressor was driven by two variable frequency 300 horsepower electric motors coupled together.

The air from the compressor outlet was ducted as shown with appropriate valving to the wing leading-edge BLC nozzles and aileron BLC nozzles.

For the first investigation, the leading edge BLC nozzle was located between the fuselage and the outboard nacelle at 0.0075c from the swept leading edge with a gap of either 0.318 cm or 0.160 cm. An air pressure ratio that ranged from 1.17 to 1.41 was used during this investigation.

For the second wind tunnel investigation, BLC nozzles were installed at the unswept leading edge sections, both sides of the inboard nacelle, and

the inboard side of the outboard nacelle. The leading-edge BLC nozzle was located 55° from the wing chord plane with a gap of 0.101 cm. The nacelle BLC nozzle was located 15° from the vertical reference line and intersected the wing leading-edge BLC nozzle. The nacelle nozzle had a length of 20.32 cm and a gap of 0.203 cm. An air pressure ratio that ranged from 1.17 to 1.33 was used at both nozzles during the second investigation.

### Trailing-edge flap system

A Coanda plate surface was installed over the double-slotted flap from $\eta$ = 0.11 to 0.70 as shown in figure 2(f). The flap was the same as reported in reference 1 except for the increased spanwise extent of the Coanda surface. Separate Coanda plates were used to provide a jet flap deflection ($\delta_f$) of 30° and 75° measured between the flap trailing edge and the wing chord plane. For $\delta_f$ = 90° a 0.254 m (0.834 ft) chord extension was added at the trailing edge of the Coanda plate used for $\delta_f$ = 75°.

### Aileron

As shown in figure 2(g) a 0.35c plain aileron with BLC extended from $\eta$ = 0.70 to 1.0 and could be deflected from 0° to 23° measured perpendicular to the hinge line. For the first wind tunnel investigation, the BLC nozzle was located 30° ahead of the 0.65c line. For the second wind tunnel investigation the nozzle was relocated 15° ahead of the 0.65c line to improve the air flow over the aileron radius. A nozzle gap of 0.089 cm with a pressure ratio that ranged from 1.16 to 1.39 was used during the investigations.

### Propulsion

The upper surface blowing flap and nozzle arrangement is shown in figure 2(h). The JT15D-1 engines were used during the investigations and were housed in nacelles as shown in the figure. The engines have a bypass ratio of 3 and a normal maximum gross thrust of 2200 pounds. The engine centerline was coincident with the nacelle centerline and was pitched up 1° with respect to the wing chord plane. The inboard and outboard engine centerlines were located at $\eta$ = 0.256 and 0.480, respectively.

The engine nozzle configuration used during both wind tunnel investigations is shown in figure 2(h). The nozzle had an aspect ratio of 5.5 and corresponded to nozzle D of reference 1.

During the investigations, two vanes were located on each side of the nacelles close to the wing leading edge as shown in figure 2(h). These were installed to generate a vortex to improve the flow along the side of the nacelle and the wing upper surface. In addition, a wing fence was installed during the investigations at $\eta$ = 0.37 as shown in figure 2(h) to decrease the exhaust flow interaction between the inboard and outboard engines. Vortex generators were also installed briefly on the wing upper surface adjacent to the inboard side of the outboard nacelle as shown in the figure.

The nacelle contours used during the investigations are defined in figure 2(i). During the first wind tunnel investigation the lower half of the inboard and outboard nacelle cross sections were modified to elliptical sections from station 2 to 7 as shown in the figure. This was done to improve the upflow over the wing leading edge.

### Tail

The geometry of the horizontal and vertical tails is shown in figure 2(a). These tails are the same ones used in reference 1. The horizontal tail detail is shown in figure 2(j). The horizontal tail incidence and elevator were set at 0° when the tail was installed. The vertical tail was on the model throughout both investigations.

## CORRECTIONS

The data were corrected for wind-tunnel wall constraints. These corrections were determined by considering only the aerodynamic lift of the model ($C_L'$) that resulted after the jet reaction components had been subtracted from the data as follows:

$$C_L' = C_L - \eta_f C_J (\sin(\delta_j + \alpha_u))$$

$$\alpha = \alpha_u + .4175 C_L'$$

$$C_D = C_{D_u} + 0.0073 C_L'^2$$

$$C_m = C_{m_u} + 0.025 C_L' \text{ (horizontal tail on tests only)}$$

The engine thrust values defining $C_J$ were based on the calibration of the engine static thrust variation with engine fan rotational speed. The calibration of each engine was obtained from wind tunnel scale measurements with the flap undeflected. The $\delta_j$ and $\eta_f$ values used in the corrections are shown in figure 3. These values were obtained in the wind tunnel with four engines operating and with the wind off. Evaluated from tunnel balance measurements, $\eta_f$ is the resultant thrust ($F_R$) divided by static thrust ($F_g$).

The data that are presented in this report are not corrected for ram drag, but for reference the variation of ram drag with $C_J$ is presented in figure 4.

## TESTING AND PROCEDURE

The data to compute static jet turning angle and resultant thrust with the flap deflected were recorded in five second intervals during the period the four engines were accelerated simultaneously from idle setting to a thrust setting of 1000 pounds per engine. This was done to obtain data before the engine thrust generated airflow in the test section. The tunnel overhead doors were opened when these data were recorded.

Forces and moments were measured through an angle-of-attack range of -8° to 28°. Tests were conducted at Reynolds numbers of $2.1 \times 10^6$ and $3.0 \times 10^6$ corresponding to dynamic pressures of 239 and 479 $N/m^2$ (5.0 and 10.0 psf), respectively, and based on a mean aerodynamic chord of 1.69 m (5.56 ft).

### Tests With Constant $C_J$ and Varying Angle of Attack

Four engines operating- A constant $C_J$ was maintained as angle of attack was varied for each flap configuration investigated. The nominal $C_J$ values used in most cases during the investigation are as follows:

| $C_J$ (4 engine) | $q_\infty$, $N/m^2$ |
|---|---|
| 0 | 239 |
| .5 | 479 |
| 1.0 | 239 |
| 2.0 | 239 |
| 3.0 | 239 |
| 4.0 | 239 |

The variables studied were jet flap deflection, leading-edge BLC, nacelle BLC, wing leading-edge inboard sweep, and leading-edge slat or flap deflection. Tests were conducted with and without the horizontal tail.

Three engines operating- Tests were conducted with either the left hand outboard or inboard engine out at $\delta_f = 30°$ and 90°. In addition, tests were conducted with the right hand outboard engine out at $\delta_f = 90°$. In most cases, the Coanda surface behind the inoperative engine was left on.

### Tests With Constant $C_J$ and Varying Angle of Sideslip

A constant $C_J$ was maintained at $\alpha_u = 4°$ as $\beta$ was varied from 8° to -19° for most cases. Tests were conducted with all engines operating, or left hand outboard engine out.

## RESULTS AND DISCUSSION

The static turning efficiencies ($\eta_f$) and static turning angles ($\delta_j$) are shown in figure 3. The variation of $C_{D_{ram}}$ with $C_J$ is shown in figure 4. The jet exhaust total pressure distributions behind the engine nozzle and at the flap trailing edge (see figure 2(h)) along the inboard and outboard engine centerline are shown in figure 5. The basic aerodynamic data are presented in figures 6 through 32. An index to these data is given in Table III. The flap chordwise surface pressures at several spanwise stations are shown in figure 33. The variation of average downwash angle with angle-of-attack at the horizontal tail location is shown in figures 34(a) and (b) for $\delta_f$ = 30° and 90°, respectively. These data were obtained from a downwash rake mounted at the tail location as shown in figure 2(a). The variation of $C_L$ with $C_{\mu_{LE}}$ with the swept and unswept leading edge is shown in figure 35. A comparison of $C_{L_{max}}$ and $\alpha_{C_{Lmax}}$ values between the two engine model of reference 1 and the four engine model with the wing fully swept is shown in figure 36. The variation of $C_y$, $C_n$, and $C_\ell$ with $C_J$ at $\alpha_u$ = 4° is shown in figures 37(a) and (b) for $\delta_f$ = 30° and 90°, respectively with either the inboard or outboard engine out case.

### Static Turning

The $\delta_j$ and $\eta_f$ values shown in figure 3 were obtained with four engines operating at equal thrust. The engine nozzle which was used during the investigations corresponded to nozzle D of reference 1. A comparison with the results of reference 1 is also shown in the figure. Slightly higher values of $\delta_j$ and $\eta_f$ were obtained with four engines operating when the results are compared with one engine operating of reference 1. However, the result is nearly the same between two engine operation of reference 1 and the four engine operation. As mentioned in reference 1, higher $\delta_j$ value was obtained with multi-engine operation. This was probably due to the jet exhaust spreading over the top of the fuselage with one engine operating.

### Improvement of Maximum Lift and Stall Angle

Reference 3 discusses the problem and the subsequent improvement of maximum lift and stall angle of the model in greater detail. As indicated in the reference, the large nacelles extending well above the wing upper surface caused high upwash angles between the nacelles and between the inboard nacelle and the fuselage. This created an adverse pressure gradient at the leading edge and led to flow separation in these areas which affected maximum lift and stall angle. The deterioration of these values when the outboard engines were installed is shown in figure 36 in a comparison between the two engine model of reference 1 and the four engine model. As mentioned previously, these models were nearly identical except for the number of engines. The values of $C_{L_{max}}$ and the stall angle were lowered approximately by 1.0 and 8° to 12°, respectively, from $C_J$ = 0 to 2.9.

Efforts were made to improve maximum lift and stall angle by changing the leading edge and nacelle configuration at the critical areas. Figure 13 shows the effect of modifying the nacelle contour (see figure 2(i)) near the wing leading edge. Maximum lift is improved slightly, but the stall angle remained the same. The effects of leading-edge BLC on the swept leading edge and unsweeping the leading edge near the critical areas are also shown in the figure. In either case, $C_{L_{max}}$ and $\alpha_{C_{Lmax}}$ increased (approximately 10 percent and 5.5°, respectively) over that without any treatment on the swept leading edge. Additional improvement was obtained with the inboard leading-edge unswept by applying blowing along the nacelle sides as shown in figure 14. $C_{L_{max}}$ and $\alpha_{C_{Lmax}}$ values increased 4 percent and 7°, respectively. The addition of leading edge BLC to the unswept leading edge sections along with nacelle blowing did not give further improvement as shown in the same figure.

The effect of slat and Krueger flap deflections at the unswept leading edge sections on $C_{L_{max}}$ is shown in figure 16. The higher slat deflection or Krueger flap deflection did not provide any significant improvement in $C_{L_{max}}$.

Neither the combination of nacelle vanes and wing vortex generator nor the combination of nacelle vanes and wing fence or nacelle vanes alone provided any sizeable maximum lift improvements as shown in figures 13 and 19, respectively.

### Longitudinal and Lateral Characteristics With an Engine Out at Zero Sideslip

The effects of engine out are shown in figures 23, 26, and 27. As shown in these figures, higher values of lift were obtained with the outboard engine out compared to the inboard engine out case, but the values of drag remained essentially the same for either case. As expected, the outboard engine out case provided a greater nose up pitching moment.

The variation of $C_y$, $C_n$, and $C_\ell$ with $C_J$ with either the outboard or the inboard engine out on the left hand side are shown in figures 37(a) and (b) for $\delta_f$ = 30° and 90°, respectively. As shown in the figures, the values of rolling moment with the outboard engine out was approximately twice those with the inboard engine out for either $\delta_f$ = 30° and 90°.

## REFERENCES

1. Aoyagi, Kiyoshi; Falarski, Michael D.; and Koenig, David G.: Wind Tunnel Investigation of a Large-Scale Upper Surface Blown-Flap Transport Model Having Two Engines. NASA TM X-62,296, 1973.

2. Falarski, Michael D.; Aoyagi, Kiyoshi; and Koenig, David G.: Acoustic Characteristics of a Large-Scale Wind-Tunnel Model of an Upper-Surface Blown Flap Transport Having Two Engines. NASA TM X-62,319, 1973.

3. Koenig, David G.; and Aoyagi, Kiyoshi: Maximum Lift of Upper Surface Blowing STOL Aircraft with Swept Wings. AIAA Paper 75-868, June, 1975.

TABLE I- MODIFIED SUPERCRITICAL AIRFOIL ORDINATES
(STREAMWISE DIRECTION)

| ROOT SECTION | | | |
|---|---|---|---|
| $\frac{x}{c}$ | x, cm | $y_u$, cm | $y_L$, cm |
| 0 | 0 | 0 | 0 |
| .0125 | 2.857 | 6.131 | 6.050 |
| .0250 | 5.715 | 8.087 | 8.229 |
| .0375 | 8.572 | 9.456 | 9.679 |
| .050 | 11.430 | 10.467 | 10.749 |
| .075 | 17.145 | 12.001 | 12.324 |
| .100 | 22.860 | 13.149 | 13.390 |
| .150 | 34.290 | 14.772 | 14.823 |
| .200 | 45.720 | 15.913 | 15.712 |
| .300 | 68.580 | 17.406 | 16.517 |
| .400 | 91.440 | 17.970 | 16.337 |
| .500 | 114.300 | 17.713 | 15.087 |
| .600 | 137.160 | 16.634 | 12.446 |
| .700 | 160.020 | 14.587 | 9.525 |
| .800 | 182.880 | 11.153 | 6.858 |
| .900 | 205.740 | 6.210 | 4.064 |
| 1.000 | 228.600 | 0 | 1.612 |

| TIP SECTION | | | |
|---|---|---|---|
| $\frac{x}{c}$ | x, cm | $y_u$, cm | $y_L$, cm |
| 0 | 0 | 0 | 0 |
| .0125 | 1.143 | 1.960 | 1.935 |
| .0250 | 2.286 | 2.588 | 2.631 |
| .0375 | 3.429 | 3.025 | 3.096 |
| .050 | 4.572 | 3.347 | 3.439 |
| .075 | 6.858 | 3.840 | 3.942 |
| .100 | 9.144 | 4.206 | 4.284 |
| .150 | 13.716 | 4.726 | 4.742 |
| .200 | 18.288 | 5.090 | 5.026 |
| .300 | 27.432 | 5.570 | 5.285 |
| .400 | 36.576 | 5.750 | 5.227 |
| .500 | 45.720 | 5.666 | 4.826 |
| .600 | 52.578 | 5.321 | 4.064 |
| .700 | 61.722 | 4.668 | 3.175 |
| .800 | 70.866 | 3.568 | 2.286 |
| .900 | 80.010 | 1.986 | 1.397 |
| 1.000 | 91.440 | 0 | .508 |

TABLE II- LEADING EDGE CONFIGURATIONS

| LE Config. no. | η = 0.087 to 0.190 | | | η = 0.321 to 0.413 | | | η = 0.546 to 1.00 | | | Reference Figure No. |
|---|---|---|---|---|---|---|---|---|---|---|
| | LE Device | Slat Chord | $\Lambda_{LE}$, deg | LE Device | Slat Chord | $\Lambda_{LE}$ deg. | LE Device | Wing LE Contour | $\Lambda_{LE}$, deg | |
| 1 | 52° slat | 0.15 c | 27.71 | 52° slat | 0.15 c | 27.71 | 52° slat | original | 27.71 | 2(c) |
| 2 | 68° Krueger | ↓ | ↓ | 68° Krueger | ↓ | ↓ | ↓ | ↓ | ↓ | ↓ |
| 3 | 70° slat | 24.10 cm | 0 | 70° slat | 24.10 cm | 0 | ↓ | ↓ | ↓ | ↓ |
| 4 | 60° slat | 33.97 cm | ↓ | 60° slat | 30.86 cm | ↓ | 65° slat | modified | ↓ | 2(d) |
| 5 | 70° slat | ↓ | ↓ | 70° slat | ↓ | ↓ | ↓ | ↓ | ↓ | ↓ |
| 6 | 70° Krueger | ↓ | ↓ | 70° Krueger | ↓ | ↓ | ↓ | ↓ | ↓ | ↓ |
| 7 | 80° Krueger | ↓ | ↓ | 80° Krueger | ↓ | ↓ | ↓ | ↓ | ↓ | ↓ |

TABLE III- LIST OF BASIC DATA FIGURES

| Test | Run | Figure | $\delta_f$ deg | $C_J$ | $\alpha_u$, deg | $q_u$ psf | $\beta$ deg | LE config. no. (see Table II) | $\Lambda_{LE}$, deg n=0.087 to 0.190 n=0.321 to 0.413 | Nacelle Contour | $C_{\mu_{NAC}}$ | $C_{\mu_{LE}}$ | $\delta_{ail}$ deg. | $C_{\mu_{ail}}$ | Hori Tail | Wing Fence | Nacelle Vane | Remark |
|---|---|---|---|---|---|---|---|---|---|---|---|---|---|---|---|---|---|---|
| 441 | 98 | 6 | 0 | 0 | -8 to 24 | 5 | 0 | plain | 0 | Modified | 0 | 0 | 0 | 0 | off | off | off | Unswept inboard LE |
| | 97 | | | 2.08 | -8 to 24 | | | | | | | | | | | | | |
| | 96 | | | 4.19 | -8 to 20 | | | | | | | | | | | | | |
| | 90 | 7 | | 0 | -8 to 30 | | | 6 | | | | | | | on | | | |
| | 89 | | | 2.02 | | | | | | | | | | | | | | |
| | 93 | | | 0 | | | | | | | | | | | off | | | |
| | 92 | | | 2.04 | | | | | | | | | | | | | | |
| | 91 | | | 4.08 | -8 to 28 | | | | | | | | | | | | | |
| | 3 | 8 | 30 | 2.02 | -8 to 30 | | | 4 | | | | 0.025 | 23 | 0.029 | off | on | on | |
| | 4 | | | 1.94 | | | | | | | | .023 | | .026 | | | | |
| | 5 | | | 1.93 | | | | | | | | 0 | | .026 | | | | |
| | 6 | | | 3.79 | | | | | | | | | | .024 | | | | |
| 434 | 62 | 9 | | 0 | -8 to 28 | | | 3 | | | | 0 | | 0.039 | | | | |
| | 61 | | | .42 | -8 to 24 | 10 | | | | | | | | | | | | |
| | 60 | | | .90 | -8 to 28 | 5 | | | | | | | | | | | | |
| | 59 | | | 2.05 | -8 to 28 | | | | | | | | | | | | | |
| | 58 | | | 3.14 | | | | | | | | | | | | | | |
| | 57 | | | 3.84 | | | | | | | | | | | | | | |
| 441 | 69 | 10 | | 0 | -8 to 30 | 10 | | 6 | | | | | 0 | 0 | on | off | off | |
| | 68 | | | .56 | | | | | | | | | | | | | | |
| | 67 | | | 1.11 | | 5 | | | | | | | | | | | | |
| | 66 | | | 2.00 | | | | | | | | | | | | | | |
| | 65 | | | 2.83 | | | | | | | | | | | | | | |
| | 64 | | | 4.06 | | | | | | | | | | | | | | |
| 434 | 14 | 11 | 75 | 0 | -4 to 20 | 10 | | 1 | 27.71 | Original | | 0 | 10 | 0 | off | | | Swept inboard LE |
| | 9 | | | .40 | -8 to 22 | | | | | | | | | | | | | |
| | 11 | | | .95 | -8 to 20 | | | | | | | | | | | | | |
| | 8 | | | 2.05 | -8 to 24 | | | | | | | | | | | | | |
| | 12 | | | 2.85 | -4 to 22 | | | | | | | | | | | | | |
| | 26 | 12 | | 1.85 | -8 to 24 | 5 | | 2 | | | | 0 | 23 | | on | on | | Swept inboard LE with BLC |
| | 27 | | | .86 | -8 to 20 | | | | | | | 0.043 | | 0.039 | | | | |
| | 24 | | | 1.88 | 0 to 22 | | | | | | | .046 | | .038 | | | | |
| | 28 | | | 2.77 | -8 to 24 | | | | | | | .040 | | .037 | | | | |

TABLE III- LIST OF BASIC DATA FIGURES - CONTINUED

| Test | Run | Figure | $\delta_f$ deg | $C_J$ | $\alpha_u$, deg | $q_u$ psf | $\beta$ deg | LE config. no. (see Table II) | $\Lambda_{LE}$, deg n=0.087 to 0.190 n=0.321 to 0.413 | Nacelle Contour | $C_{\mu_{NAC}}$ | $C_{\mu_{LE}}$ | $\delta_{ail}$ deg. | $C_{\mu_{ail}}$ | Horiz Tail | Wing Fence | Nacelle Vane | Remark |
|---|---|---|---|---|---|---|---|---|---|---|---|---|---|---|---|---|---|---|
| 434 | 33 | 13 | 75 | 1.96 | -8 to 24 | 5 | 0 | 2 | 27.72 | Modified | 0 | 0 | 23 | 0 | off | on | on | LE BLC effect with swept inbound LE and effect of unswept inboard LE |
| | 32 | | | 1.97 | -8 to 24 | | | | | | | 0.076 | | .064 | | | | |
| | 35 | | | 1.89 | -8 to 18 | | | | | | | .076 | | .067 | | | off | |
| | 36 | | | 2.00 | -8 to 28 | | | 3 | 0 | | | 0 | | .046 | | | | |
| 434 | 45 | 14 | 90 | 0 | -8 to 20 | | | | | | 0 | 0 | | 0.034 | | | on | Unswept inboard LE |
| | 42 | | | 0.52 | | 10 | | | | | | | | .018 | | | | |
| | 41 | | | 1.02 | -8 to 24 | 5 | | | | | | | | .034 | | | | |
| | 38 | | | 2.11 | -8 to 28 | | | | | | | | | .042 | | | off | |
| | 39 | | | 2.18 | -8 to 26 | | | | | | | | | | | | on | |
| | 40 | | | 3.30 | | | | | | | | | | .036 | | | | |
| 441 | 7 | 15 | | 2.01 | -8 to 30 | | | 4 | | | | | | 0.025 | | | | Effect of nacelle BLC with and without LE BLC |
| | 9 | | | | | | | | | | 0.033 | .025 | | | | | | |
| | 10 | | | 2.00 | | | | | | | .029 | | | .028 | | | | |
| | 10 | 16 | | | | | | | | | | | | | | | | Effect of unswept LE devices |
| | 11 | | | | | | | 5 | | | | | | | | | | |
| | 12 | | | 1.98 | | | | | | | | | | | | | | |
| | 13 | 17 | | 1.95 | | | | | | | | | 0 | 0 | | | | Effect of aileron deflection |
| | 12 | | | 1.98 | | | | | | | | | 23 | 0.028 | | | | |
| | 16 | 18 | | 2.02 | -8 to 24 | | | 6 | | | 0 | 0 | 0 | 0 | | | | Effect of LE BLC |
| | 14 | | | 1.96 | -8 to 30 | | | | | | 0.030 | 0.026 | | | | | | |
| | 15 | | | | 8 to 30 | | | | | | .038 | .037 | | | | | | |
| | 17 | | | 1.99 | -8 to 30 | | | 5 | | | 0 | 0 | | | | | | |
| | 19 | 19 | | 1.96 | | | | | | | | | | | | off | off | Effect of nacelle vanes and wing fence |
| | 18 | | | 1.98 | | | | | | | | | | | | off | on | |
| | 17 | | | 1.99 | | | | | | | | | | | | on | on | |
| | 26 | 20 | | 0 | -8 to 20 | | | | | | | | | | | off | off | |
| | 25 | | | 0.56 | | 10 | | | | | | | | | | | | |
| | 24 | | | 1.13 | -8 to 24 | 5 | | | | | | | | | | | | |
| | 19 | | | 1.96 | -8 to 30 | | | | | | | | | | | | | |
| | 23 | | | 2.91 | | | | | | | | | | | | | | |
| | 20) | | | | | | | | | | | | | | | | | |
| | 21) | | | 3.97 | | | | | | | | | | | | | | |
| | 22) | | | | | | | | | | | | | | | | | |
| | 32 | 21(a) | | 0 | -8 to 24 | | | | | | | | | | on | | | Unswept inboard LE without LE BLC, tail on |
| | 35 | | | 0.56 | -8 to 28 | 10 | | | | | | | | | | | | |
| | 34 | | | 1.13 | -8 to 30 | 5 | | | | | | | | | | | | |
| | 33 | | | 2.00 | | | | | | | | | | | | | | |
| | 31 | | | 2.97 | | | | | | | | | | | | | | |
| | 30 | | | 3.93 | | | | | | | | | | | | | | |

TABLE III- LIST OF BASIC DATA FIGURES - CONTINUED

| Test | Run | Figure | $\delta_f$ deg | $C_J$ | $\alpha_u$, deg | $q_u$ psf | $\beta$ deg | LE config. no. (see Table II) | $\Lambda_{LE}$, deg $\eta$=0.087 to 0.190 $\eta$=0.321 to 0.413 | Nacelle Contour | $C_{\mu_{NAC}}$ | $C_{\mu_{LE}}$ | $\delta_{ail}$ deg. | $C_{\mu_{ail}}$ | Horiz Tail | Wing Fence | Nacelle Vane | Remark |
|---|---|---|---|---|---|---|---|---|---|---|---|---|---|---|---|---|---|---|
| 441 | 62 | 21(b) | 90 | 0.56 | -8 to 30 | 10 | 0 | 5 | 0 | Modified | 0.011 | 0.009 | 0 | 0 | on | off | off | Unswept inboard LE with LE BLC |
| | 61 | | | 1.12 | -4 to 28 | 5 | | | | | .021 | .018 | | | | | | |
| | 60 | | | 2.00 | ↓ | | | | | | | | | | | | | |
| | 59 | | | 3.04 | -4 to 30 | | | | | | | | | | | | | |
| 434 | 55 | 22(a) | 30 | 0 | -8 to 28 | | | 3 | | | 0 | 0 | 23 | 0.034 | off | on | on | L.H. outboard engine out longitudinal and lateral characteristics. Coanda surface on behind engine out |
| | 54 | and | | 0.68 | ↓ | | | | | | | | | | | | | |
| | 53 | (b) | | 1.50 | | | | | | | | | | | | | | |
| | 52 | | | 2.14 | -8 to 30 | | | | | | | | | | | | | |
| | 51 | | | 3.06 | | | | | | | | | | | | | | |
| 441 | 86 | 23(a) | 30 | 1.49 | | | | 6 | | | | | 0 | 0 | on | off | off | L.H.outboard engine out |
| | 85 | and | | 0.84 | | | | | | | | | | | | | | L.H.inboard engine out |
| | 84 | (b) | | 1.50 | | | | | | | | | | | | | | |
| | 83 | | | 2.09 | | | | | | | | | | | | | | |
| 434 | 50 | 24(a) | 90 | 0 | -8 to 16 | | | 3 | | | | | 23 | 0.039 | off | on | on | L.H. outboard engine out with Coanda surface from $\eta$ = 0.43 to 1.0 on L.H. side off |
| | 49 | and | | 0.63 | -8 to 20 | | | | | | | | | | | | | |
| | 46 | (b) | | 1.40 | -8 to 24 | | | | | | | | | | | | | |
| | 48 | | | 2.19 | ↓ | | | | | | | | | | | | | |
| | 47 | | | 2.91 | -8 to 30 | | | | | | | | | | | | | |
| 441 | 42 | 25(a) | | 0 | -8 to 24 | | | 5 | | | | | 0 | 0 | on | off | off | |
| | 41 | and | | 0.43 | -8 to 28 | 10 | | | | | | | | | | | | |
| | 40 | (b) | | .84 | ↓ | 5 | | | | | | | | | | | | |
| | 39 | | | 1.39 | -8 to 30 | | | | | | | | | | | | | |
| | 38 | | | 2.28 | | | | | | | | | | | | | | |
| | 37 | | | 3.05 | | | | | | | | | | | | | | |
| | 49 | 26(a) | | 0.87 | -8 to 24 | | | | | | | | | | | | | L.H.outboard engine out with Coanda surf. on behind engine |
| | 48 | and | | 1.50 | -8 to 30 | | | | | | | | | | | | | |
| | 50 | (b) | | 1.47 | ↓ | | | | | | | | | | | | | R.H.outboard engine out |
| | 58 | 27(a) | | 0.86 | -8 to 30 | | | | | | | | | | | | | L.H. inboard engine out. Coanda surf. on behind engine out. |
| | 57 | and (b) | | 1.51 | ↓ | | | | | | | | | | | | | |
| | 60 | 28(a) | | 2.02 | -4 to 30 | | | | | | 0.021 | 0.018 | | | | | | All engs at equal thrust |
| | 63 | and (b) | | 2.01 | -8 to 30 | 7.7 | | | | | .029 | .025 | | | | | | Inboard engine thrusts outboard engines |

TABLE III- LIST OF BASIC DATA FIGURES - CONCLUDED

| Test | Run | Figure | $\delta_f$ deg | $C_J$ | $\alpha_u$, deg | $q_u$ psf | $\beta$ deg | LE config. no. (see Table II) | $\Lambda_{LE}$, deg $\eta$=0.087 to -.190 $\eta$=0.321 to 0.413 | Nacelle Contour | $C_{\mu_{NAC}}$ | $C_{\mu_{LE}}$ | $\delta_{ail}$ deg. | $C_{\mu_{ail}}$ | Horiz Tail | Wing Fence | Nacelle Vane | Remark |
|---|---|---|---|---|---|---|---|---|---|---|---|---|---|---|---|---|---|---|
| 441 | 79 | 29 | 30 | .94 | 4 | 5 | 8 to -8 | 6 | 0 | Modified | 0 | 0 | 0 | 0 | on | off | off | Sideslip effect with 4 engines |
| | 87 | | | 2.01 | | | 8 to -16 | | | | | | | | | | | |
| | 78 | | | 3.04 | | | 8 to -8 | | | | | | | | | | | |
| | 80 | 30 | | 1.51 | | | 8 to -19 | | | | | | | | | | | L.H.outboard engine out. Coanda surface on |
| | 82 | | | 0.84 | | | 4 to -16 | | | | | | | | | | | L.H.inboard engine out. Coanda surface on behind engine out |
| | 81 | | | 1.53 | | | 8 to -16 | | | | | | | | | | | |
| | 80 | | | 2.28 | | | 8 to -16 | | | | | | | | | | | |
| | 47 | 31 | 90 | 0 | | | 8 to -19 | 5 | | | | | | | | | | Sideslip effect with 4 engines |
| | 46 | | | 0.56 | | 10 | | | | | | | | | | | | |
| | 45 | | | 1.25 | | 5 | | | | | | | | | | | | |
| | 44 | | | 2.82 | | | | | | | | | | | | | | |
| | 43 | | | 2.99 | | | | | | | | | | | | | | |
| | 53 | 32(a) | | 0.83 | | | | | | | | | | | | | | L.H.outboard engine out. Coanda surface on behind engine out |
| | 51 | | | 1.45 | | | | | | | | | | | | | | |
| | 52 | | | 2.20 | | | | | | | | | | | | | | |
| | 56 | 32(b) | | 0.84 | | | | | | | | | | | | | | L.H.inboard engine out. Coanda surface on behind engine out |
| | 55 | | | 1.51 | | | | | | | | | | | | | | |
| | 54 | | | 2.25 | | | | | | | | | | | | | | |

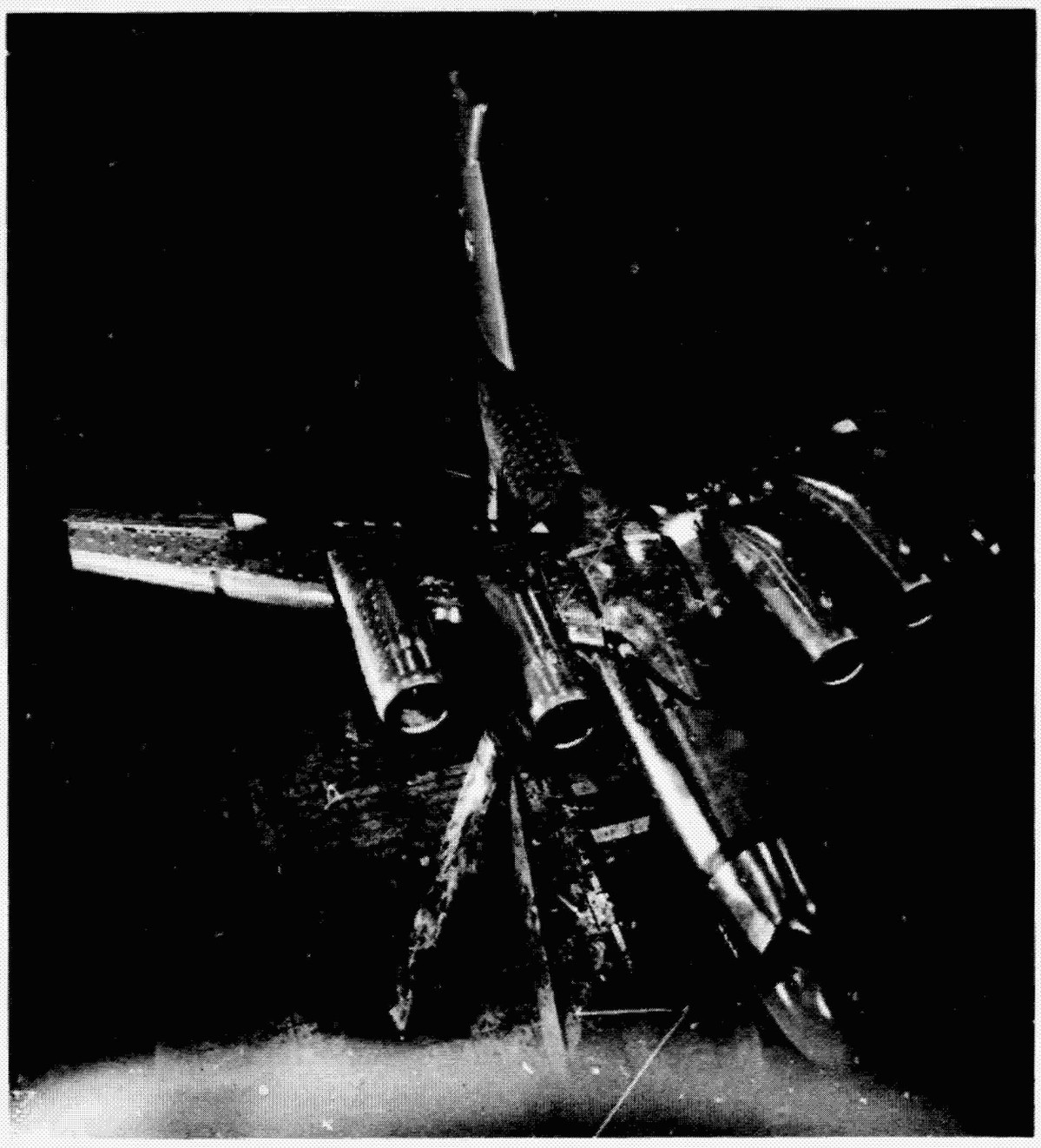

(a) Swept wing leading edge.

Figure 1.- Photograph of the model as mounted in the Ames 40- by 80-Foot Wind Tunnel.

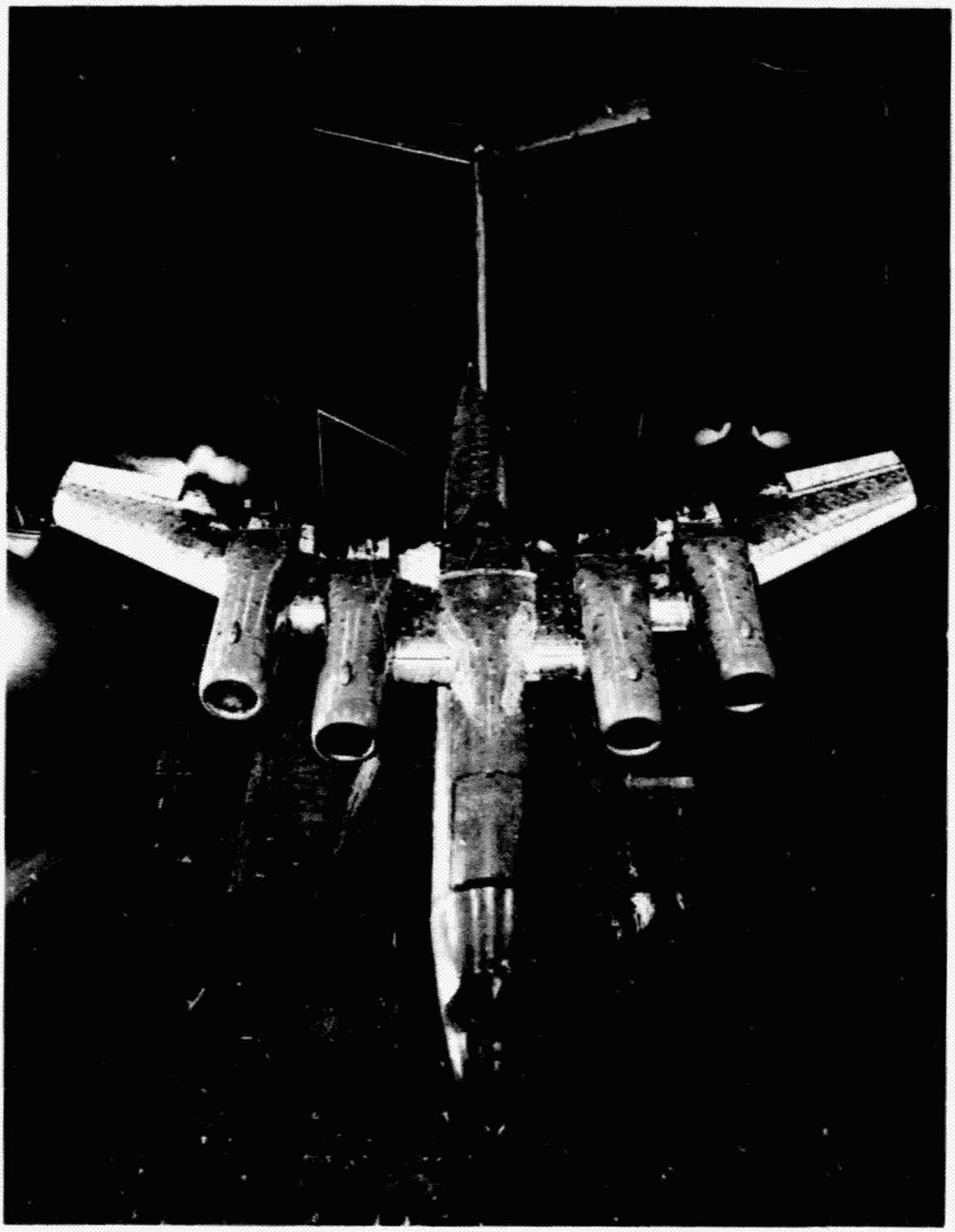

(b) Unswept wing leading edge at the inboard sections.

Figure 1.- Concluded.

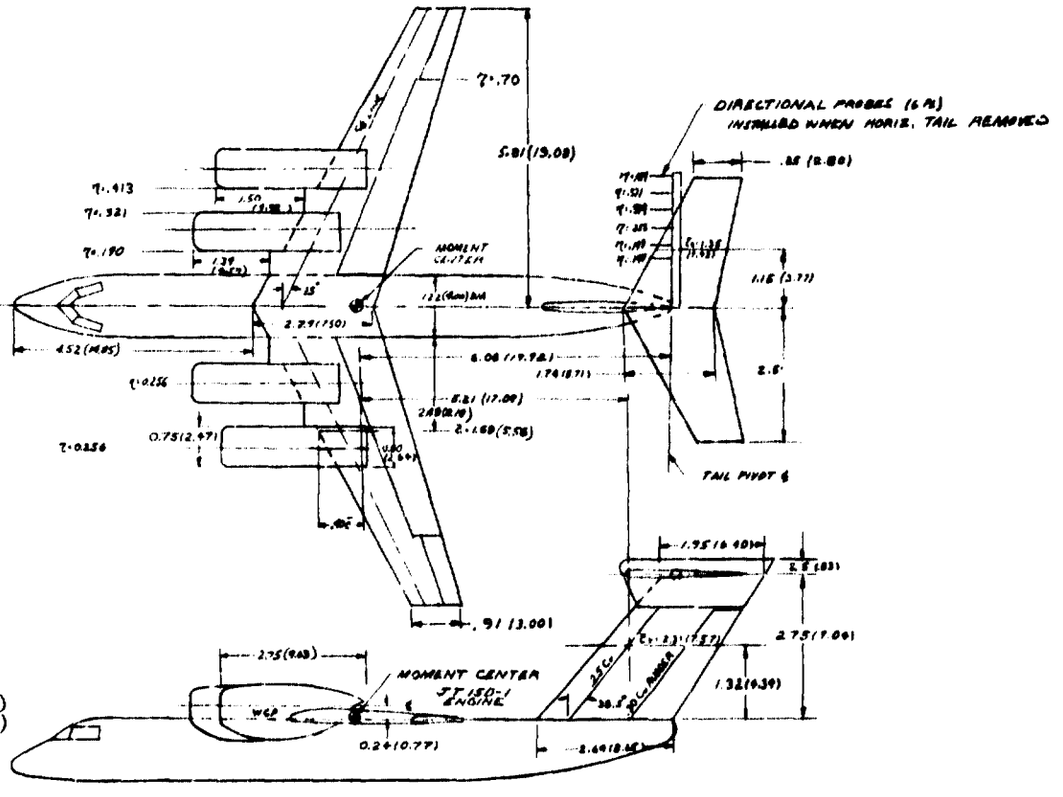


| | WING | HORIZ. TAIL | VERT. TAIL |
|---|---|---|---|
| ASPECT RATIO | 7.28 | 4.00 | 1.20 |
| SWEEP DEG | 25.0 | 25.0 | 38.5 |
| TAPER RATIO | .40 | .49 | .74 |
| AREA, METER$^2$(FT$^2$) | 19.67 (200.34) | 6.72 (72.30) | 6.32 (68.00) |
| AIRFOIL SECTION | SEE NOTE 2 | NACA 64-012 | NACA 0012 |
| MAC, METER (FT) | 1.69 (5.56) | 1.35 (4.43) | 2.31 (7.57) |

NOTE:
1. ALL DIMENSIONS IN METER (FEET) EXCEPT AS NOTED.
2. ROOT - MODIFIED SWEPT CRITICAL AIRFOIL ($t/c$ 0.15)
TIP - " " " ($t/c$ 0.12)

(a) General arrangement of the model.

Figure 2.- Geometric details of the model.

| SEC C-C | | | SEC D-D | | SEC B-B | | | SEC A-A | | SEC E-E | | | SEC F-F | | |
|---|---|---|---|---|---|---|---|---|---|---|---|---|---|---|---|
| x, cm | $Y_u$, cm | $Y_L$, cm | $Y_u$, cm | $Y_L$, cm | x, cm | $Y_u$, cm | $Y_L$, cm | $Y_u$, cm | $Y_L$, cm | x, cm | $Y_u$, cm | $Y_L$, cm | x, cm | $Y_u$, cm | $Y_L$, cm |
| 0 | — | -2.16 | — | -2.16 | 0 | — | -1.18 | — | -1.32 | 0 | -2.16 | -2.16 | 0 | -.86 | -.86 |
| 2.54 | 3.98 | -7.21 | 5.08 | -7.42 | 2.54 | 4.70 | -7.11 | 4.57 | -7.32 | 2.03 | 2.39 | -5.99 | .51 | .58 | -1.93 |
| 5.08 | 5.49 | -8.79 | 6.60 | -8.89 | 5.08 | 6.48 | -9.04 | 6.38 | -8.99 | 4.06 | 3.96 | -7.09 | 1.52 | 1.70 | -2.79 |
| 7.62 | 6.99 | -9.63 | 7.98 | -9.73 | 7.62 | 8.13 | -10.26 | 8.66 | -10.36 | 6.35 | 5.21 | -7.70 | 2.79 | 2.96 | -3.20 |
| 10.15 | 8.18 | -10.16 | 8.69 | -10.39 | 10.15 | 9.50 | -11.13 | 9.73 | -11.18 | 8.38 | 6.05 | -7.96 | 3.61 | 3.77 | -3.45 |
| 12.7 | 9.12 | -10.46 | 9.53 | -10.69 | 12.70 | 10.34 | -11.63 | 10.67 | -11.68 | 10.41 | 6.68 | -8.10 | 4.66 | 3.07 | -3.63 |
| 15.24 | 9.94 | -10.53 | 10.10 | -10.67 | 15.24 | 11.13 | -11.84 | 11.30 | -11.88 | 12.45 | 7.21 | -8.15 | 5.64 | 3.33 | -3.73 |
| 17.78 | 10.57 | -10.62 | 10.64 | -10.79 | 17.78 | 11.79 | -11.89 | 12.09 | -11.91 | 14.48 | 7.65 | -8.23 | 6.6 | 3.53 | -3.88 |
| 20.32 | 10.96 | -10.76 | 11.00 | -10.89 | 20.96 | 12.65 | -11.7 | 12.57 | -11.74 | 16.51 | 8.05 | -8.43 | 7.67 | 3.73 | -3.91 |
| 22.86 | 11.23 | -10.74 | 11.33 | -10.84 | 23.39 | 13.05 | -11.84 | 12.96 | -12.60 | 18.54 | 8.38 | -8.66 | 8.70 | 4.06 | -4.22 |
| 25.4 | 11.53 | -11.15 | 11.68 | -10.89 | 25.09 | 13.21 | -12.34 | 13.41 | -12.83 | 20.57 | 8.69 | -8.86 | 11.73 | 4.34 | -4.50 |
| 30.48 | 11.99 | -11.58 | 11.99 | -10.74 | 27.12 | 13.62 | -12.90 | 13.97 | -13.19 | 22.61 | 8.99 | -9.07 | 12.77 | 4.50 | -4.58 |
| 35.56 | 12.34 | -11.94 | 12.37 | -10.85 | 30.20 | 14.27 | -13.57 | 14.63 | -14.06 | 24.67 | 9.42 | -9.47 | 15.80 | 4.76 | -4.70 |
| 38.34 | 12.57 | -12.10 | — | — | 32.28 | 14.63 | -13.85 | 14.88 | -14.38 | 30.72 | 9.86 | -9.78 | 17.83 | 4.90 | -4.80 |
| 42.52 | 13.11 | -12.30 | — | — | 35.04 | 14.99 | -13.98 | 15.75 | -15.19 | 33.02 | 10.01 | -9.91 | 20.88 | 5.13 | -4.98 |
| 38.77 | 12.96 | -12.98 | — | — | 36.80 | 15.11 | -13.36 | 15.76 | -15.42 | | | | | | |
| 63.50 | — | — | 13.00 | -11.31 | 71.76 | 15.29 | -13.67 | — | — | | | | | | |

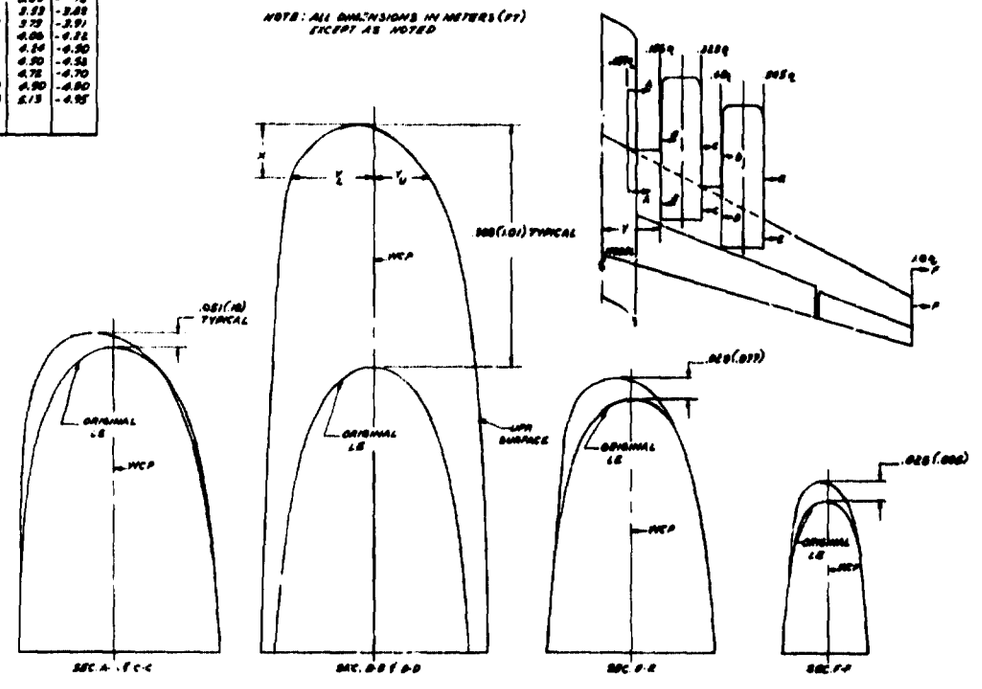


(b) Wing leading edge modification.

Figure 2.- Continued.

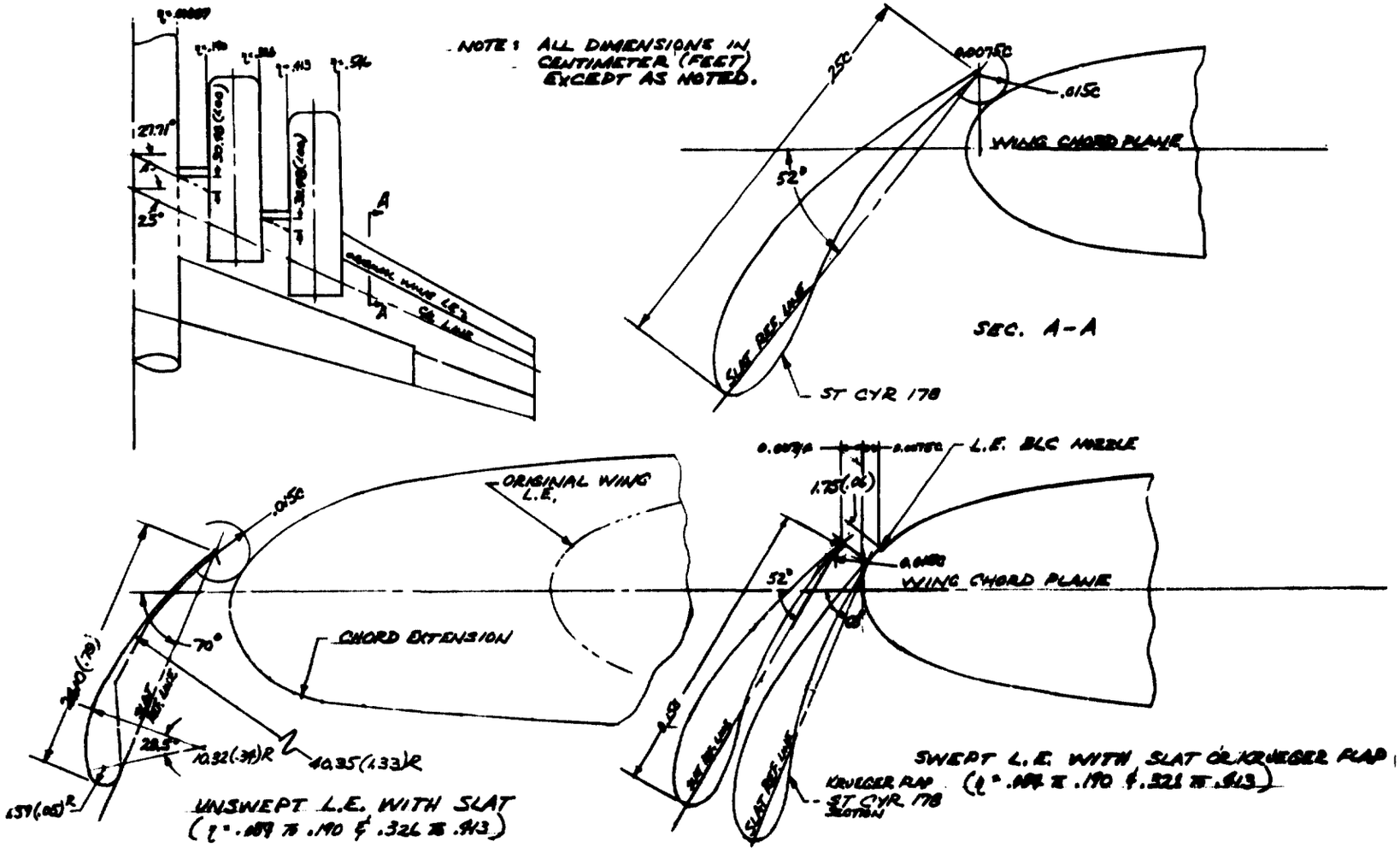


(c) Leading edge configurations used during Test 434.

Figure 2.- Continued.

| SEC. A-A | | | SEC. B-B | | | SEC. C-C | | |
|---|---|---|---|---|---|---|---|---|
| X,cm | $Y_u$,cm | $Y_L$,cm | X,cm | $Y_u$,cm | $Y_L$,cm | X % c | $Y_u$ % c | $Y_L$ % c |
| .356 | 2.464 | - | 0 | .673 | - | 0 | 0 | 0 |
| 1.016 | 3.607 | - | .419 | 2.540 | - | .31 | .95 | -.54 |
| 1.524 | 4.2[illegible] | - | .838 | 3.353 | - | .62 | 1.30 | -.74 |
| 2.032 | 4.750 | - | 1.270 | 3.962 | - | 1.25 | 1.82 | -.99 |
| 2.540 | 5.131 | - | 1.702 | 4.458 | - | 1.87 | 2.22 | -1.06 |
| 3.048 | 5.410 | - | 2.540 | 5.296 | - | 2.50 | 2.50 | -1.13 |
| 3.810 | 5.842 | - | 3.391 | 5.944 | - | 3.75 | 2.96 | -1.04 |
| 5.080 | 6.375 | - | 4.242 | 6.414 | - | 5.00 | 3.28 | -.97 |
| 6.350 | 6.782 | 0 | 5.098 | 6.820 | - | 6.25 | 3.50 | -.79 |
| 7.620 | 7.061 | 1.422 | 6.794 | 7.417 | .876 | 7.50 | 3.67 | -.47 |
| 8.890 | 7.163 | 2.616 | 8.484 | 7.772 | 2.489 | 10.00 | 1.24 | .10 |
| 10.160 | 7.165 | 3.353 | 10.185 | 7.912 | 3.531 | 12.50 | 3.50 | .59 |
| 11.430 | 7.137 | 3.810 | 11.887 | 7.886 | 4.229 | 15.00 | 2.90 | .68 |
| 12.700 | 7.036 | 4.115 | 13.589 | 7.762 | 4.653 | 17.50 | 2.10 | .55 |
| 13.970 | 6.833 | 4.293 | 16.985 | 7.082 | 4.892 | 20.00 | 1.20 | .35 |
| 15.240 | 6.807 | 4.267 | 20.384 | 6.081 | 4.567 | 22.50 | .10 | 1.11 |
| 17.780 | 5.918 | 4.115 | 23.779 | 4.823 | 3.820 | 23.75 | -.50 | -.04 |
| 20.320 | 5.055 | 3.632 | 27.178 | 3.363 | 2.751 | 25.00 | -.90 | -.16 |
| 22.860 | 4.039 | 3.023 | 30.574 | 1.816 | 1.359 | | | |
| 25.400 | 2.896 | 2.159 | 33.972 | .135 | -.135 | | | |
| 27.940 | 1.753 | 1.245 | LER | 2.176 | | | | |
| 28.423 | - | 1.016 | | | | | | |
| 30.861 | 229 | - | | | | | | |
| LER | 2.175 | | | | | | | |

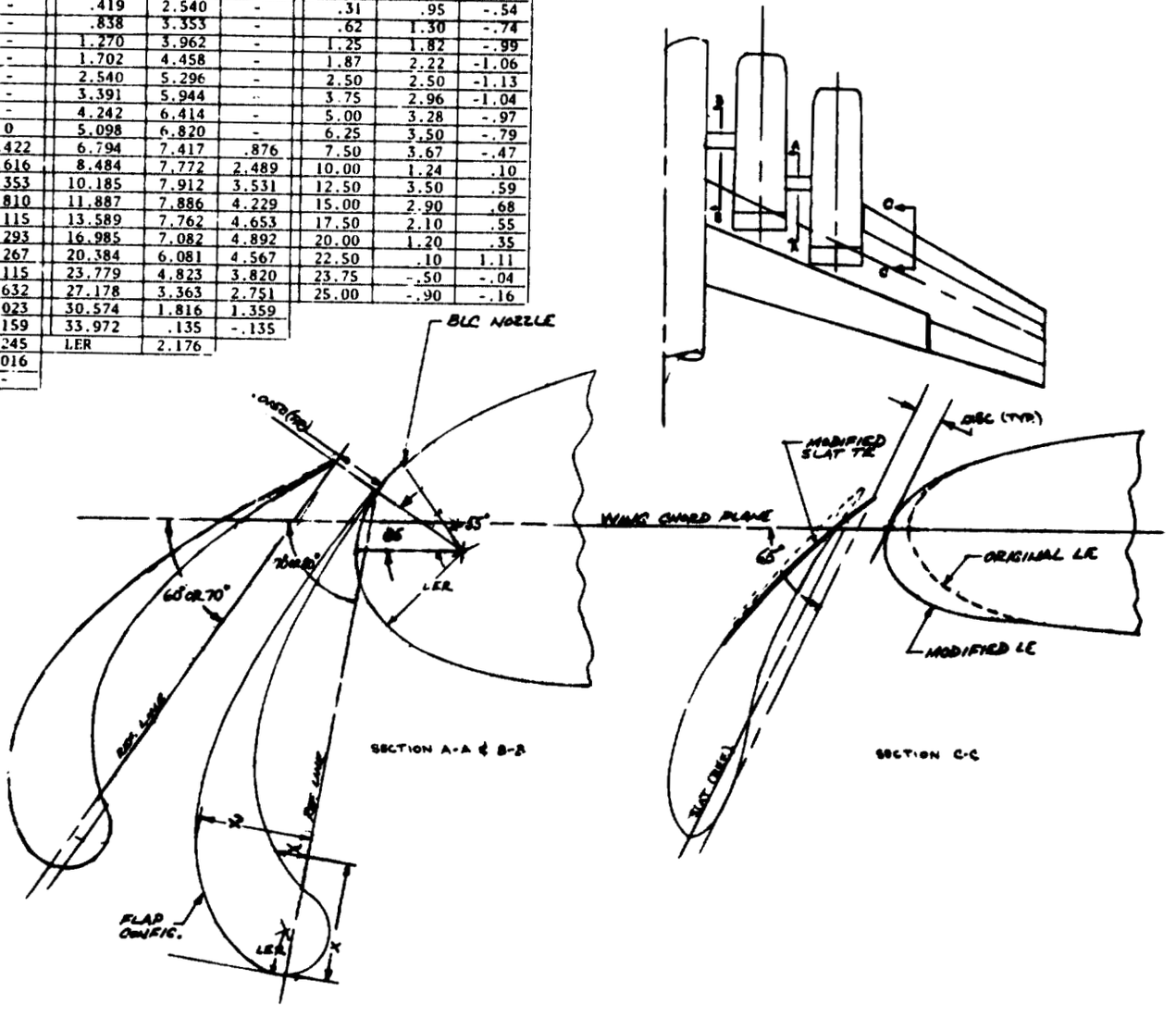


(d) Leading-edge slat arrangement used during Test 441.

Figure 2.- Continued.

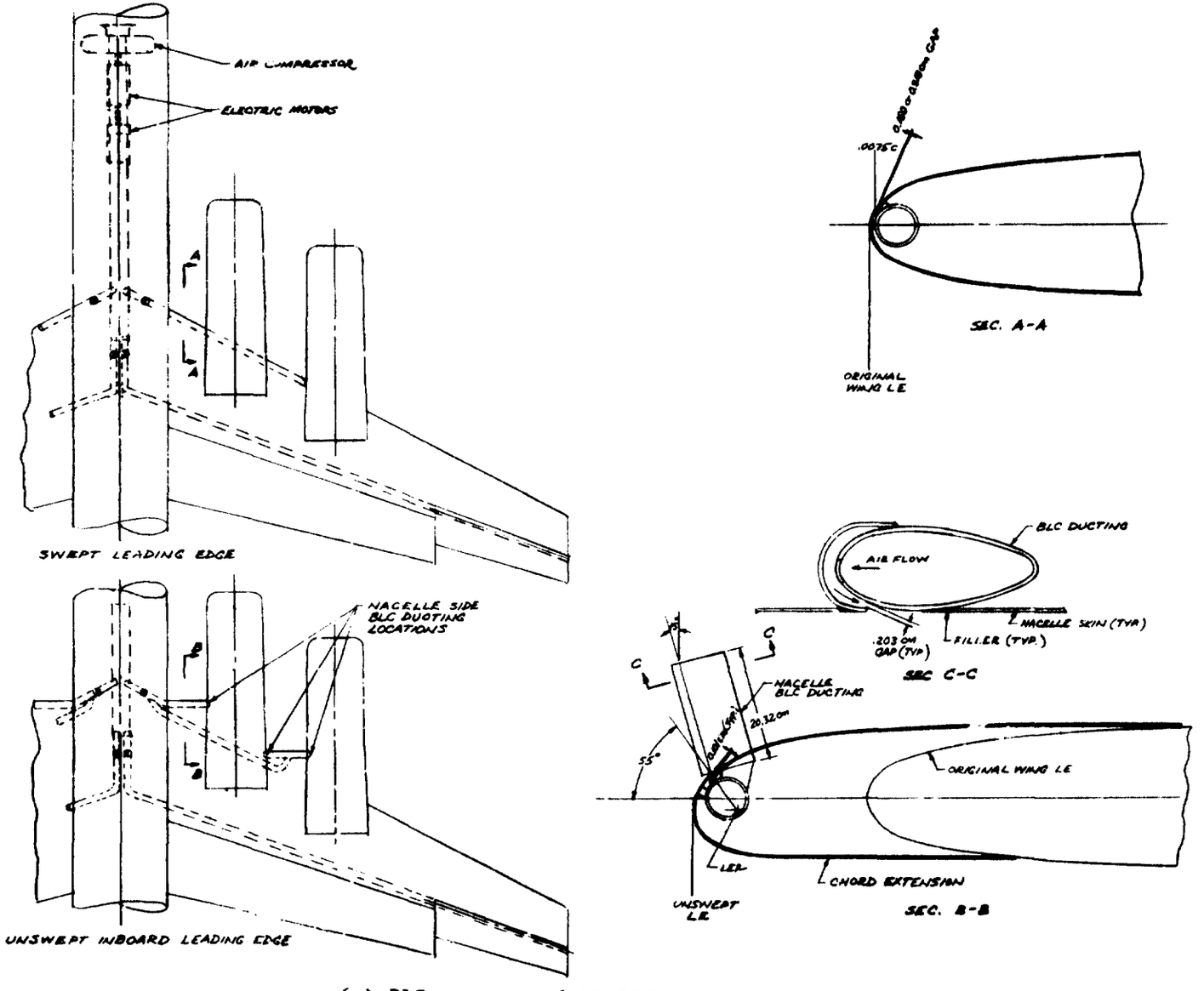


(e) BLC system and LE BLC nozzle arrangement.

Figure 2.- Continued.

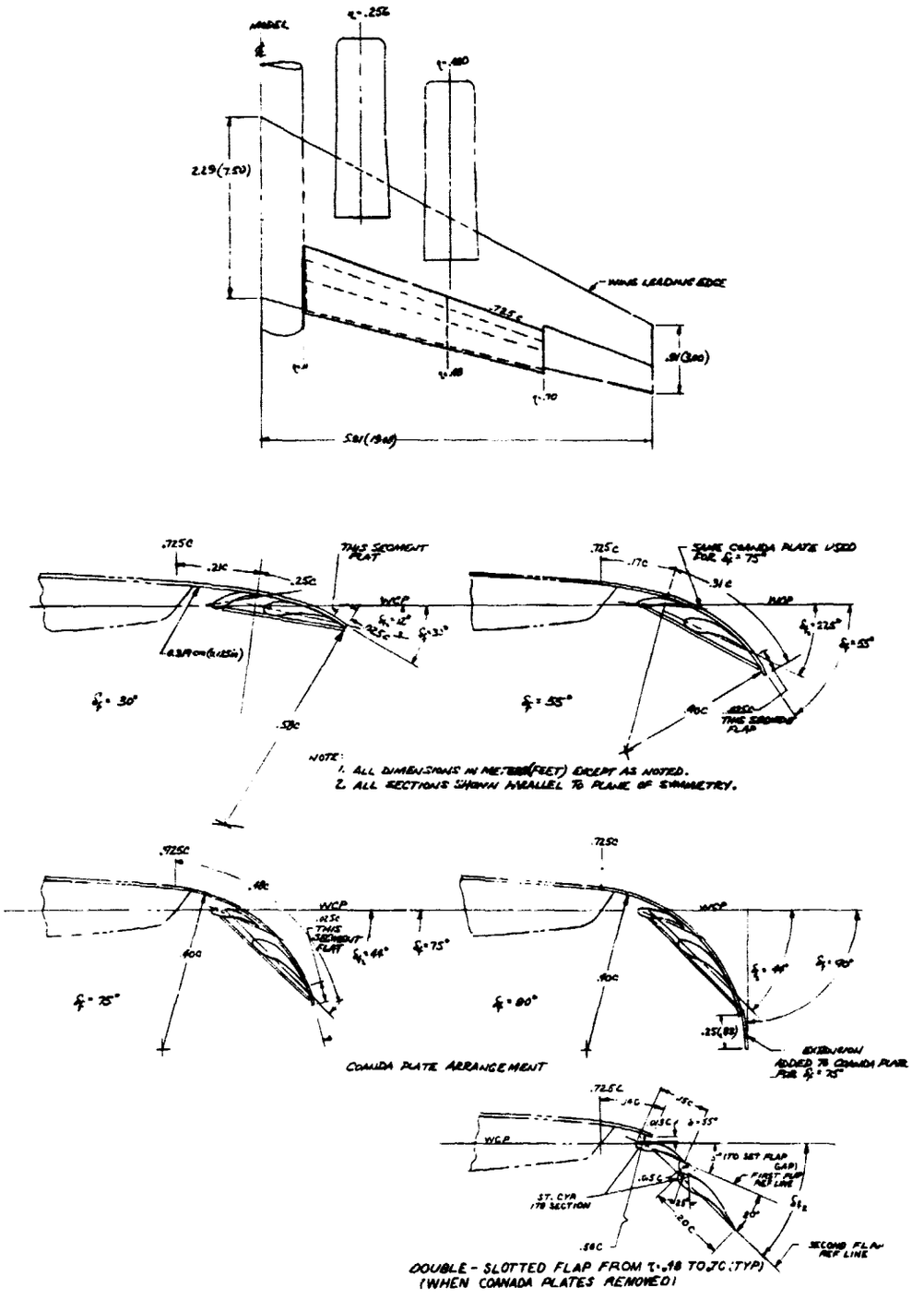


(f) Trailing-edge flap arrangement.

Figure 2.- Continued.

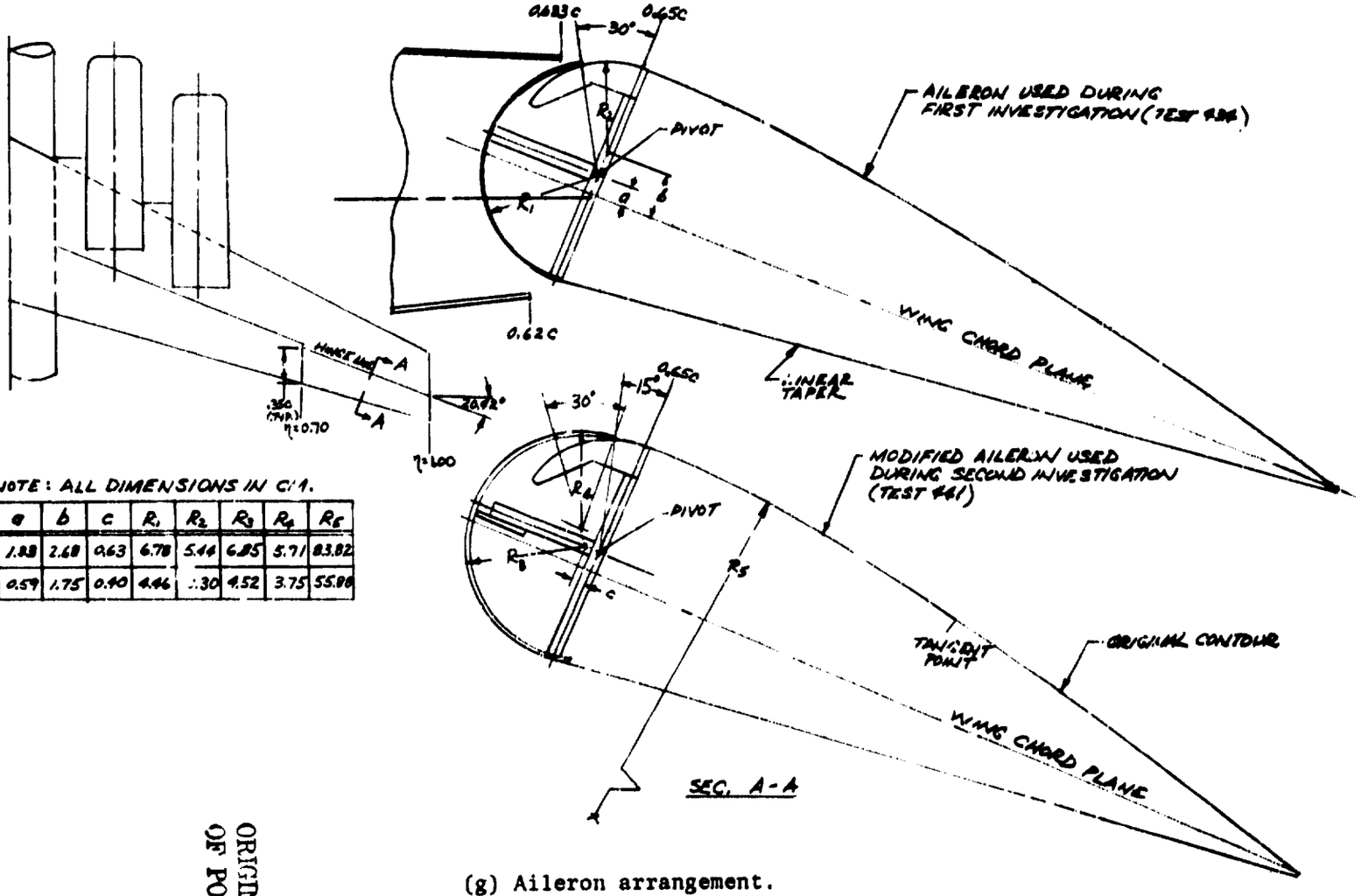


NOTE: ALL DIMENSIONS IN c/4.

| η | a | b | c | $R_1$ | $R_2$ | $R_3$ | $R_4$ | $R_5$ |
|---|---|---|---|---|---|---|---|---|
| .70 | 1.88 | 2.68 | 0.63 | 6.78 | 5.44 | 6.85 | 5.71 | 83.82 |
| 1.00 | 0.59 | 1.75 | 0.40 | 4.46 | .30 | 4.52 | 3.75 | 55.98 |

(g) Aileron arrangement.

Figure 2.- Continued

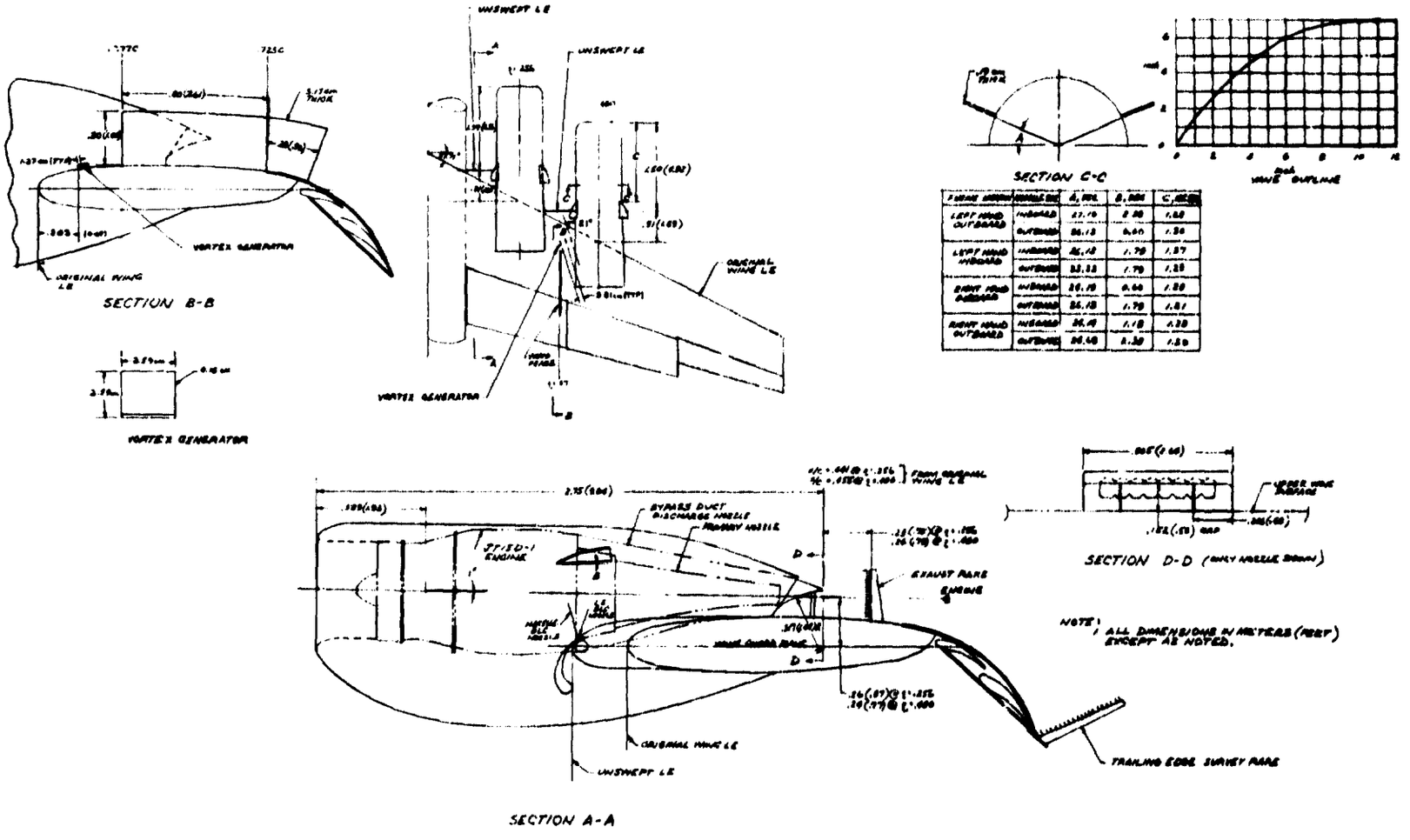


(h) Upper surface blowing flap and nozzle arrangement.

Figure 2 - Continued.

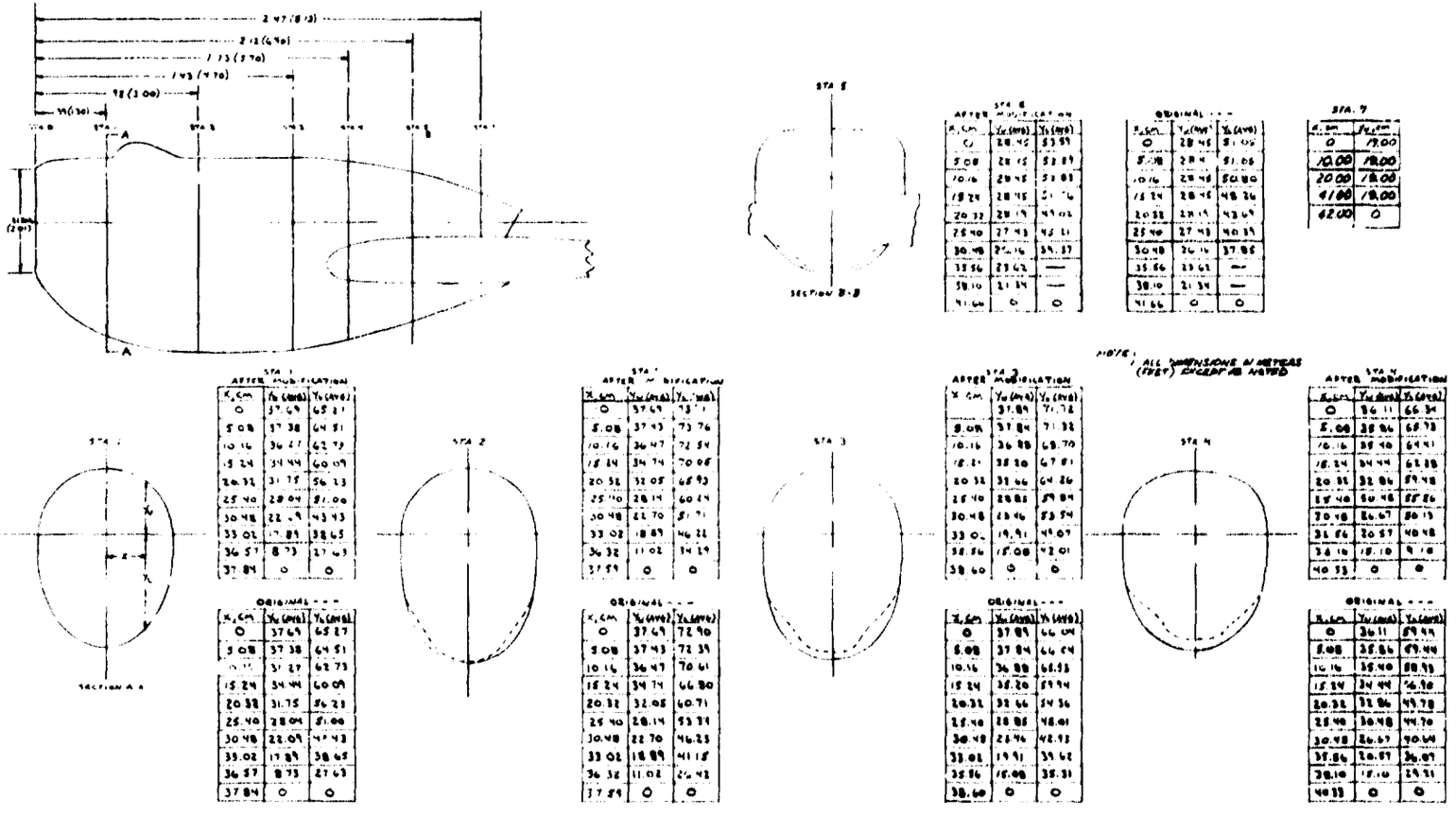

(i) Nacelle contour.

Figure 2.- Continued.

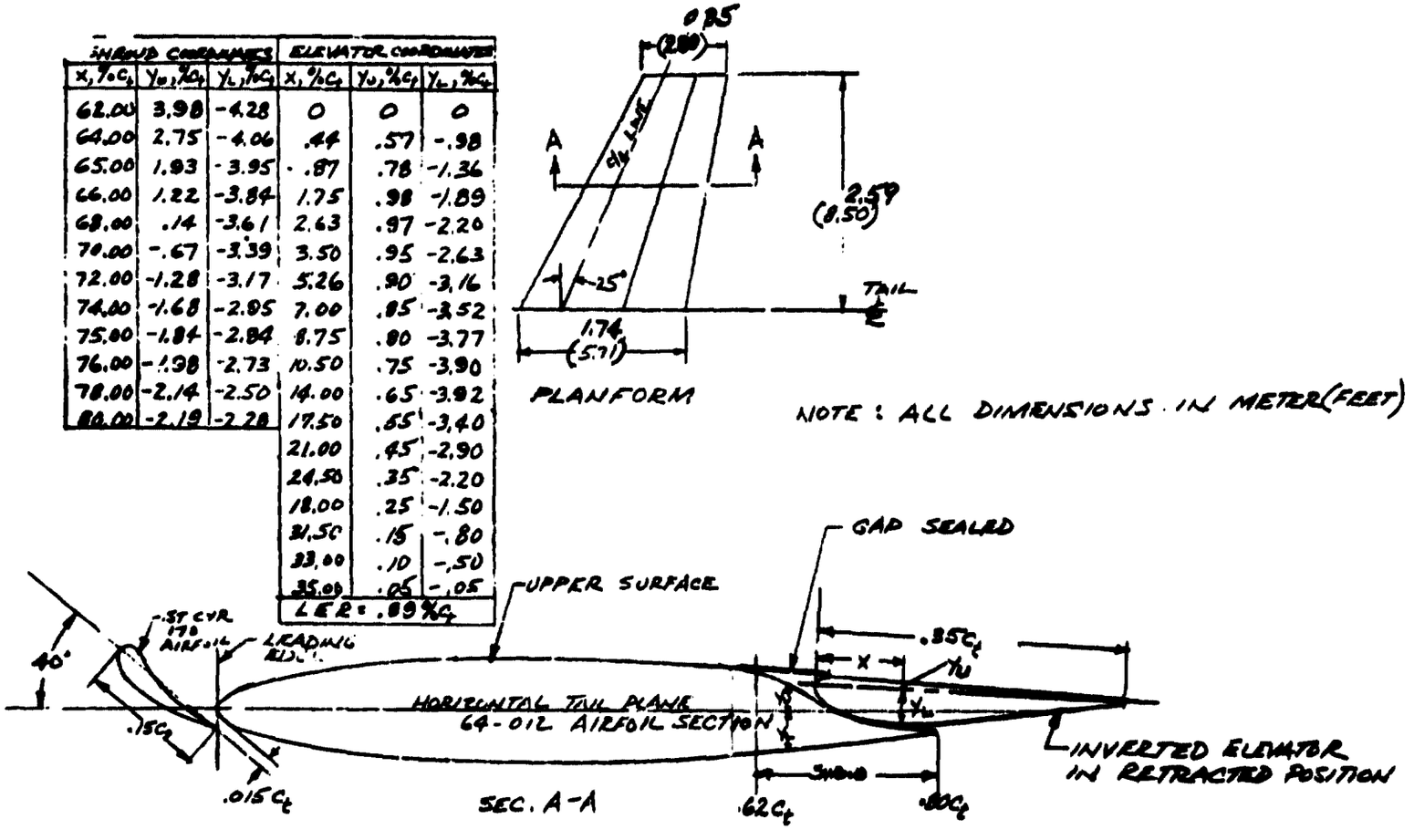


(j) Horizontal tail detail.

Figure 2.- Concluded.

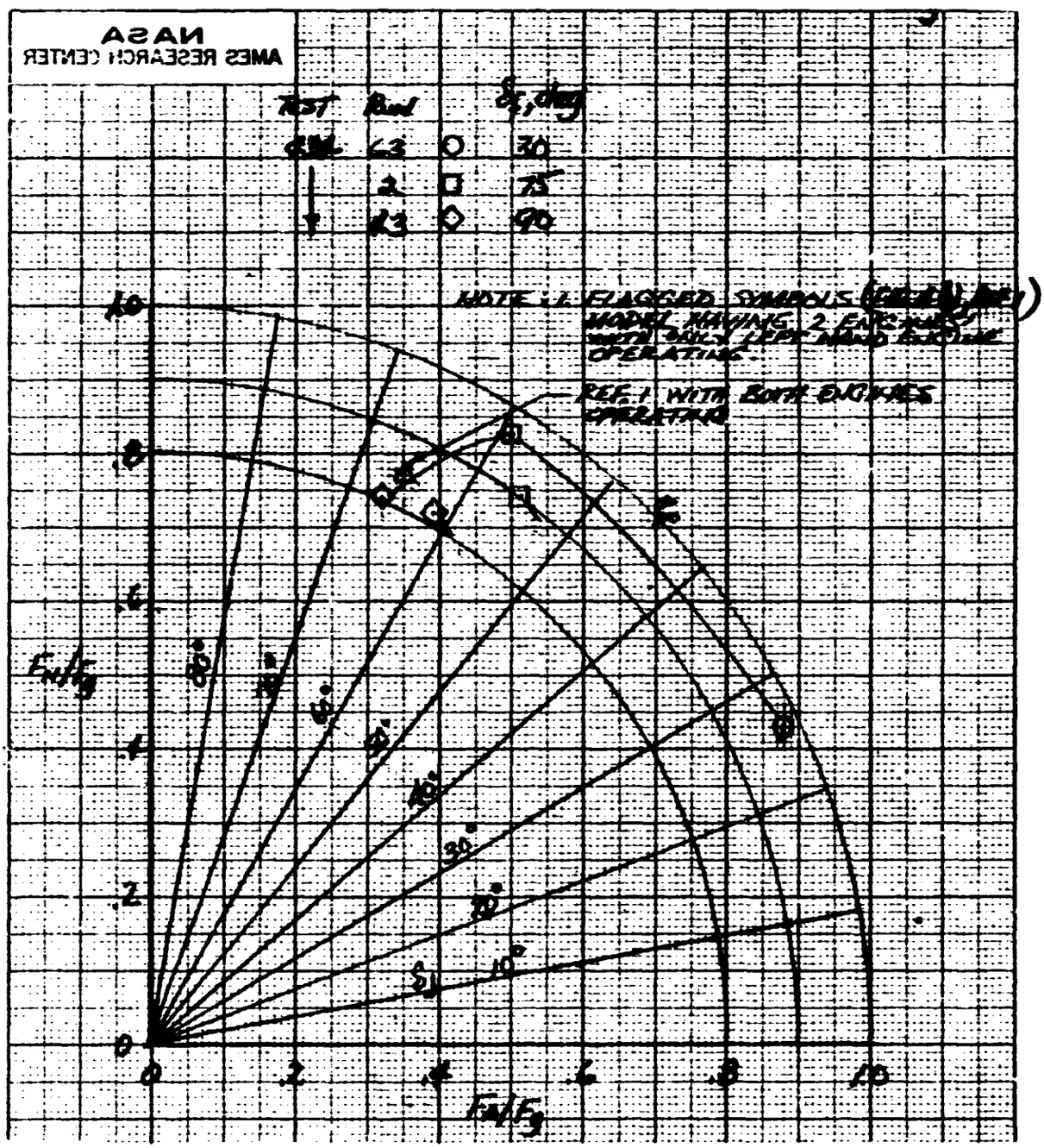


Figure 3.- Flap static turning efficiency and turning angle.

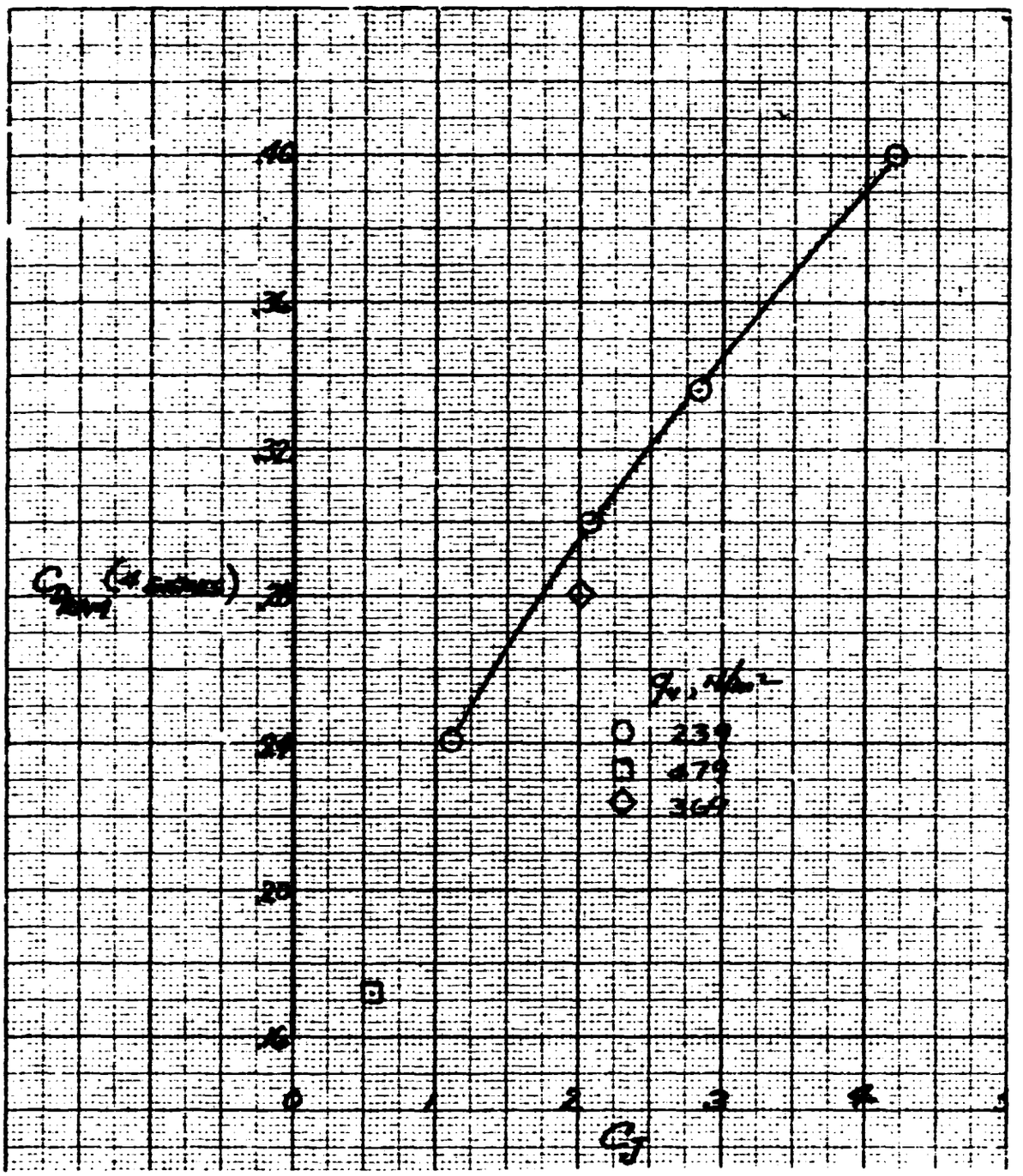


Figure 4.- Variation of $C_{D_{ram}}$ with $C_J$.

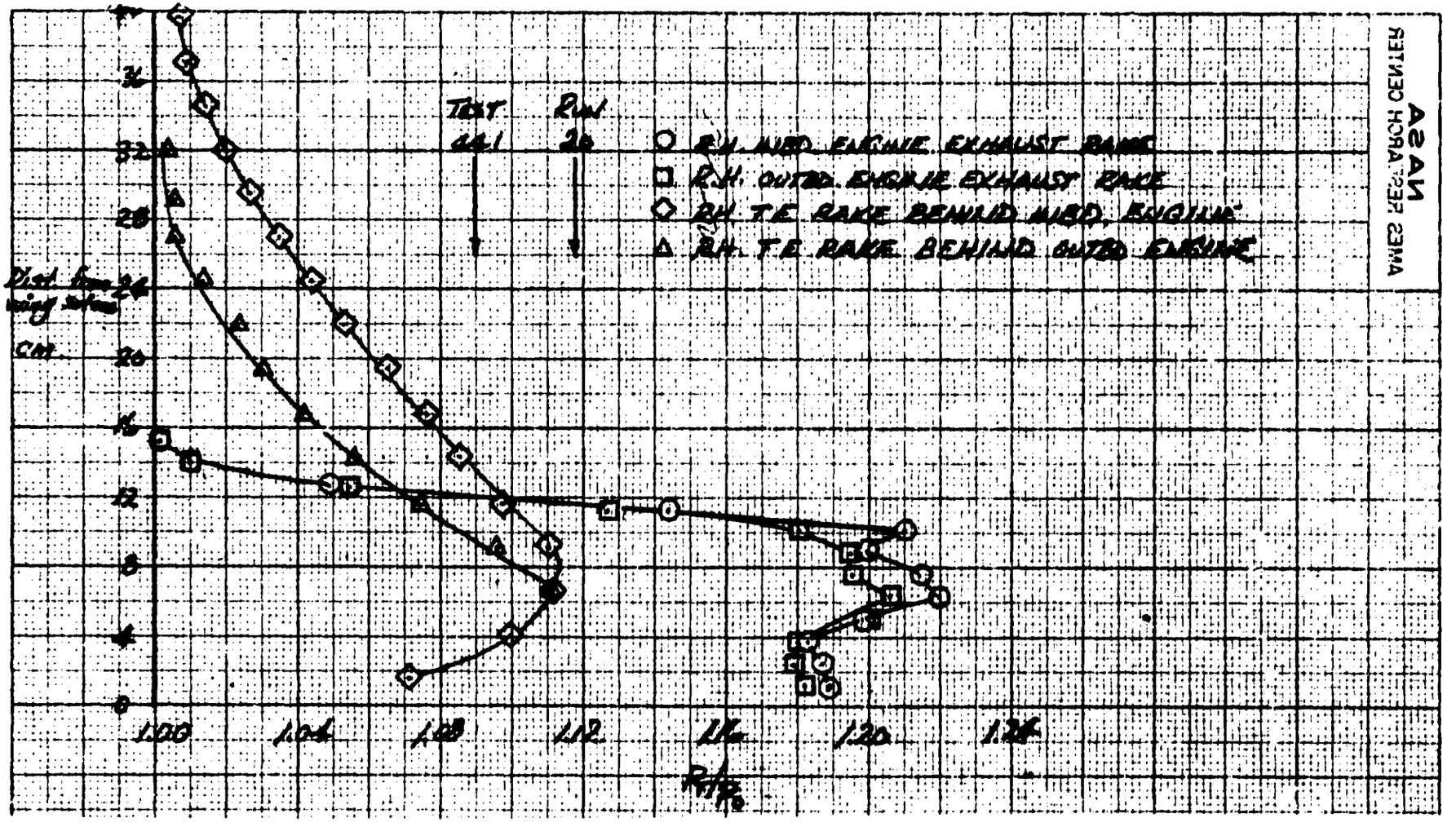


Figure 5.- Engine exhaust pressure ratio behind the engine nozzle and the flap trailing edge; $\delta_f = 90°$, $C_J = 3.97$, $\alpha_u = 0°$, $q_u = 239$ N/m$^2$.

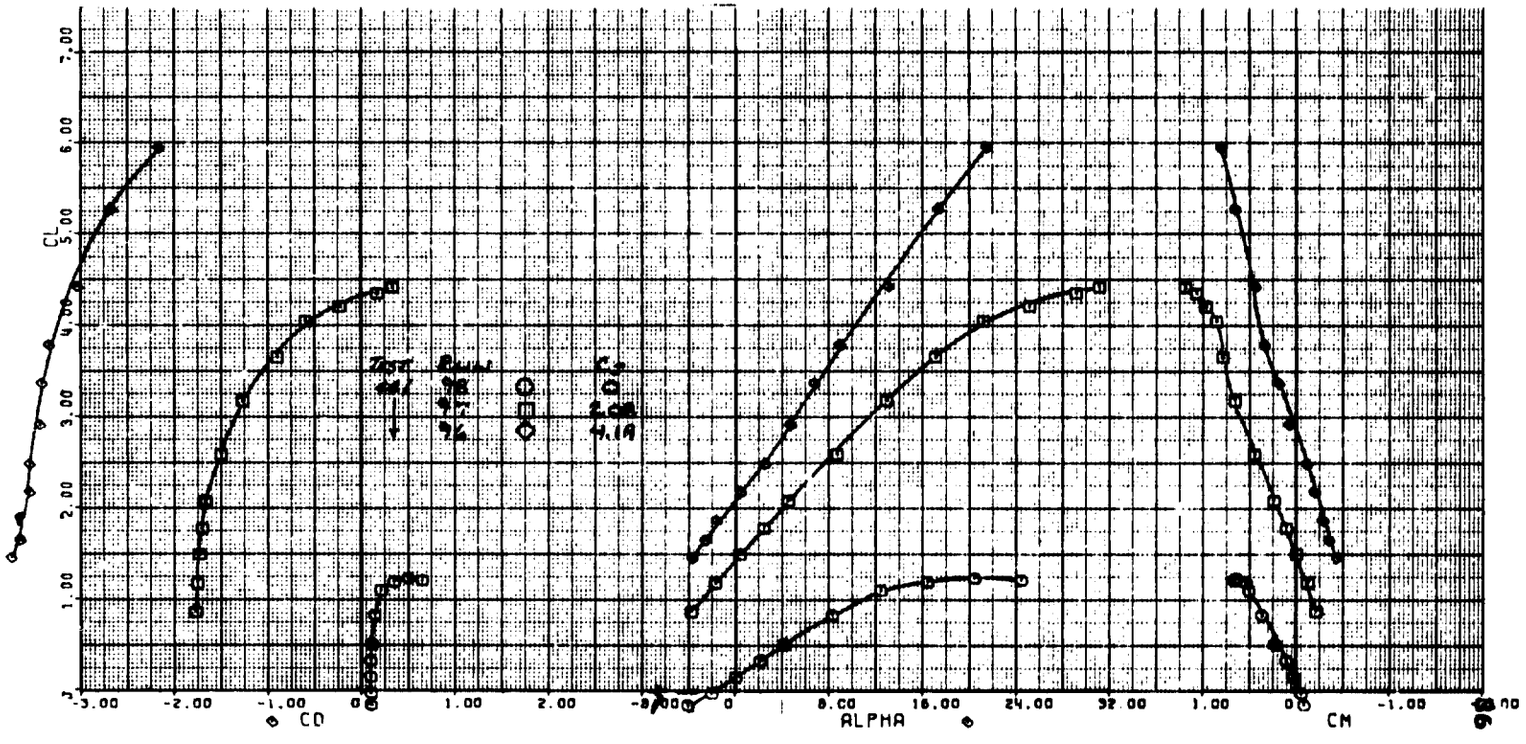


Figure 6.- Longitudinal characteristics of the model with unswept inboard LE: $\delta_f$ = 0°, $\delta_{ail}$ = 0°, wing fence off, nacelle vane on, plain LE, tail off.

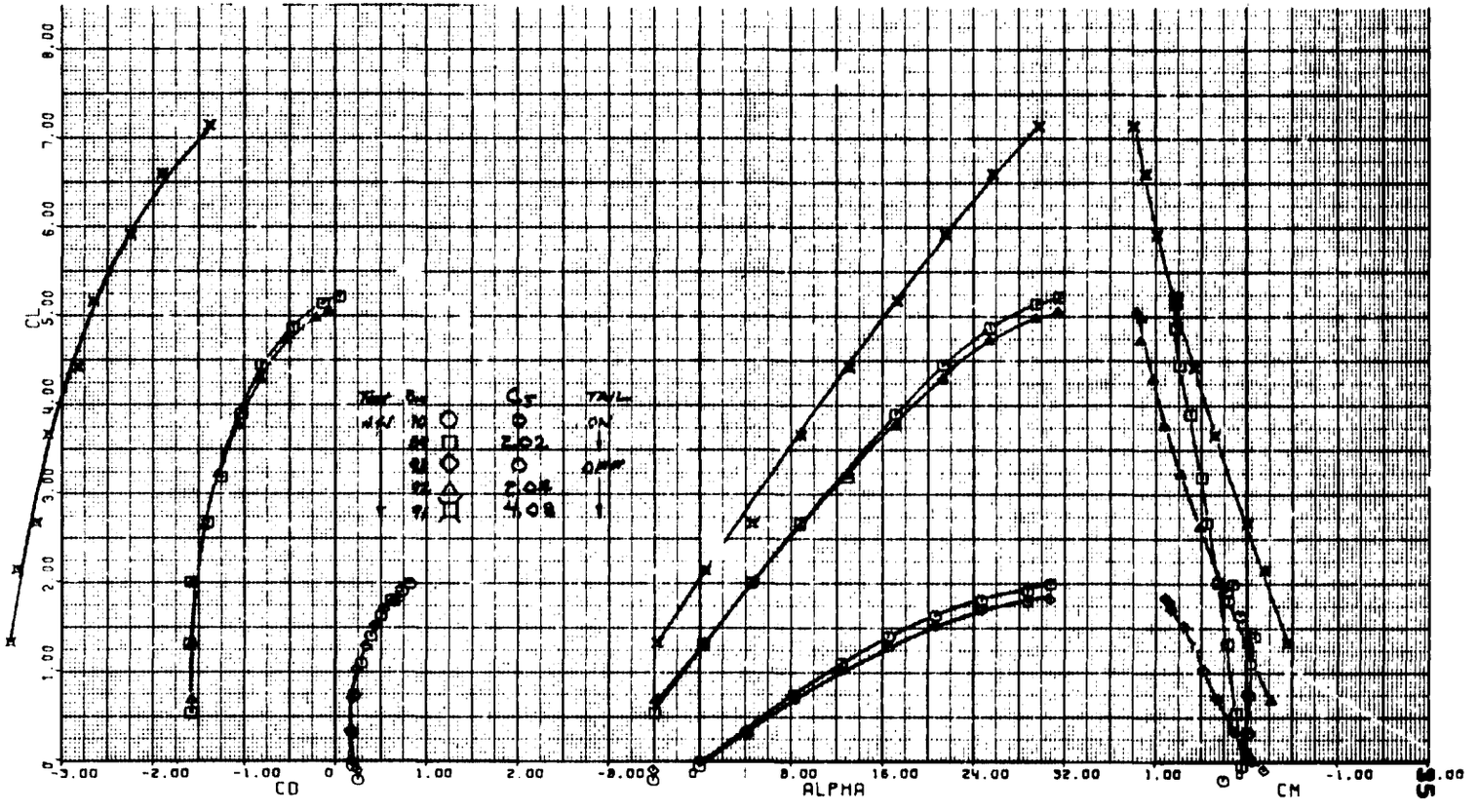


Figure 7.- Longitudinal characteristics of the model with unswept inboard LE; $\delta_f = 0°$, $\delta_{ail} = 0°$, wing fence off, nacelle vane off, LE configuration 6.

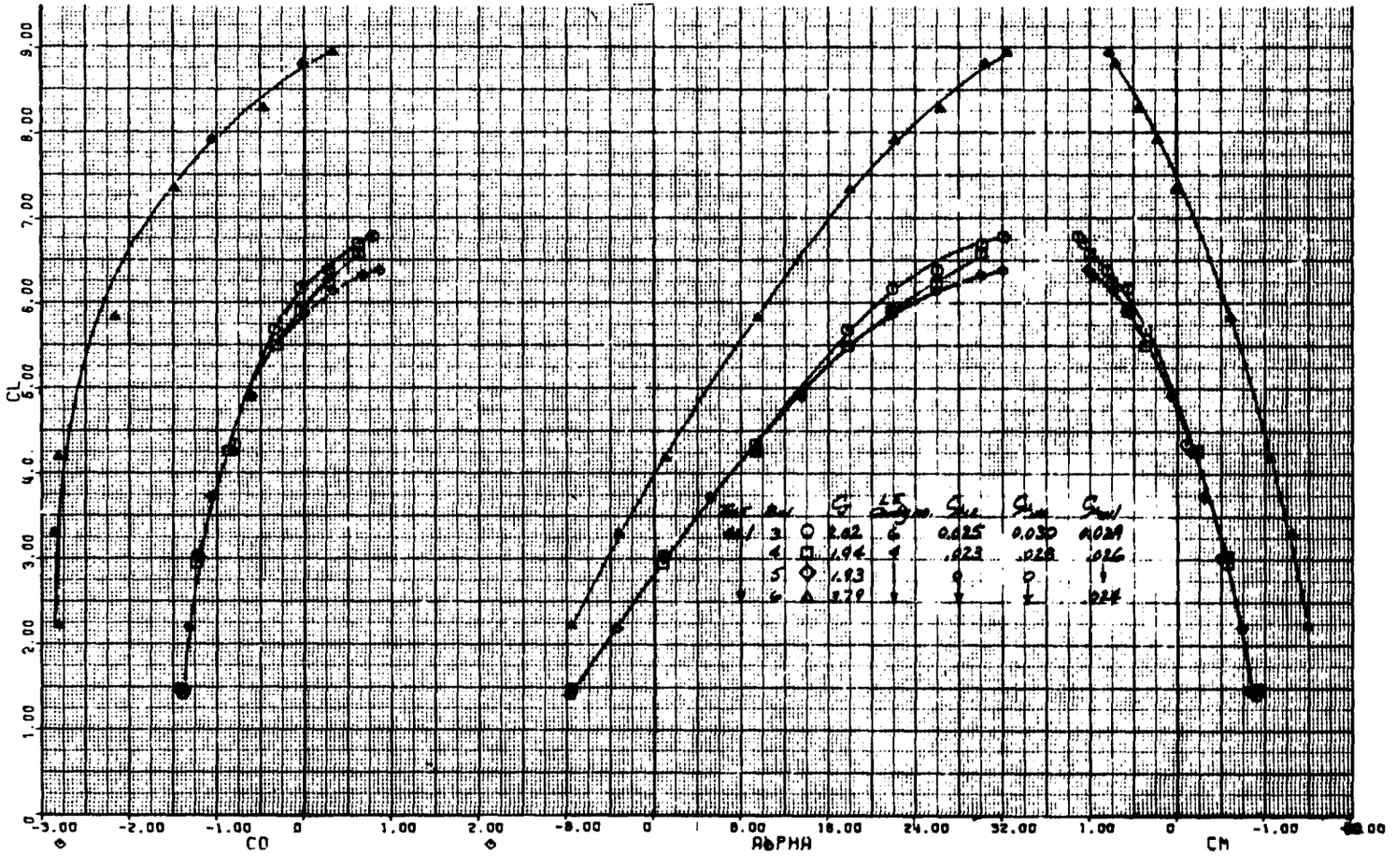


Figure 8.- Longitudinal characteristics of the model with unswept inboard LE; $\delta_f$ = 30°, $\delta_{ail}$ = 23°, wing fence on, nacelle vane on, tail off.

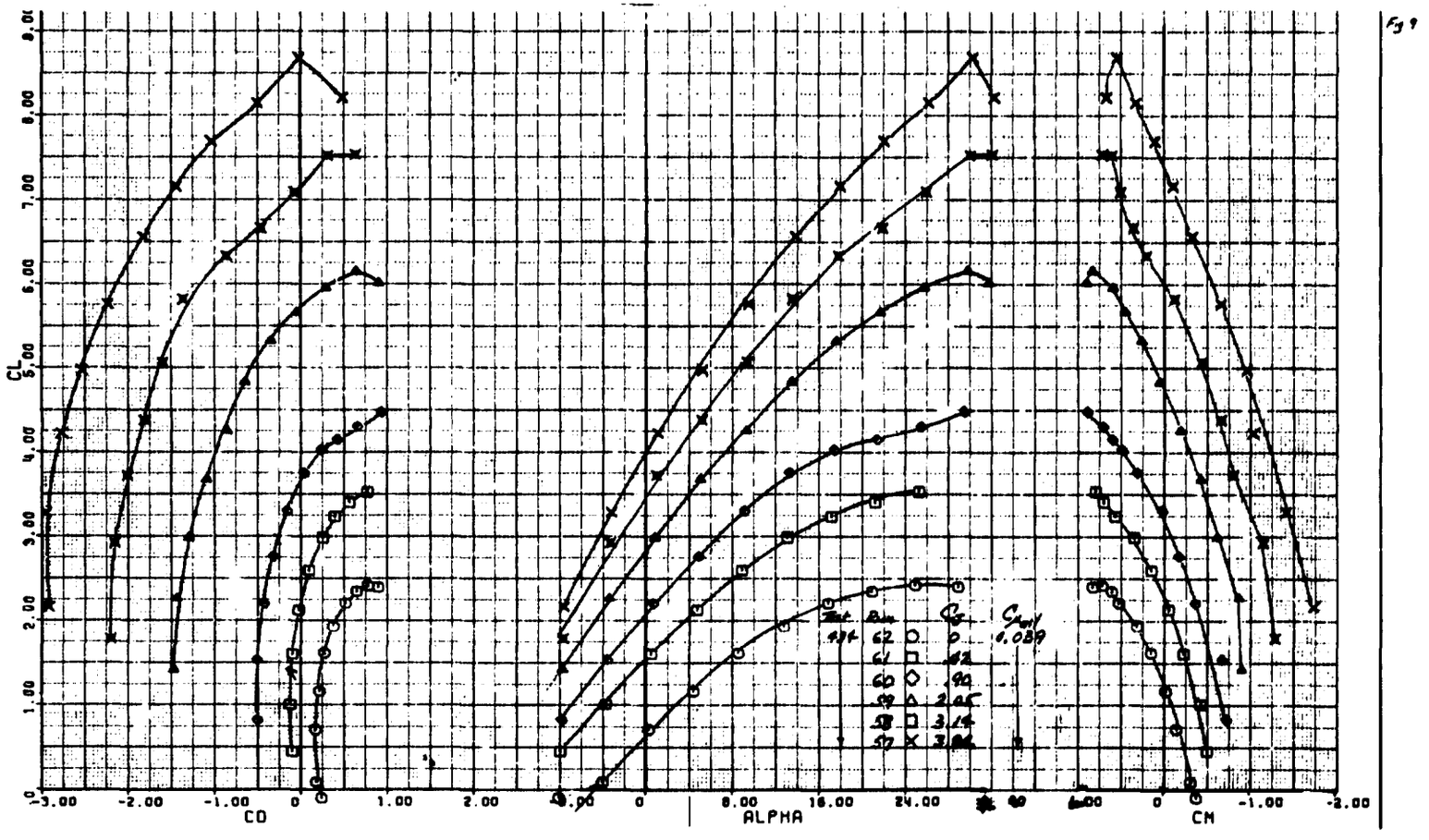


Figure 9.- Longitudinal characteristics of the model with unswept inboard LE; $\delta_f$ = 30°, $\delta_{ail}$ = 23°, $C_{\mu_{LE}}$ = 0, $C_{\mu_{NAC}}$ = 0, wing fence on, nacelle vane on, LE configuration 3, tail off.

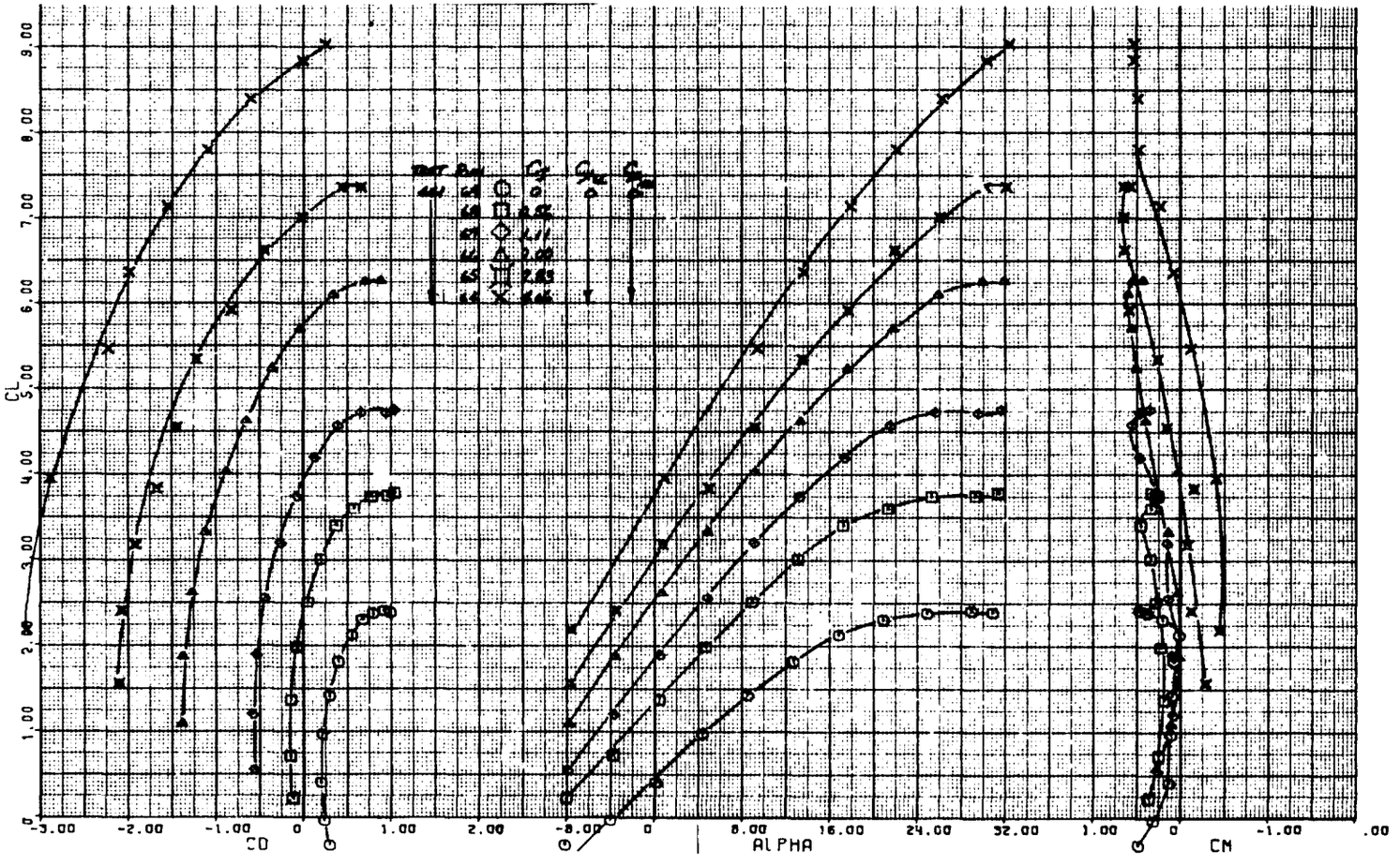


Figure 10.- Longitudinal characteristics of the model with unswept inboard LE; $\delta_f$ = 30°, $\delta_{ail}$ = 0°, $C_{\mu_{ail}}$ = 0, wing fence off, nacelle vane off, LE configuration 6, tail on.

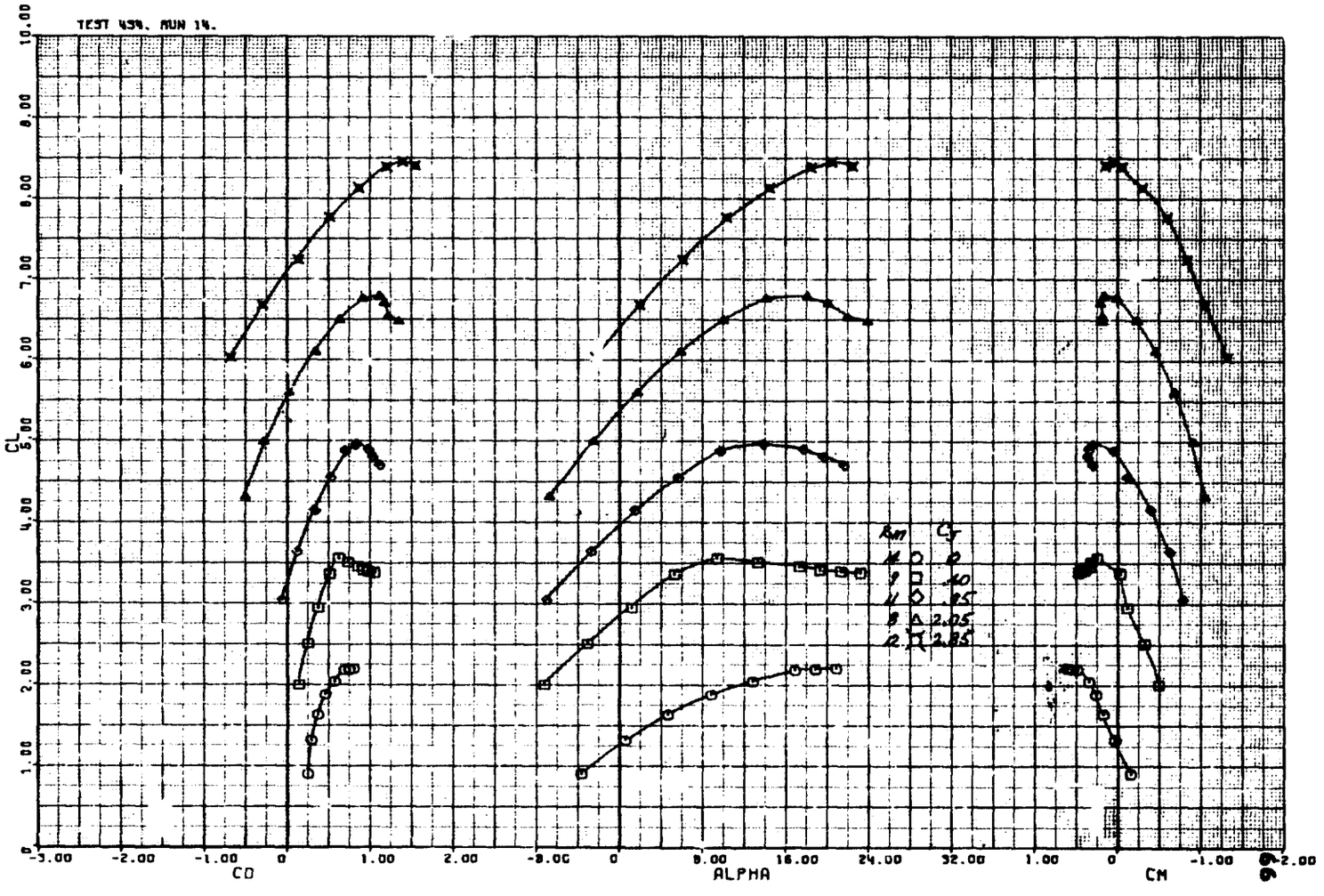


Figure 11.- Longitudinal characteristics of the model with swept inboard LE without LE BLC; $\delta_f$ = 75°, $\delta_{ail}$ = 10°, $C_{\mu_{ail}}$ = 0, wing fence off, nacelle vane off, LE configuration 1, tail off.

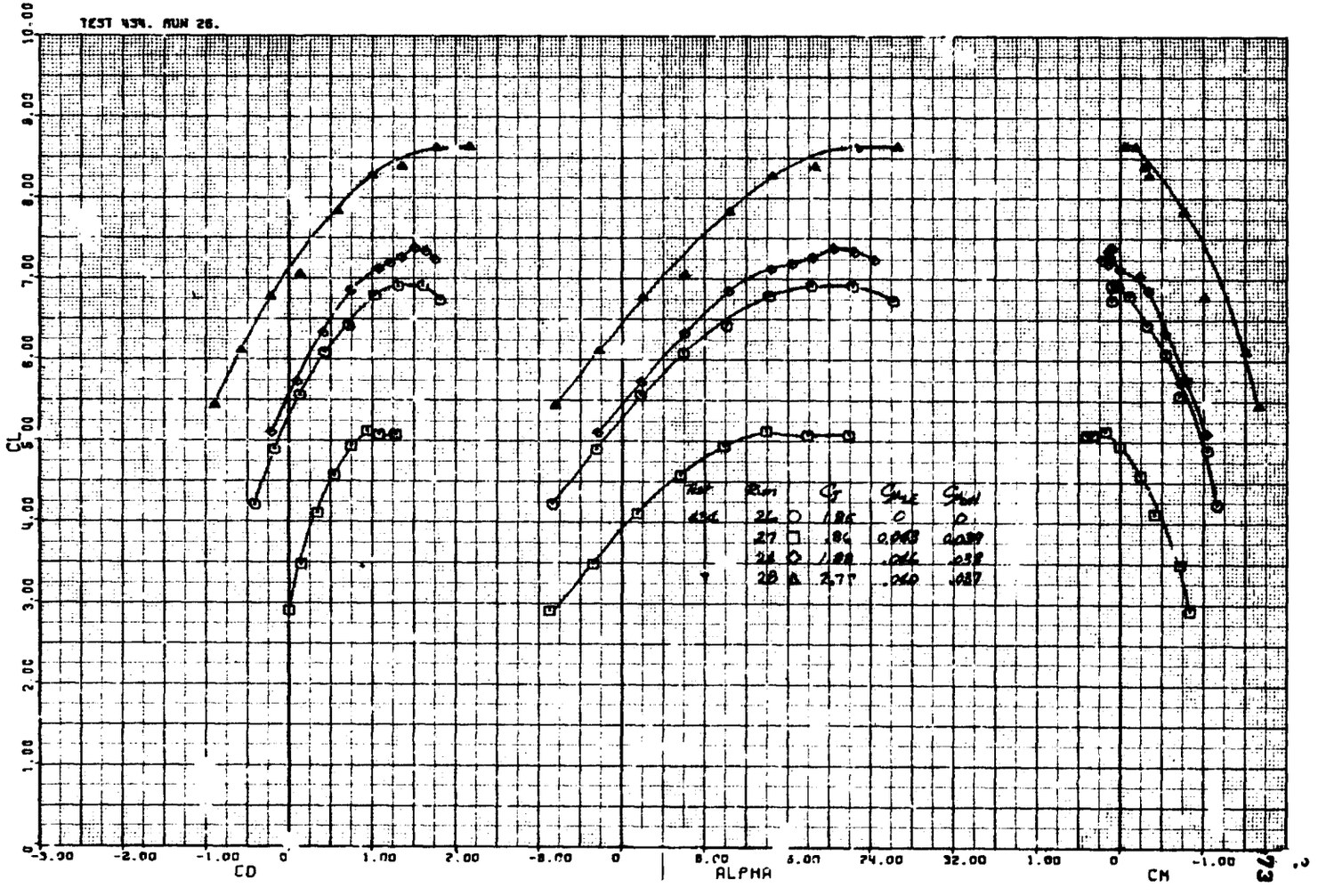


Figure 12.- Longitudinal characteristics of the model with BLC on the swept inboard LE; $\delta_f = 75°$, $\delta_{ail} = 23°$, wing fence on, LE configuration 2, tail off.

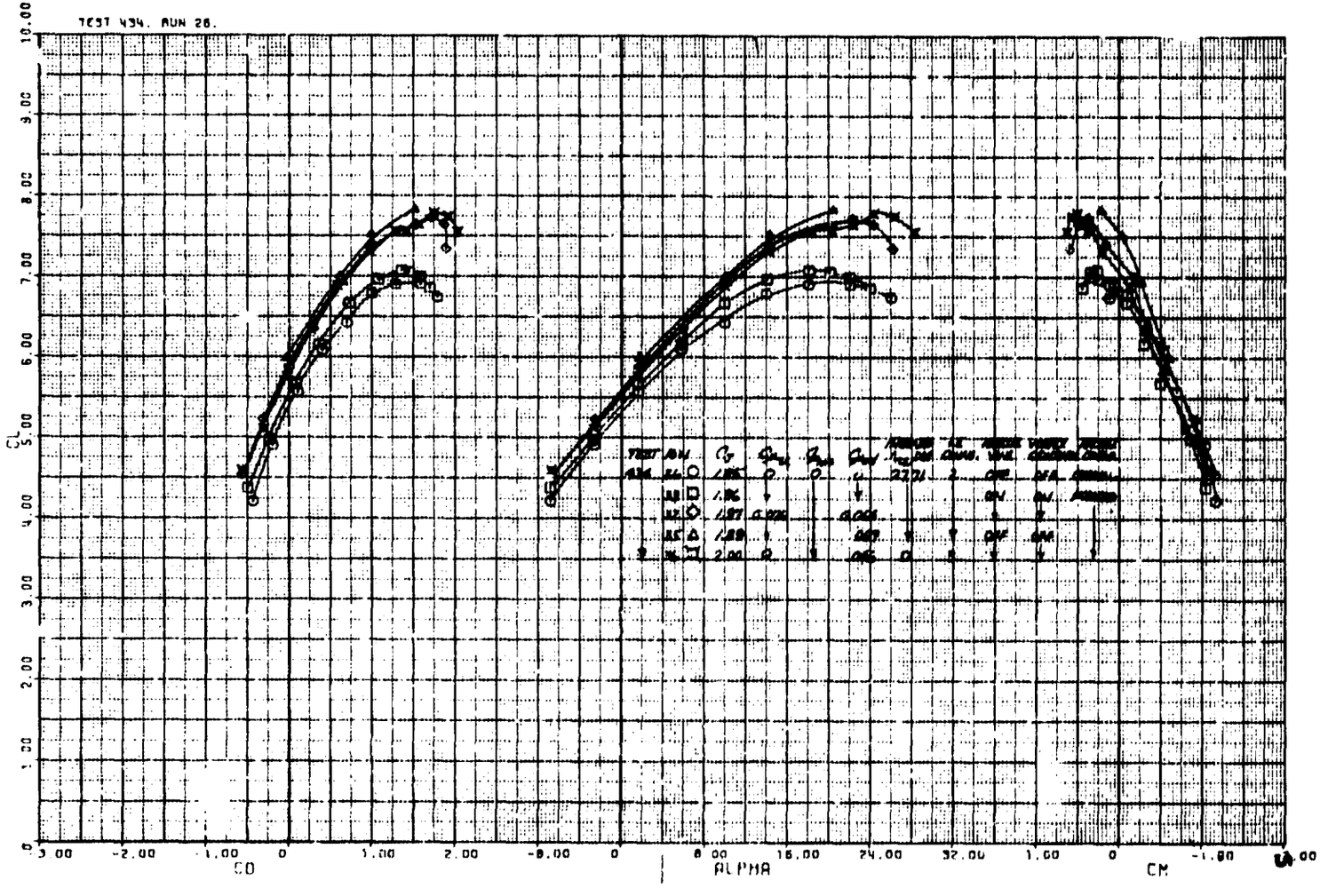


Figure 13.- Effect of LE treatment on the longitudinal characteristics of the model; $\delta_f$ = 75°, $\delta_{ail}$ = 23°, wing fence on, tail off.

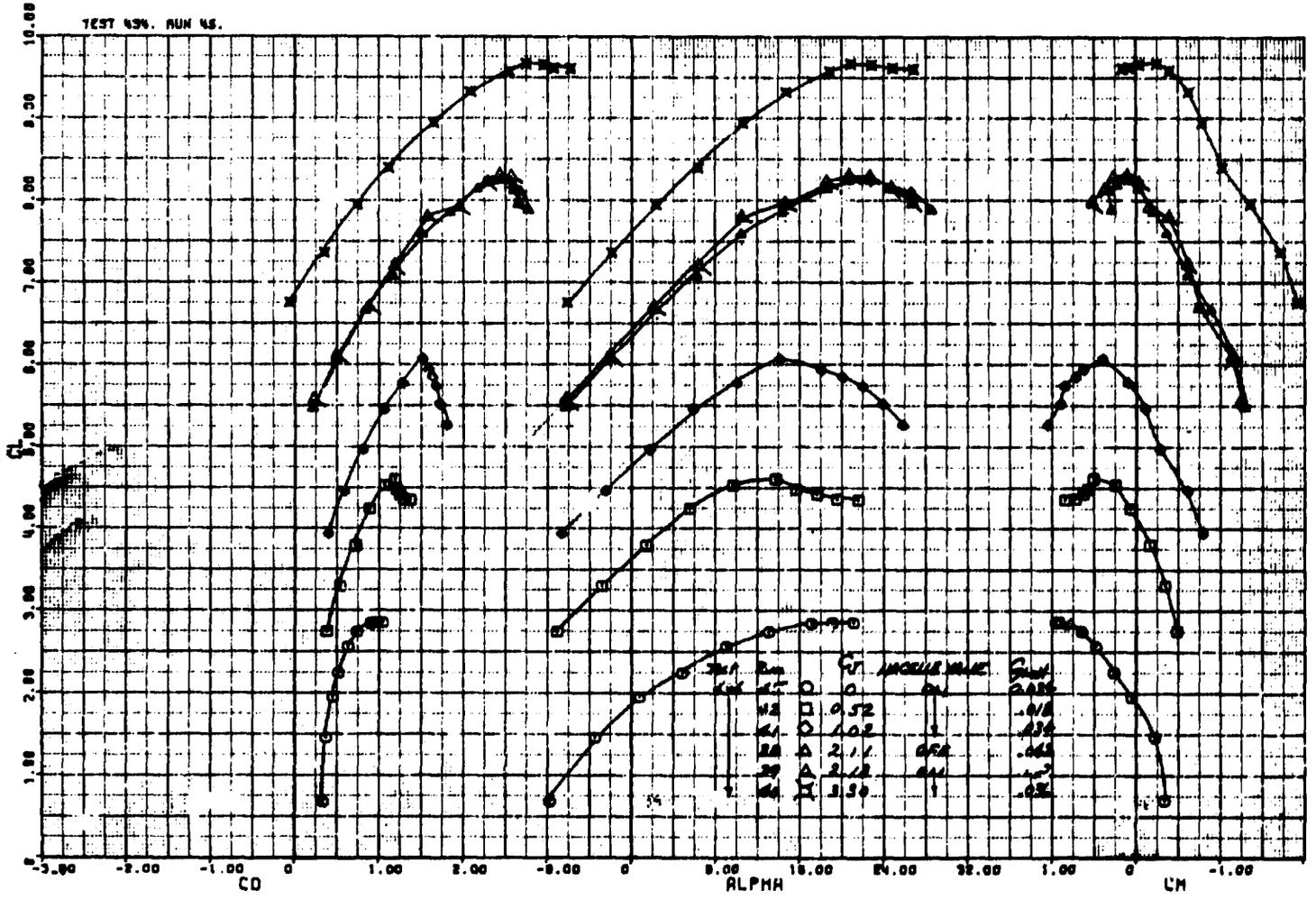


Figure 14.- Longitudinal characteristics of the model with unswept inboard LE; $\delta_f$ = 90 , $\delta_{ail}$ = 23°, $C_{\mu_{LE}}$ = 0, $C_{\mu_{NAC}}$ = 0, wing fence on, LE confirugration 3, tail off.

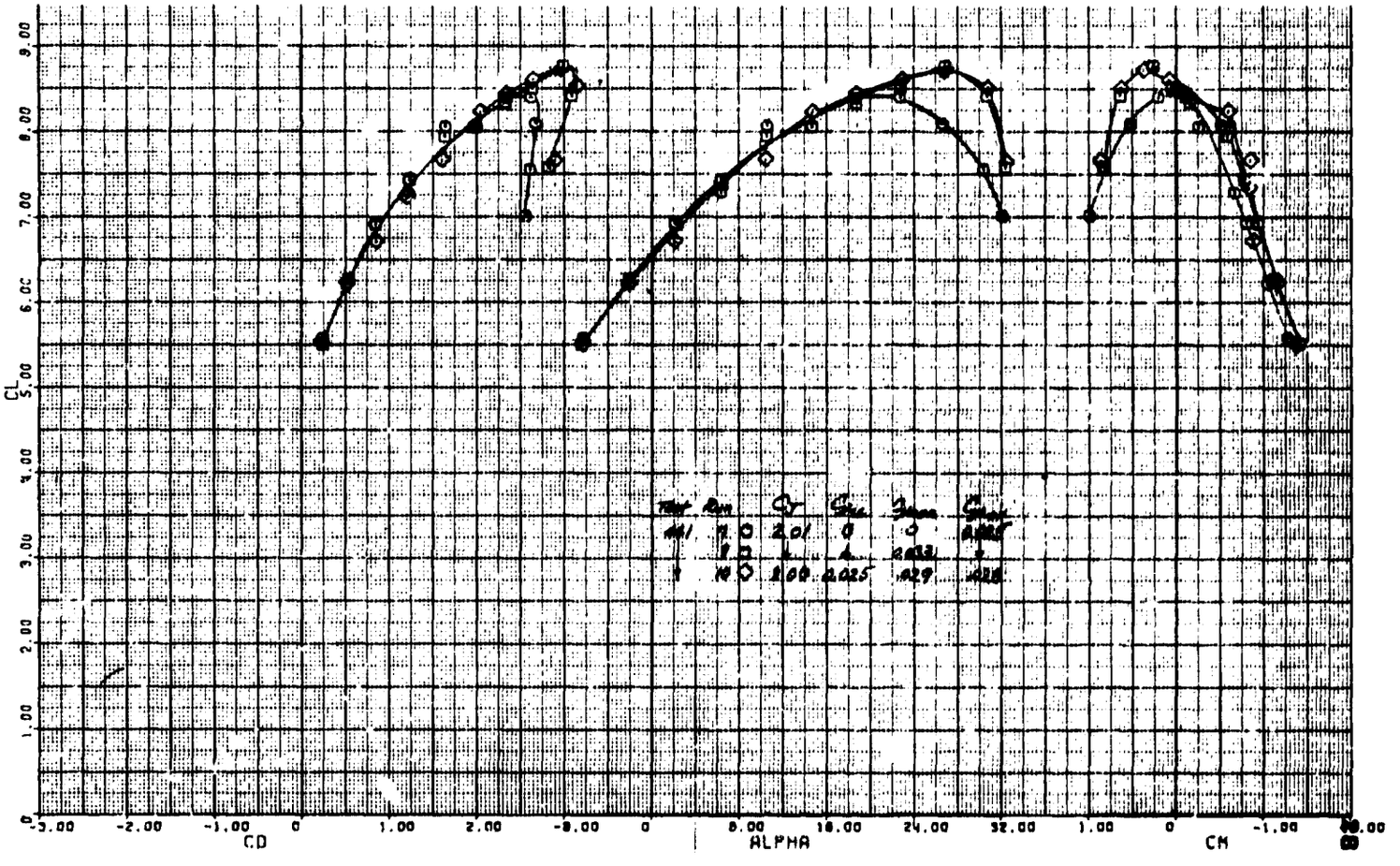


Figure 15.- Effect of LE BLC on the longitudinal characteristics of the model with unswept inboard LE; $\delta_f$ = 90°, $\delta_{ail}$ = 23°, wing fence on, nacelle vane on, LE configuration 4, tail off.

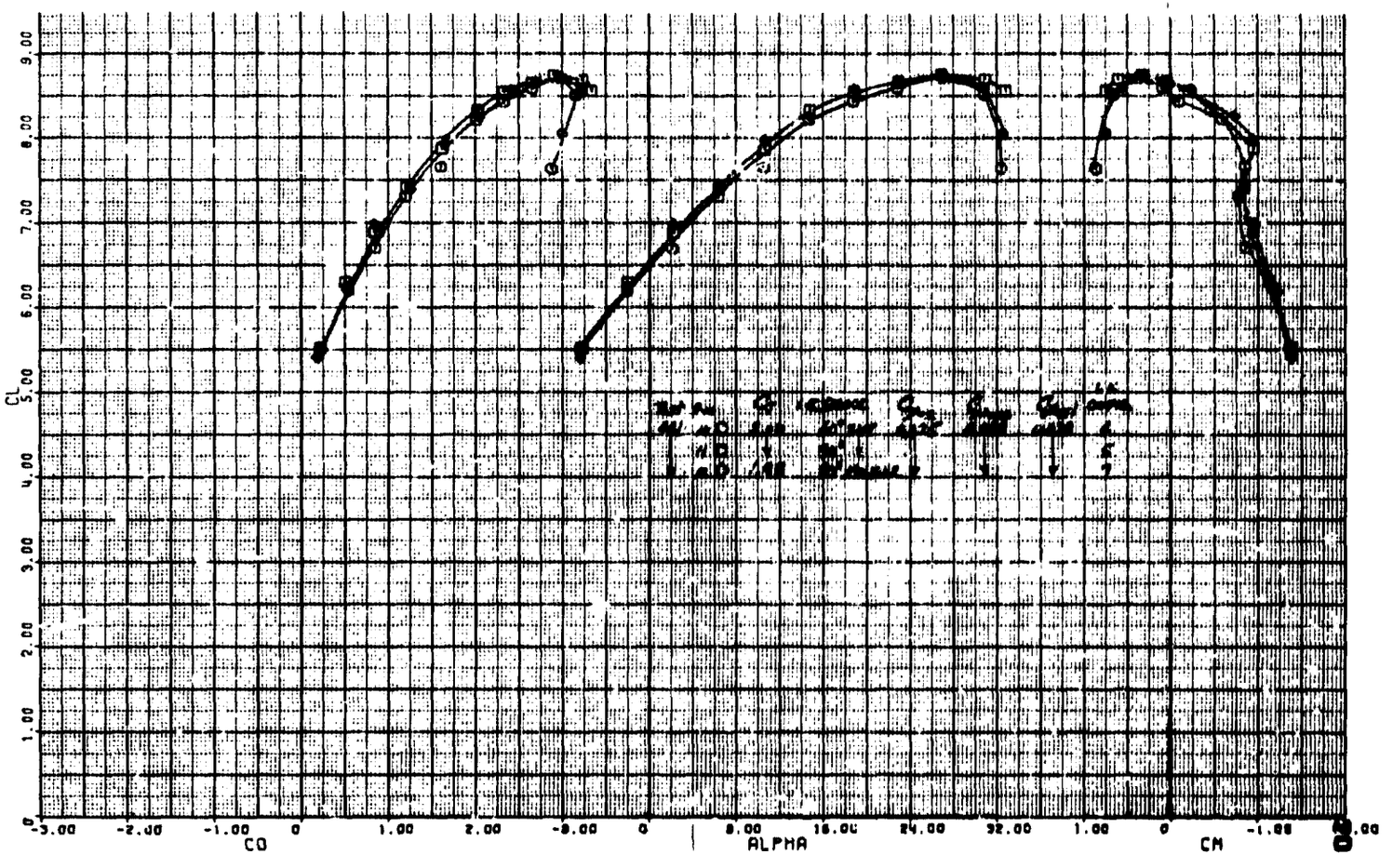


Figure 16.- Effect of LE devices on the longitudinal characteristics of the model with unswept inboard LE; $\delta_f$ = 90°, $\delta_{ail}$ = 23°, wing fence on, nacelle vane on, tail off.

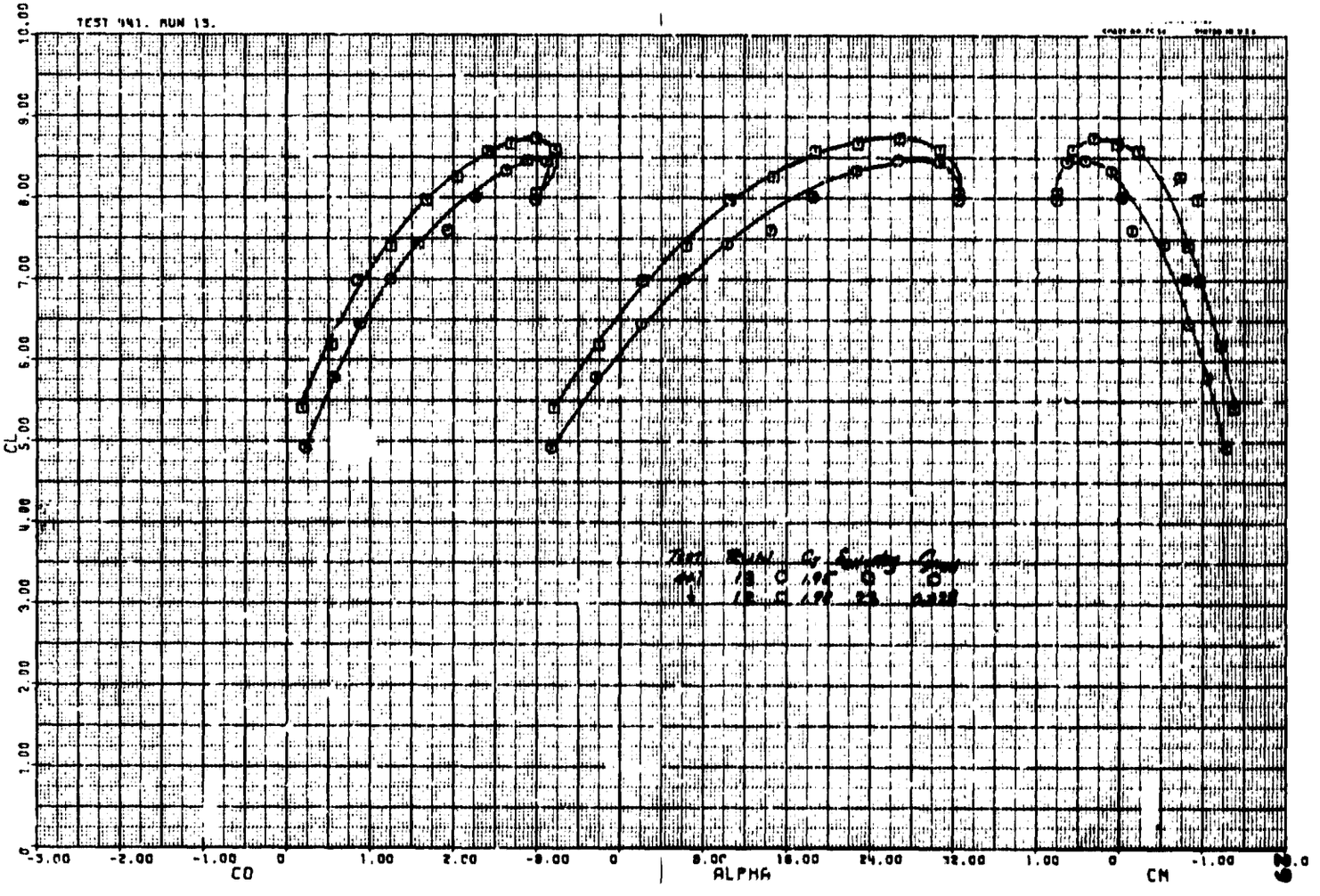


Figure 17.- Longitudinal characteristics of the model with the aileron deflected; $\delta_f$ = 90°, $C_{\mu_{LE}}$ = 0.025, $C_{\mu_{NAC}}$ = 0.029, wing fence on, nacelle vane on, LE configuration 7, tail off.

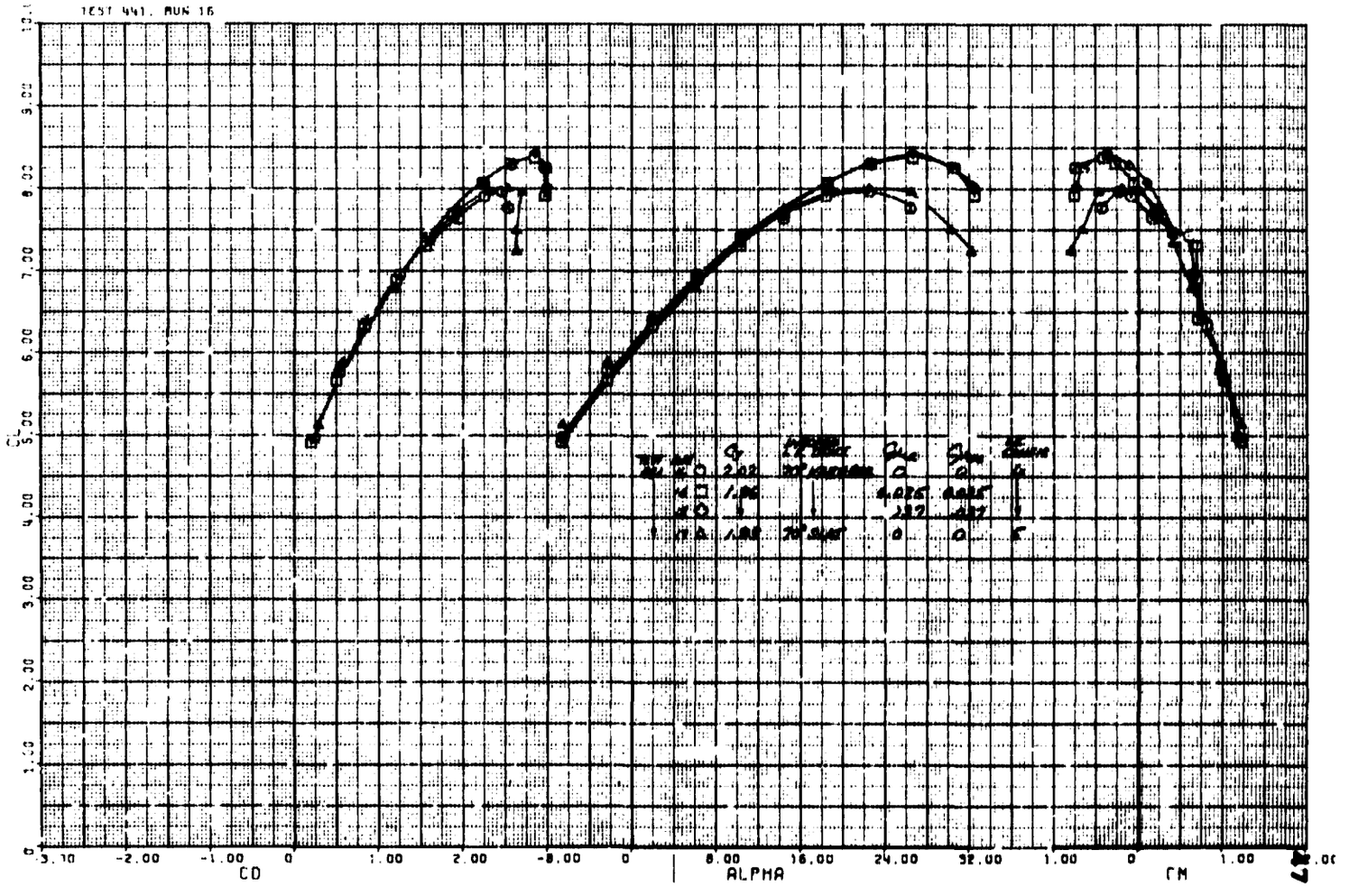


Figure 18.- Effect of LE BLC on the longitudinal characteristics of the model with the unswept inboard LE; $\delta_f$ = 90°, $\delta_{ail}$ = 0°, wing fence on, nacelle vane on, tail on.

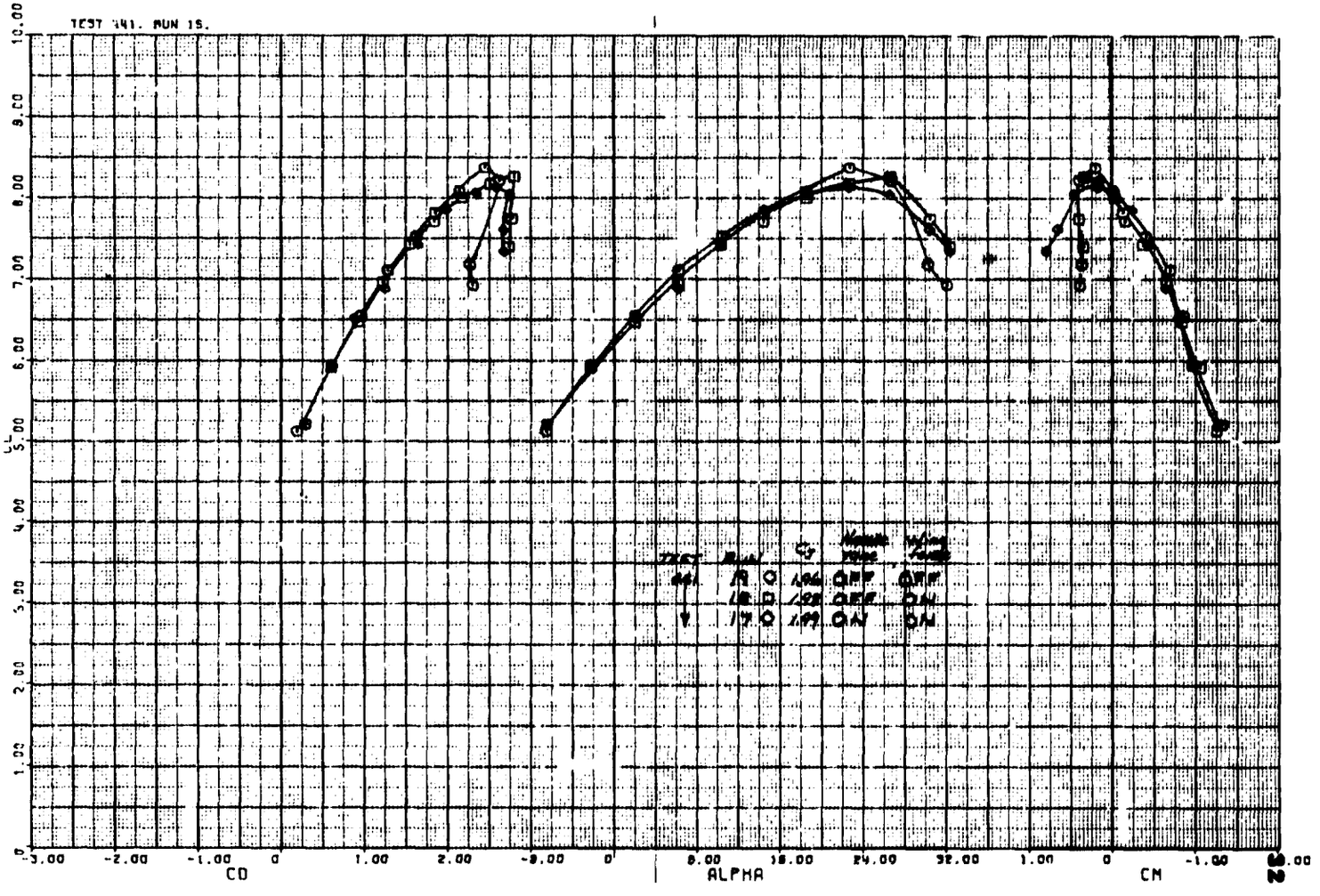


Figure 19.- Effect of wing fence and nacelle vane on the longitudinal characteristics of the model with unswept inboard LE; $\delta_f = 90°$, $\delta_{ail} = 0°$, $C_{\mu_{LE}} = 0$, $C_{\mu_{NAC}} = 0$, LE configuration 5, tail off.

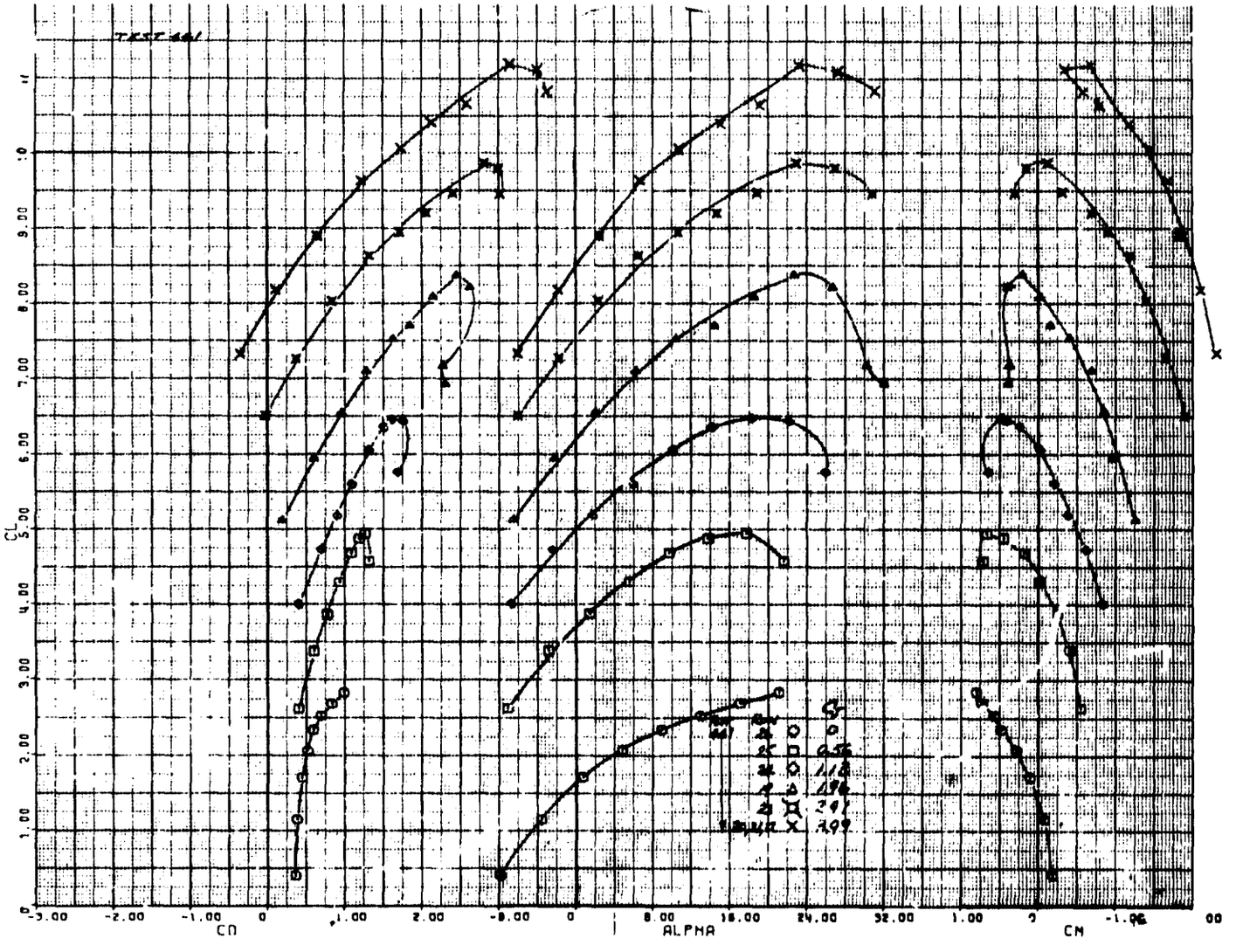


Figure 20.- Longitudinal characteristics of the model with unswept inboard LE; $\delta_f = 90°$, $\delta_{ail} = 0°$, $C_{\mu_{LE}} = 0$, $C_{\mu_{NAC}} = 0$, wing fence off, nacelle vane off, LE configuration 5, tail off.

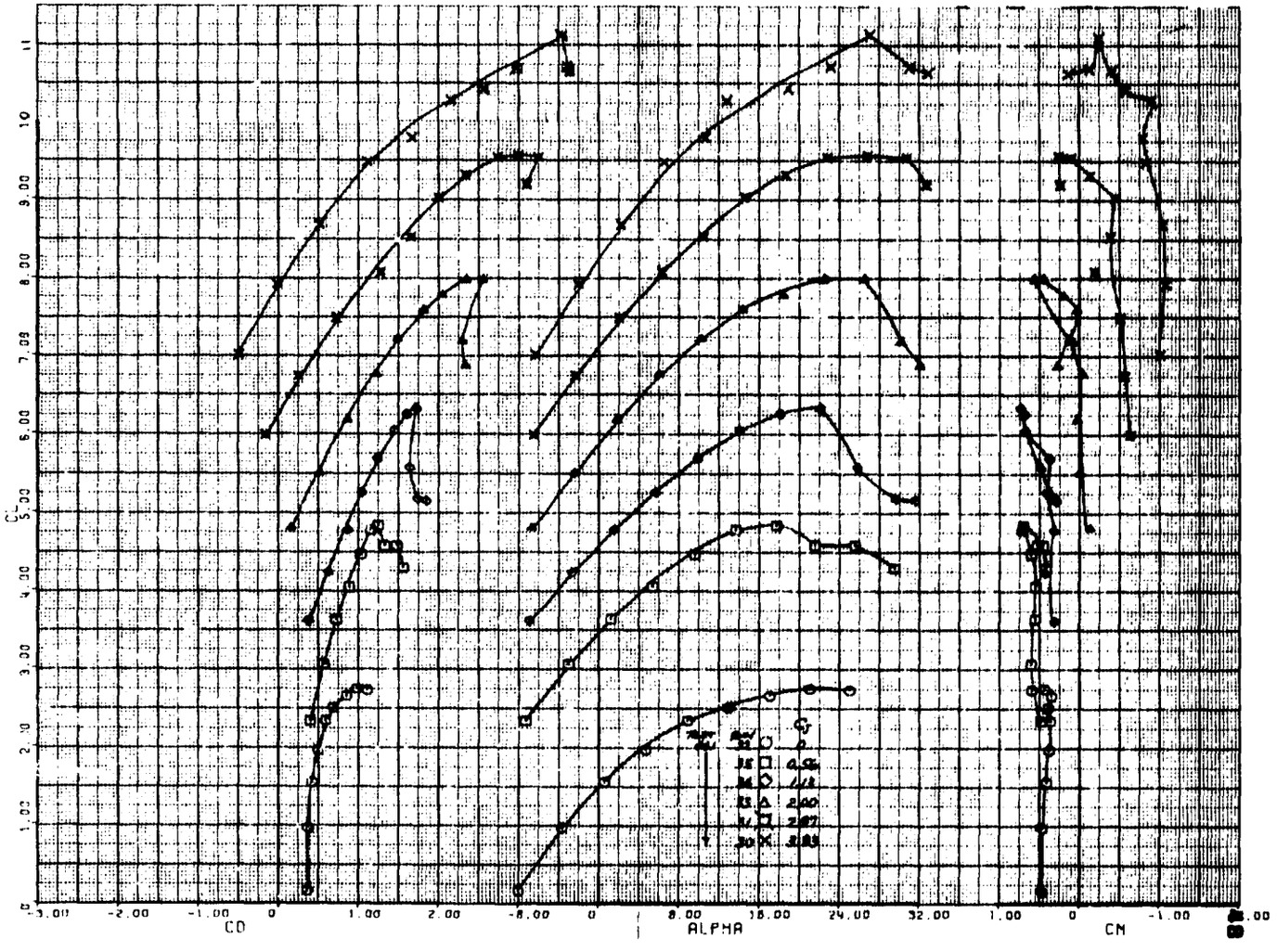


(a) LE BLC off.

Figure 21.- Longitudinal characteristics of the model with unswept inboard LE; $\delta_f$ = 90°, $\delta_{ail}$ = 0°, wing fence off, nacelle vane off, LE configuration 5, tail on.

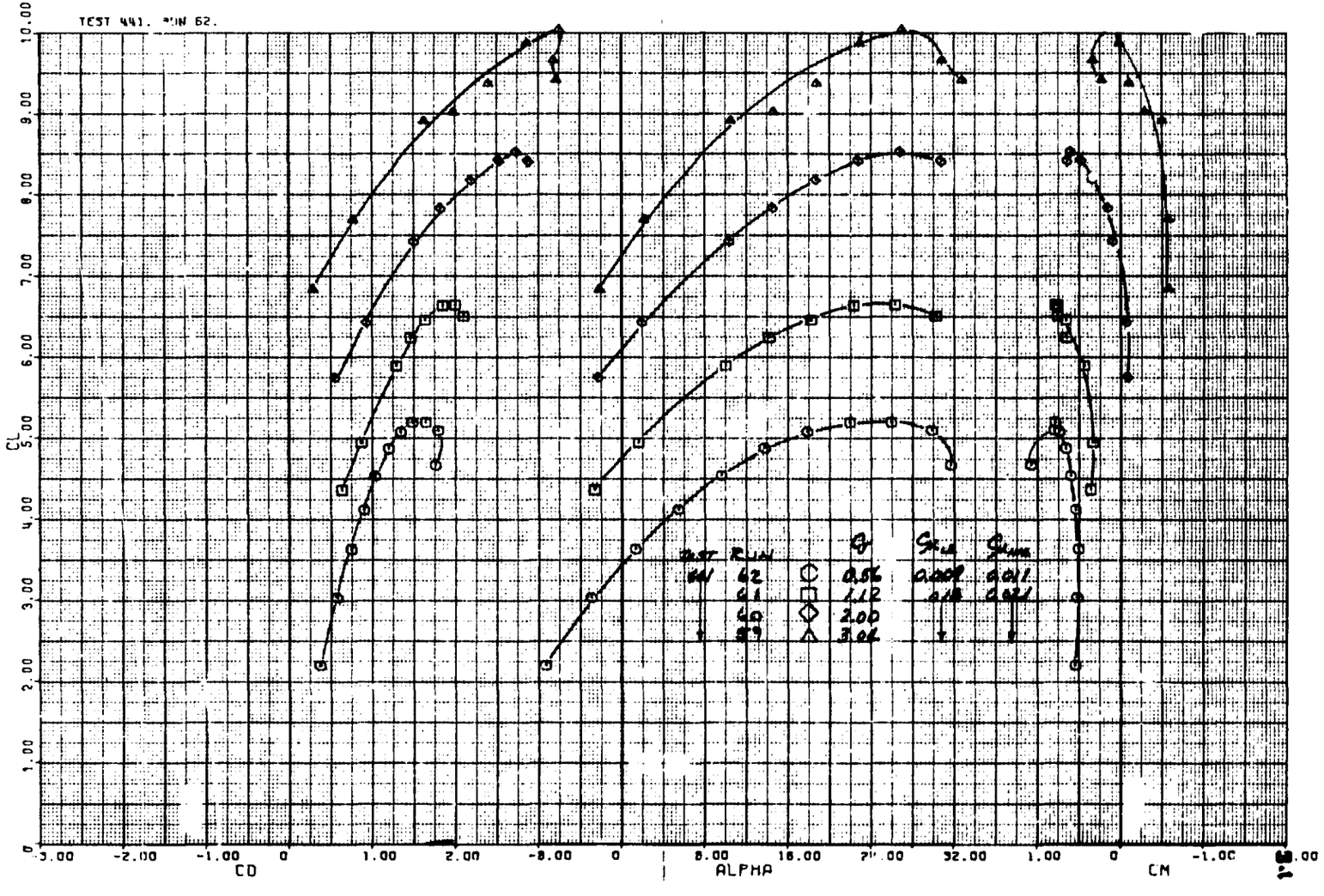


(b) LE BLC on.

Figure 21.- Concluded.

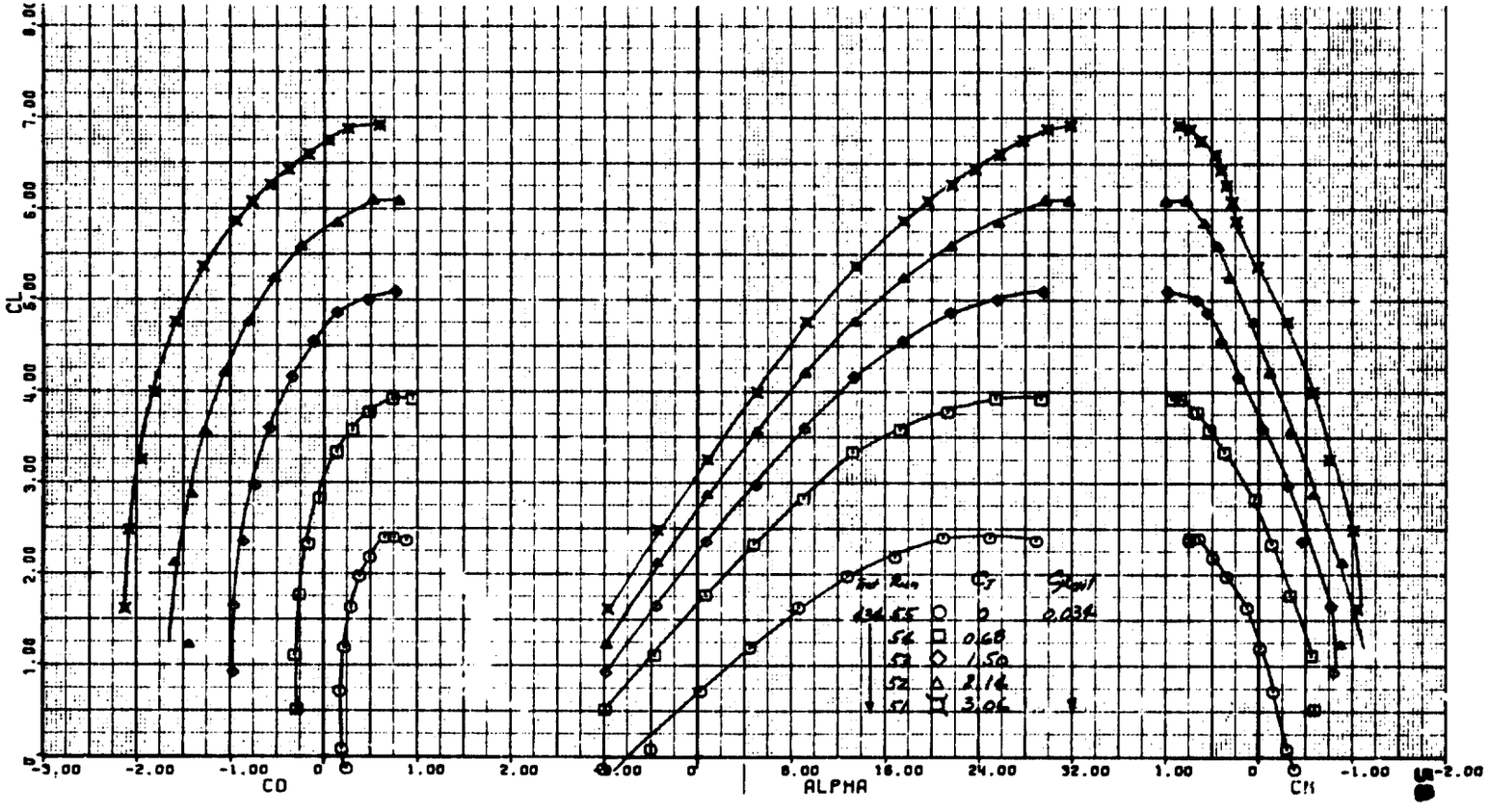


(a) Longitudinal characteristics.

Figure 22.- Aerodynamic characteristics of the model with unswept inboard LE and L.H. outboard engine out; $\delta_f$ = 30°, $\delta_{ail}$ = 23°, $C_{\mu_{LE}}$ = 0, $C_{\mu_{NAC}}$ = 0, wing fence on, nacelle vane on, LE configuration 3, tail off.

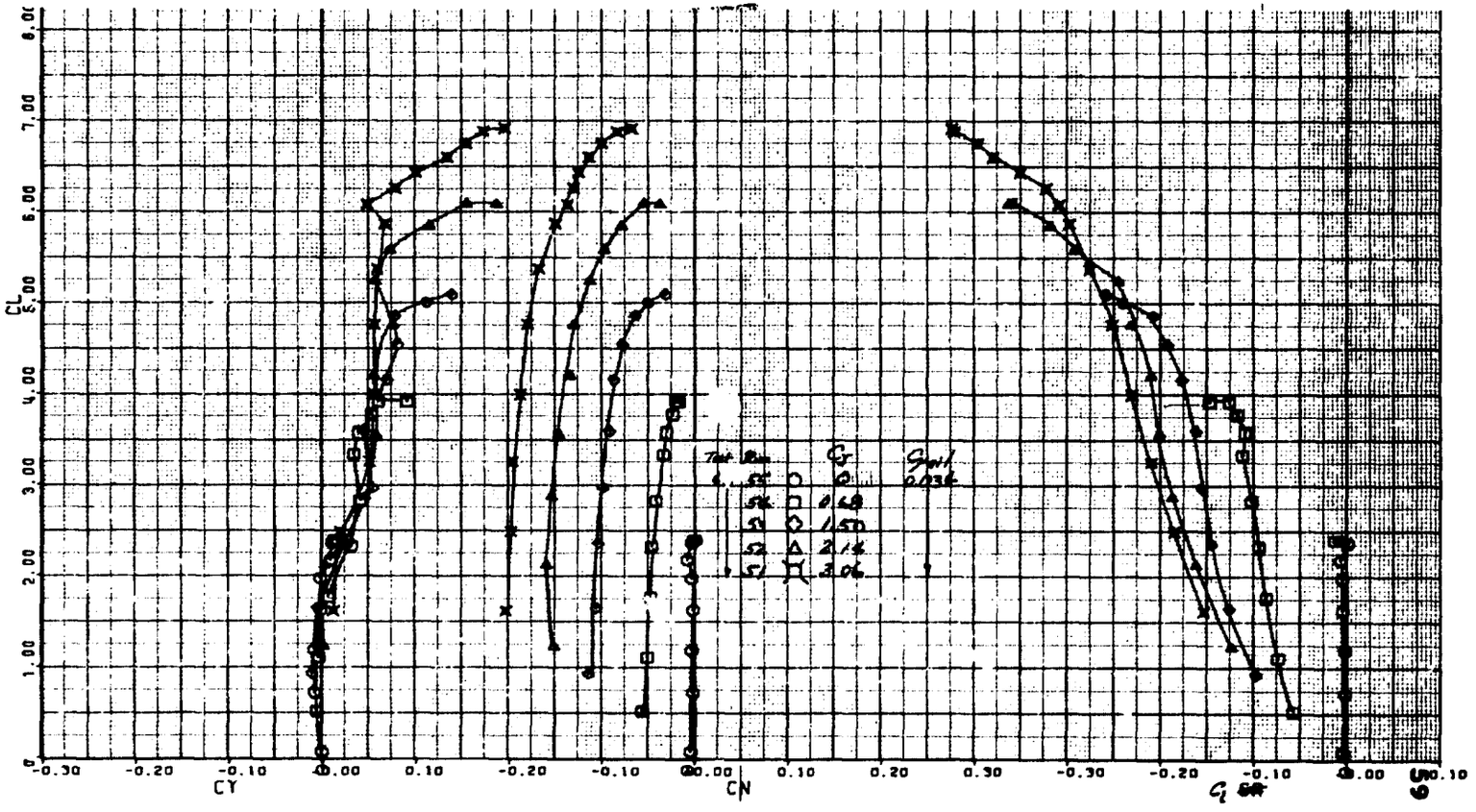


(b) Lateral characteristics.

Figure 22.- Concluded.

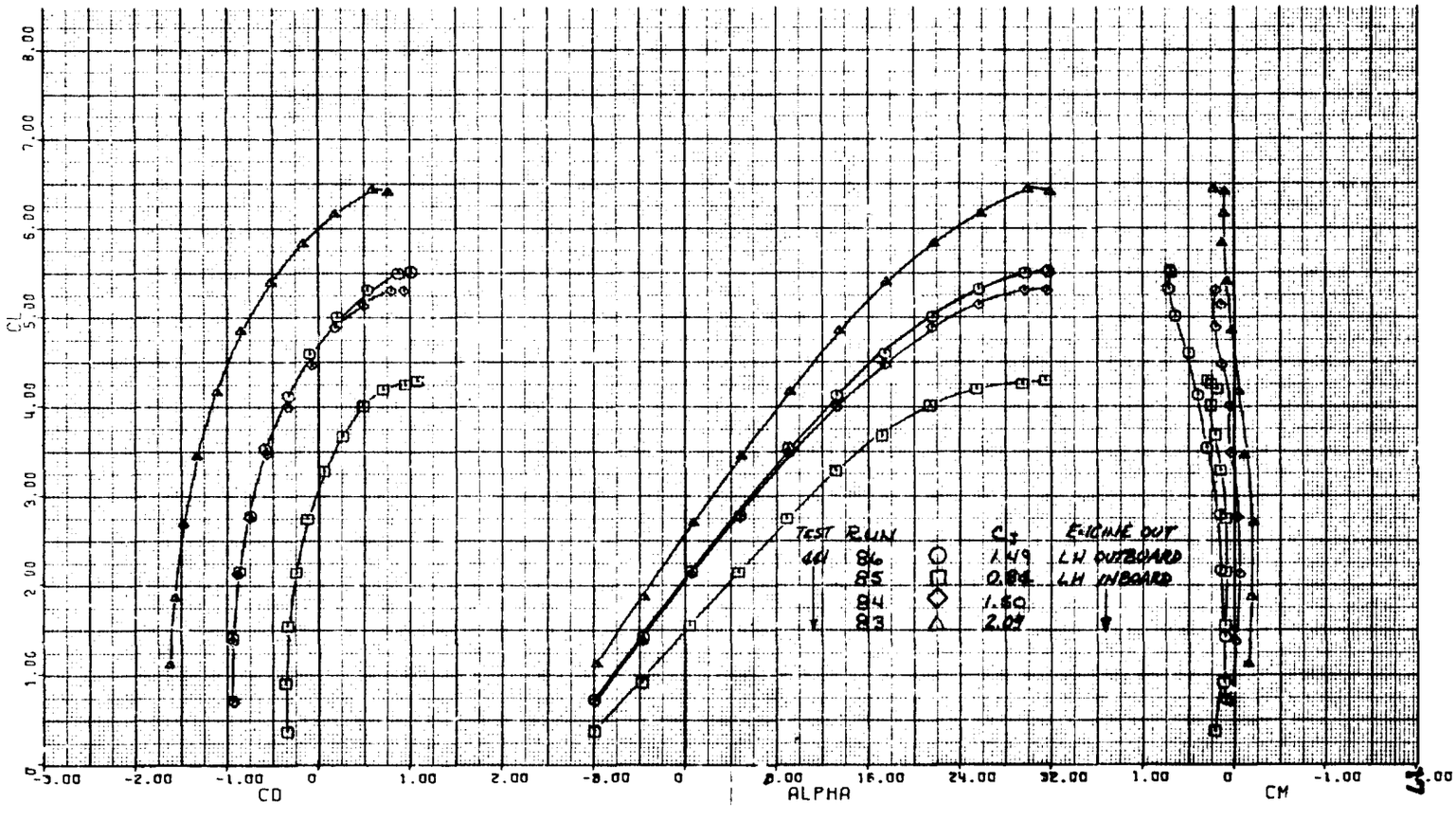


(a) Longitudinal characteristics.

Figure 23.- Aerodynamic characteristics of the model with an engine out; $\delta_f = 30°$, $\delta_{ail} = 0$, $C_{\mu_{LE}} = 0$, $C_{\mu_{NAC}} = 0$, wing fence off, nacelle vane off, LE configuration 6, tail off.

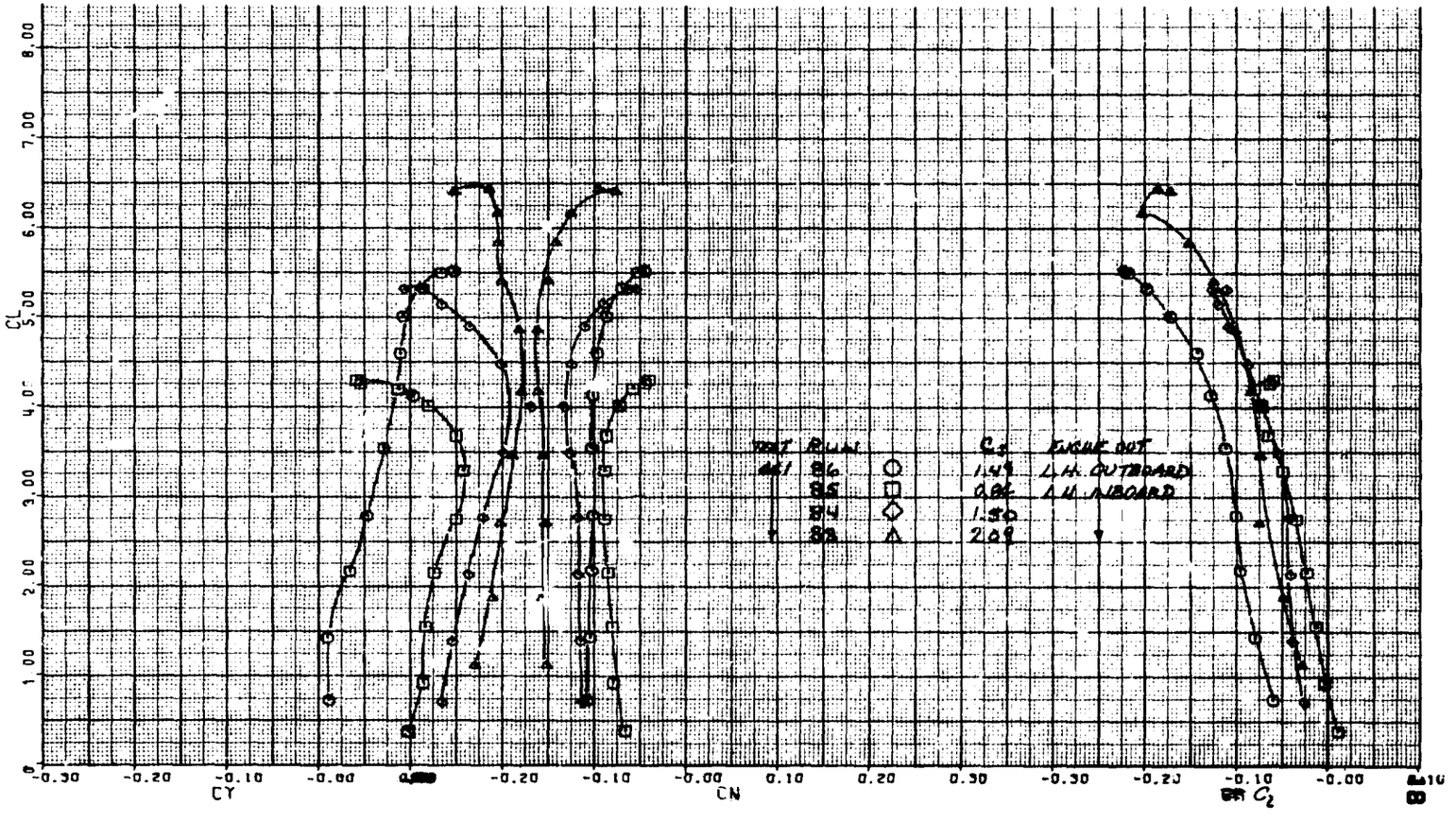


(b) Lateral characteristics.

Figure 23.- Concluded.

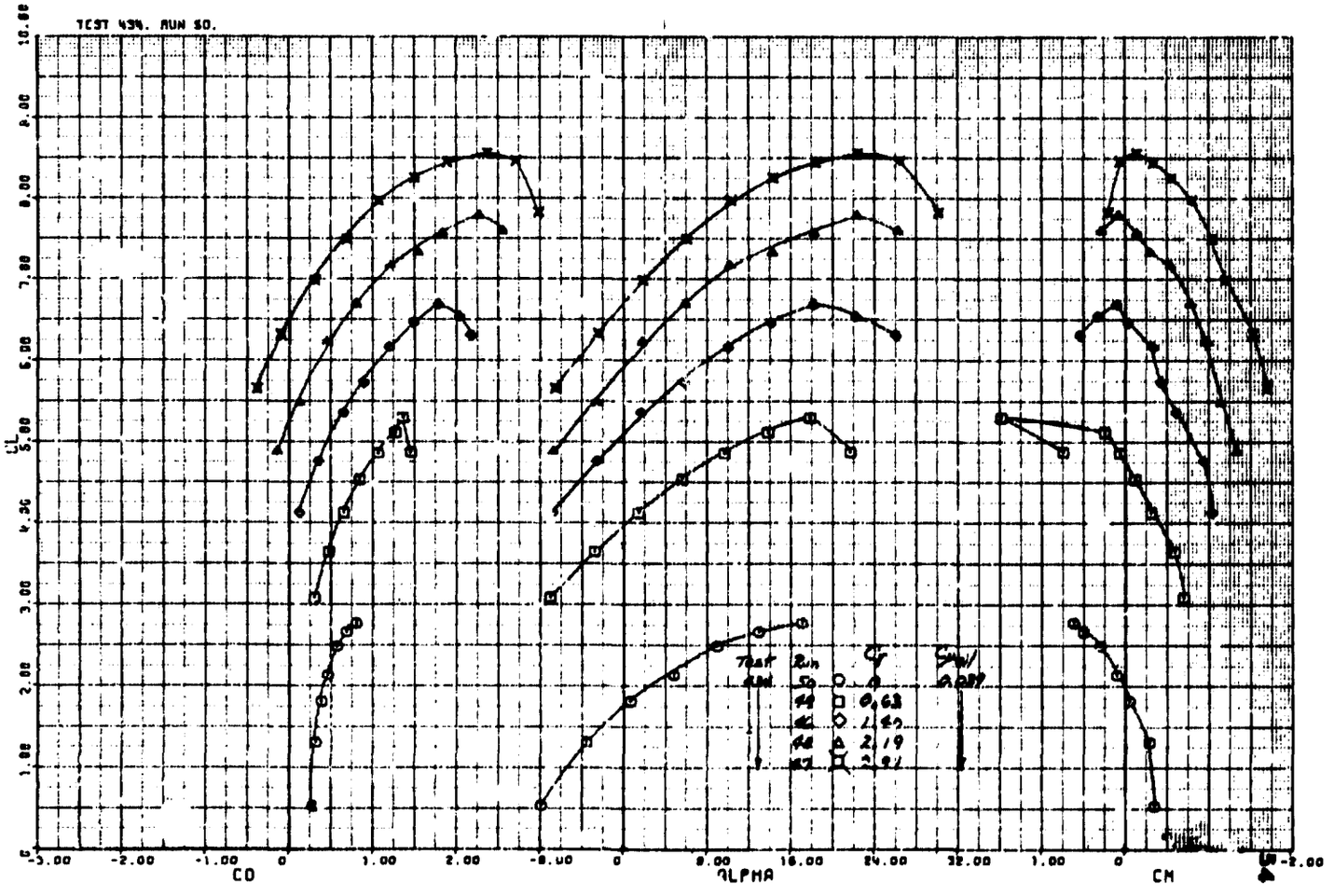


(a) Longitudinal characteristics.

Figure 24.- Aerodynamic characteristics of the model with unswept inboard LE and L.H. outboard engine out; $\delta_f$ = 90°, $\delta_{ail}$ = 23°, $C_{\mu_{LE}}$ = 0, $C_{\mu_{NAC}}$ = 0, wing fence on, nacelle vane on, LE configuration 3, tail off.

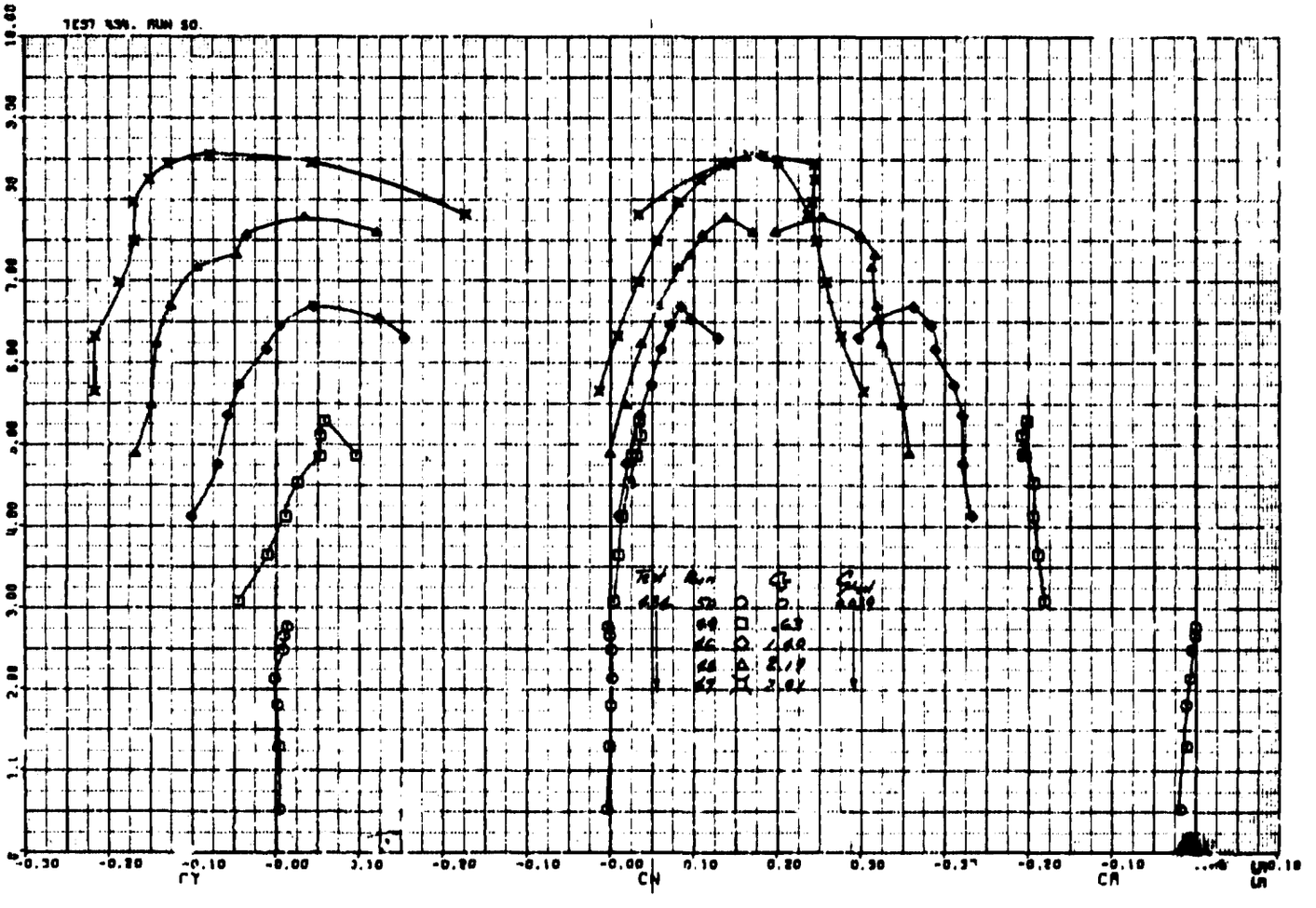

(b) Lateral characteristics.

Figure 24.- Concluded.

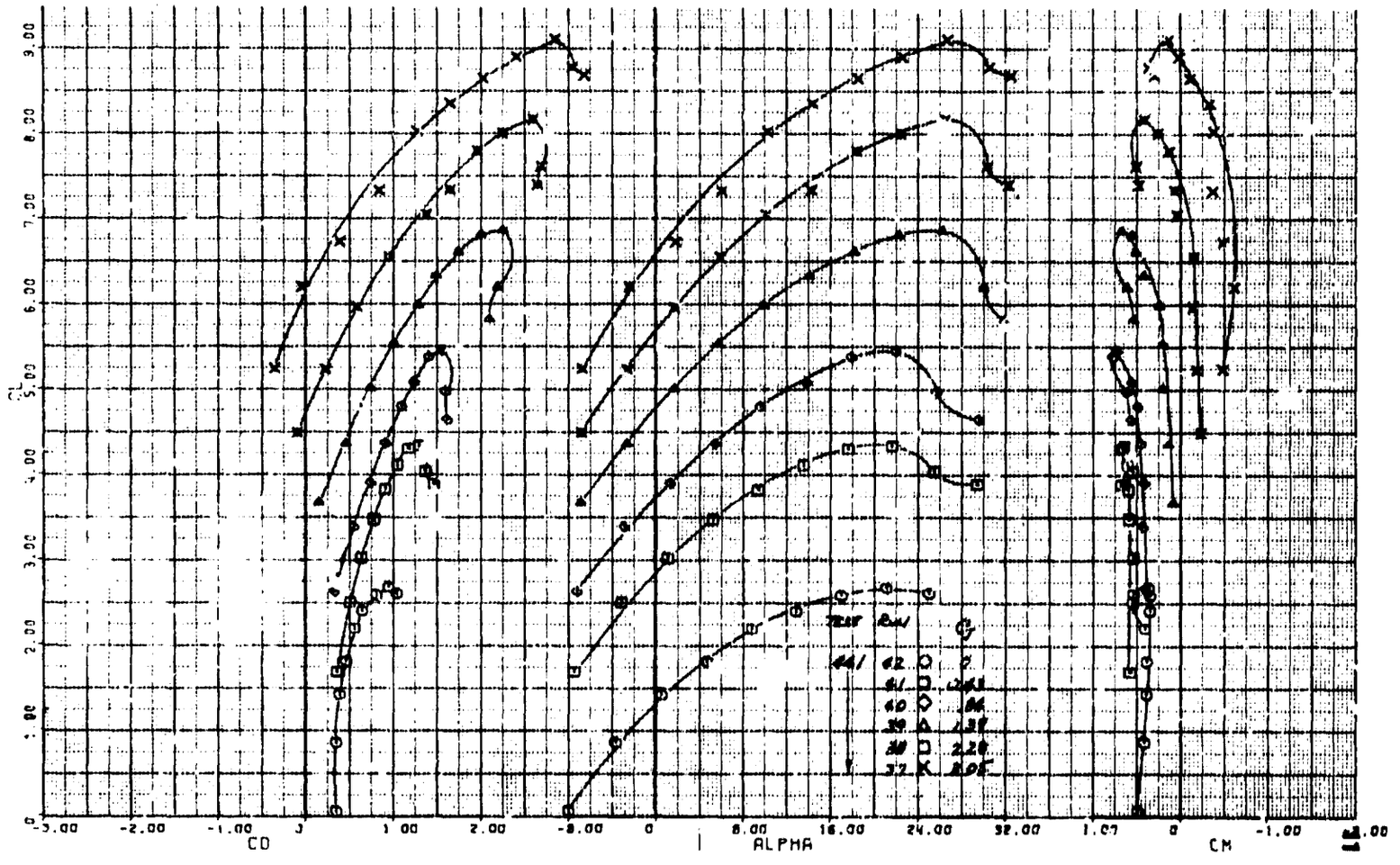


(a) Longitudinal characteristics.

Figure 25.- Aerodynamic characteristics of the model with L.H. outboard engine out; $\delta_f$ = 90°, $\delta_{ail}$ = 0, $C_{\mu_{LE}}$ = 0, $C_{\mu_{NAC}}$ = 0, wing fence off, nacelle vane off, LE configuration 5, tail on.

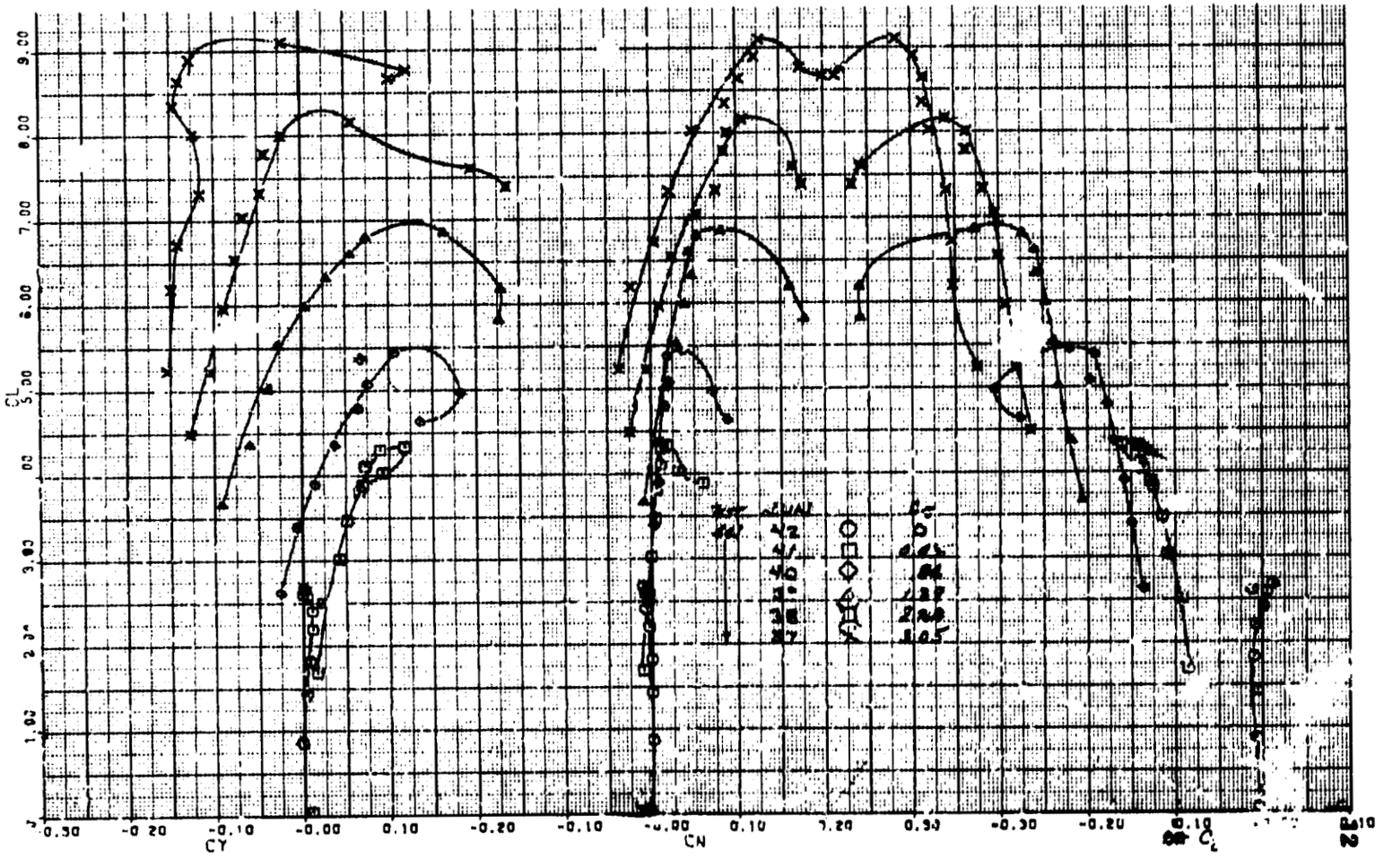


(b) Lateral characteristics.

Figure 25.- Concluded.

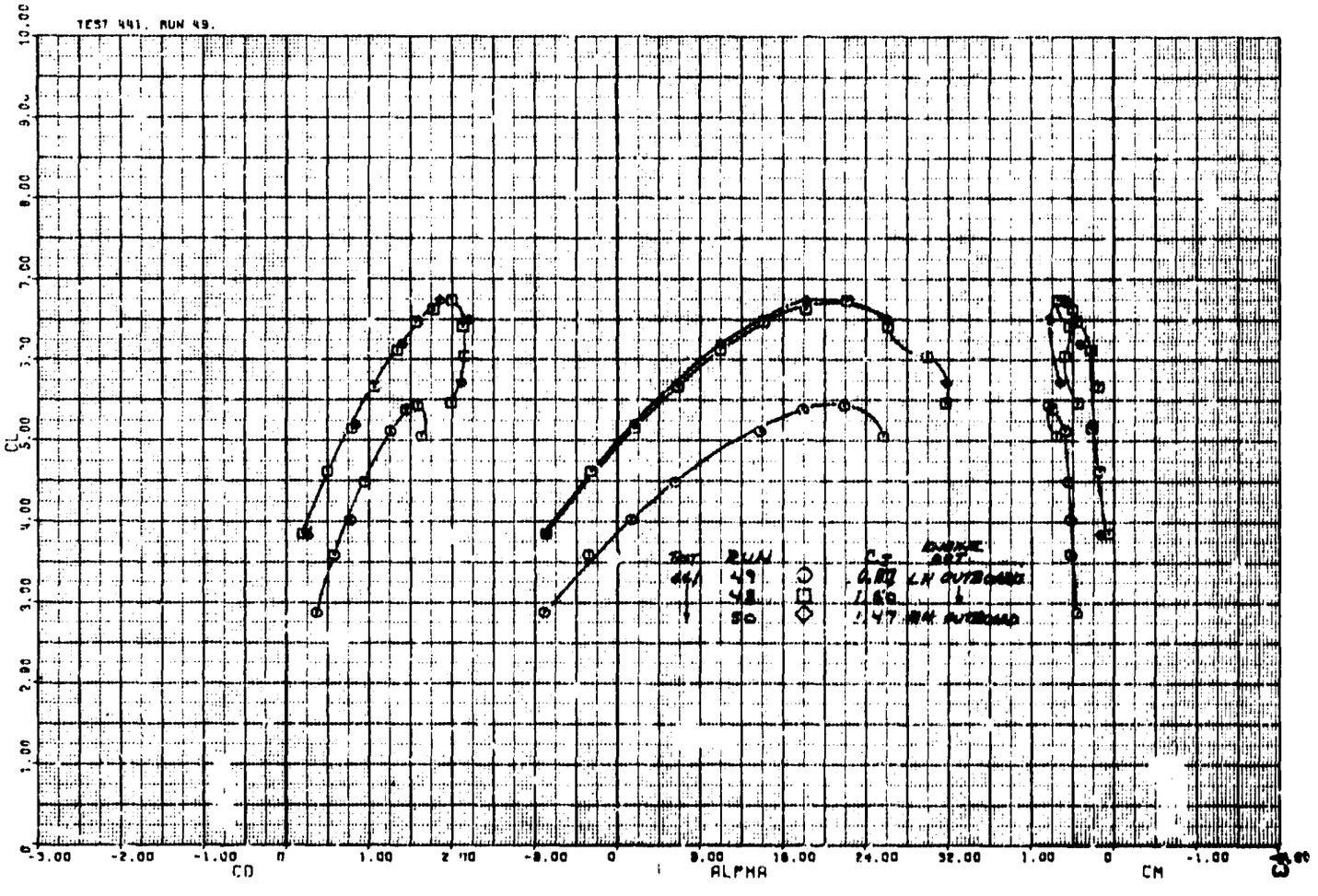


(a) Longitudinal characteristics.

Figure 26.- Aerodynamic characteristics of the model with an outboard engine out and with the Coanda surface behind the engine out; $\delta_f = 90°$, $\delta_{ail} = 0°$, $C_{\mu_{LE}} = 0$, $C_{\mu_{NAC}} = 0$, wing fence off, nacelle vane off, LE configuration 5, tail on.

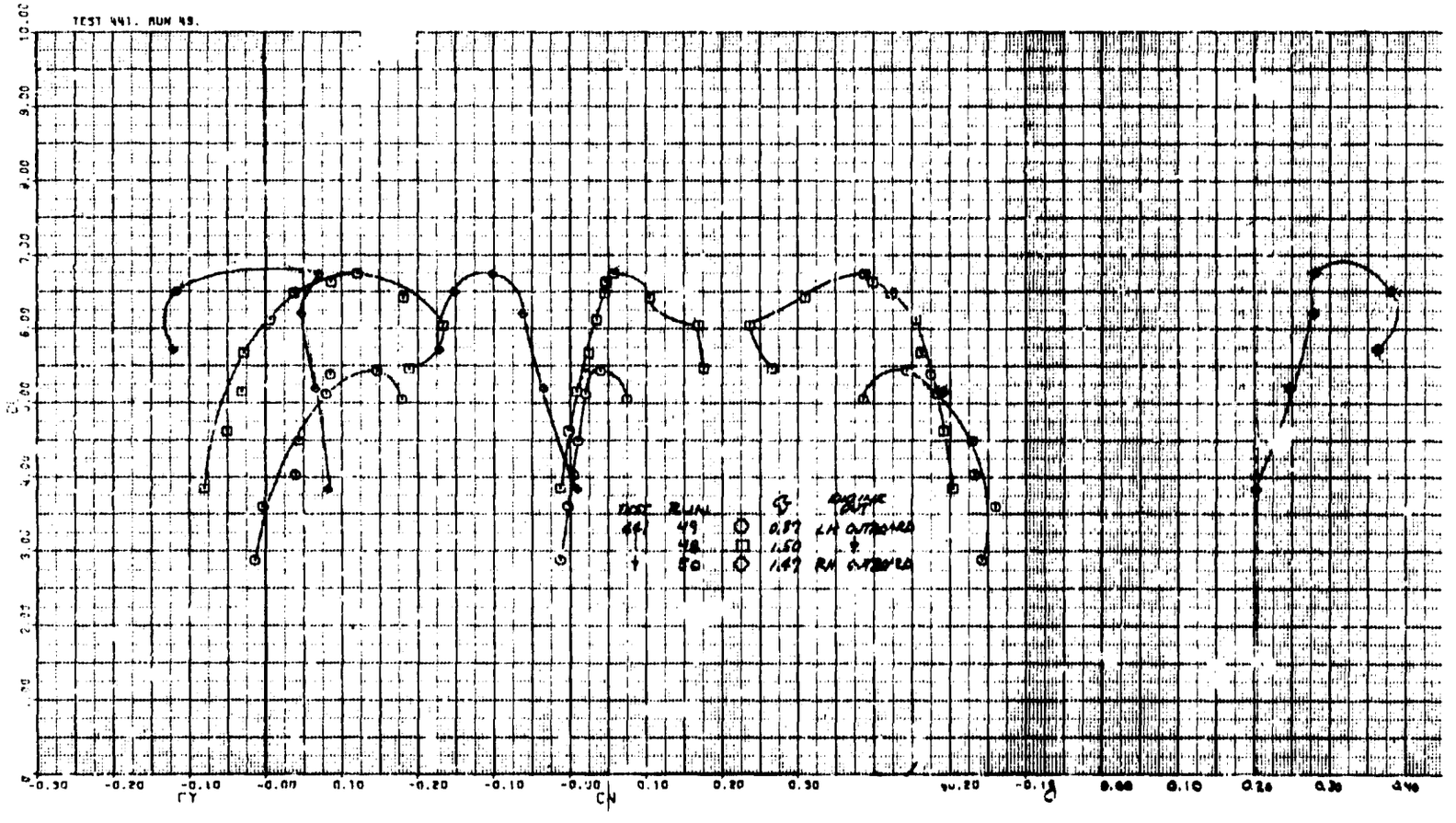


(! Lateral characteristics.

Figure 26.- Concluded.

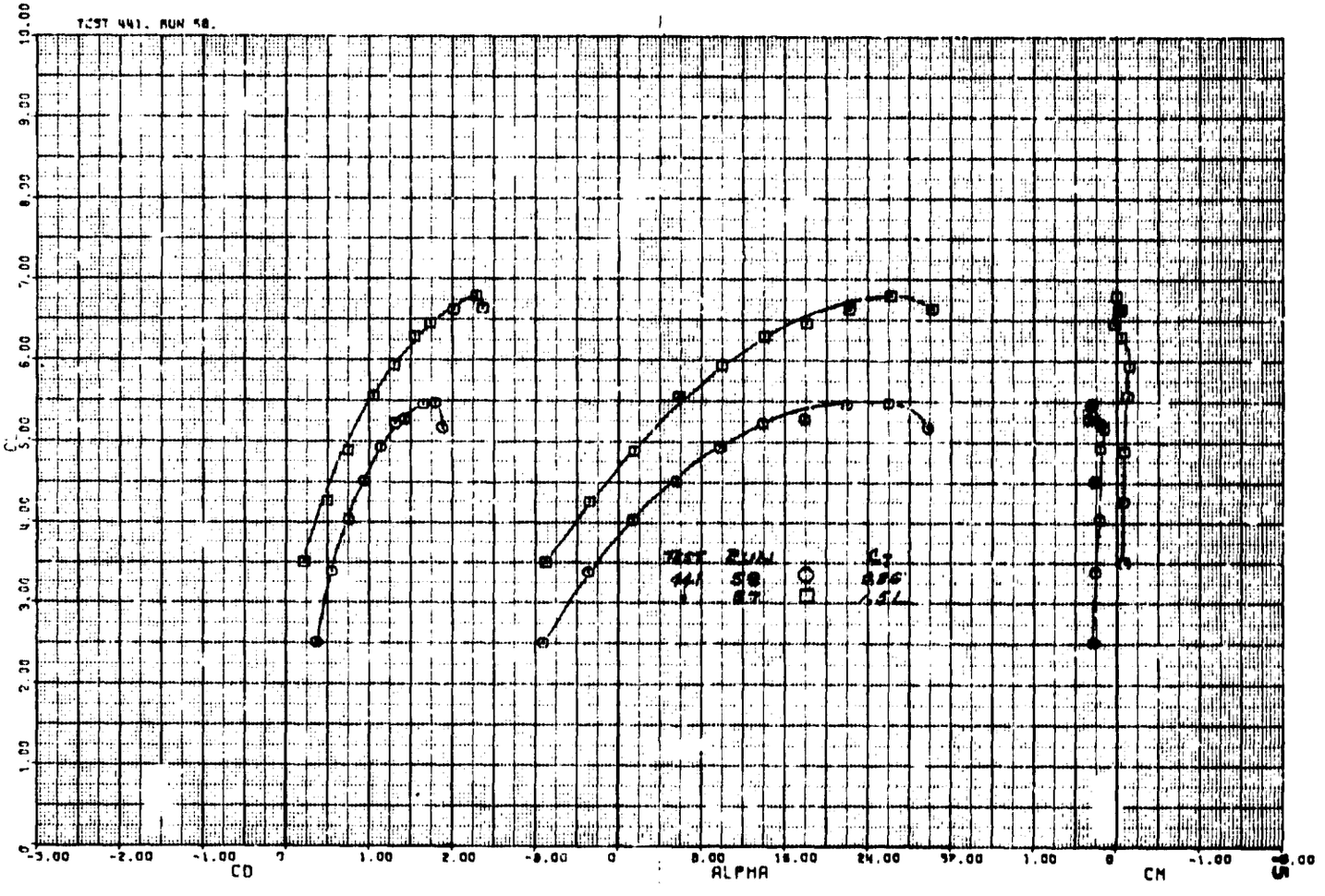


(a) Longitudinal characteristics.

Figure 27.- Aerodynamic characteristics of the model with L.H. inboard engine out; $\delta_f = 90°$, $\delta_{ail} = 0°$, $C_{\mu_{LE}} = 0$, $C_{\mu_{NAC}} = 0$, wing fence off, nacelle vane off, LE configuration 5, tail on.

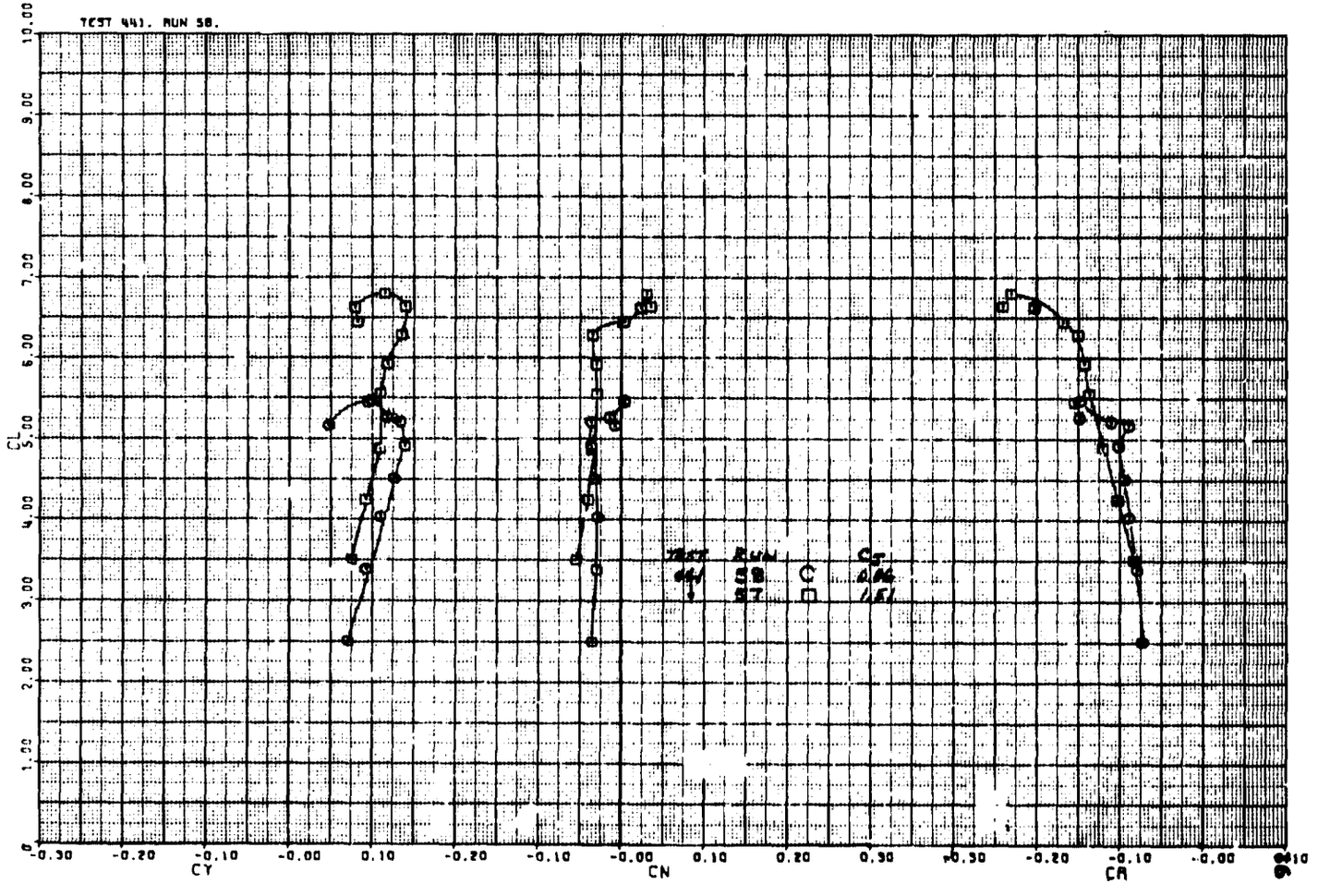


(b) Lateral characteristics.

Figure 27.- Concluded.

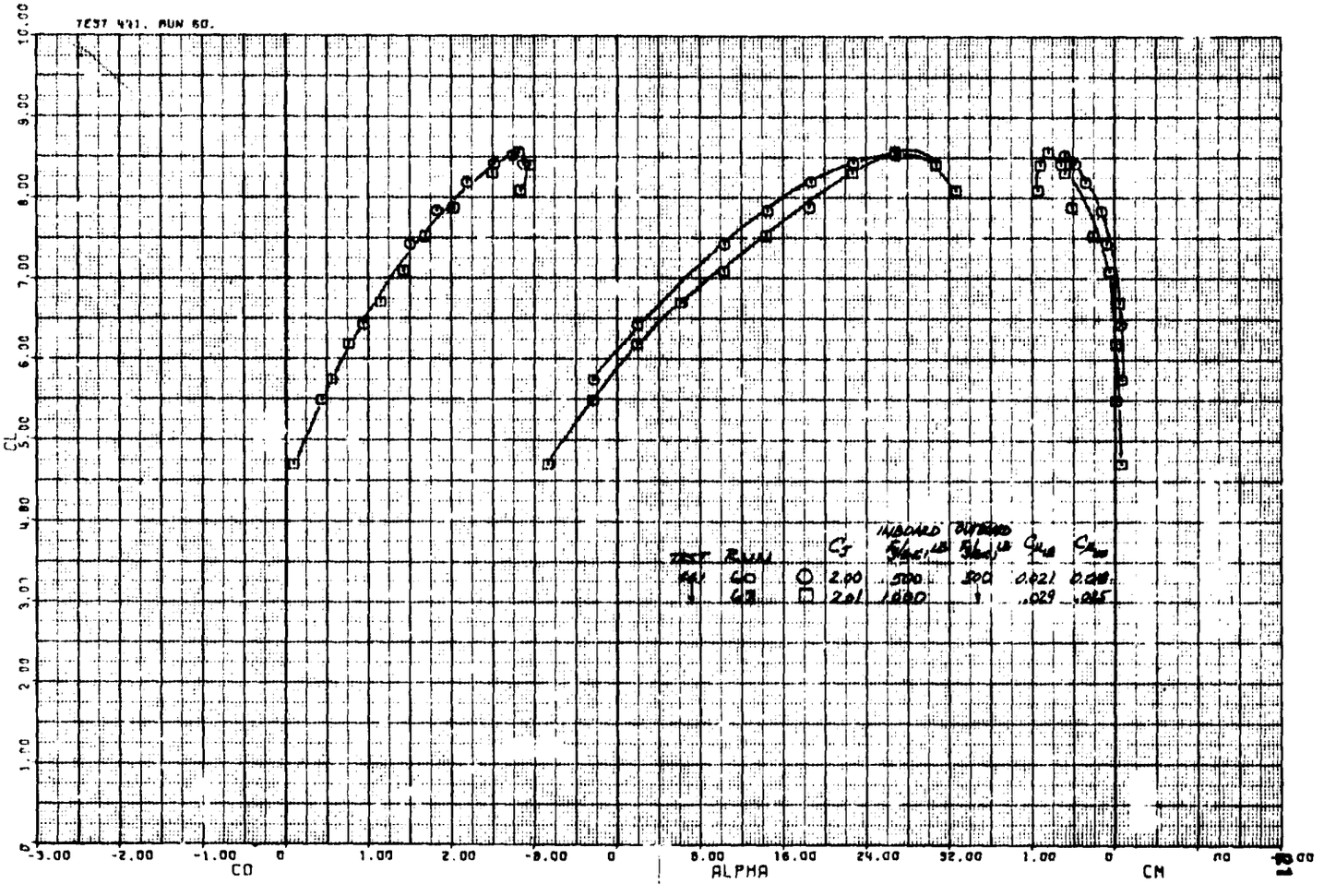


(a) Longitudinal characteristics.

Figure 28.- Effect of engine thrust distribution on the aerodynamic characteristics of the model; $\delta_f$ = 90°, $\delta_{ail}$ = 0°, wing fence off, nacelle vane off, LE configuration 5, tail on.

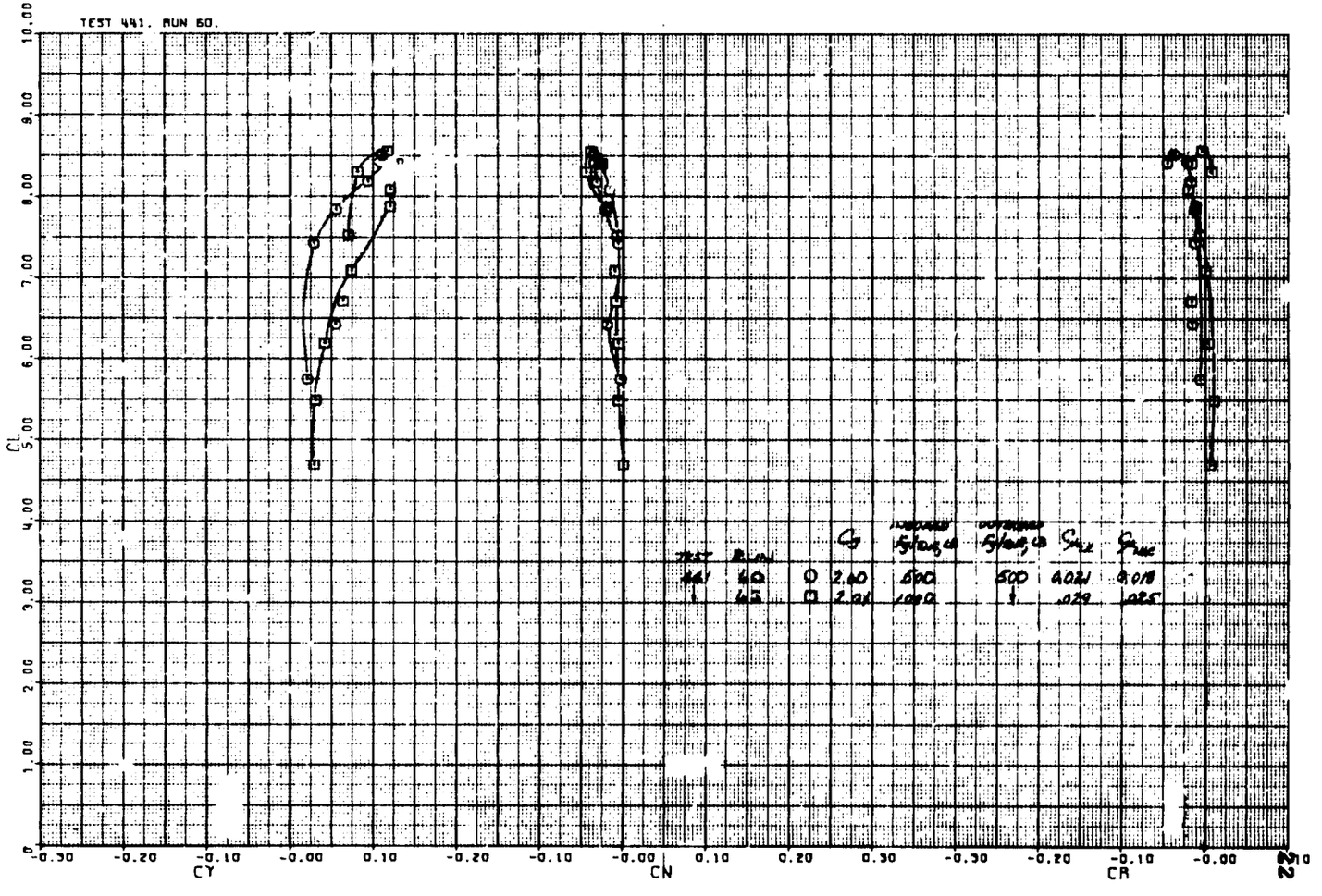


(b) Lateral characteristics.

Figure 28.- Concluded.

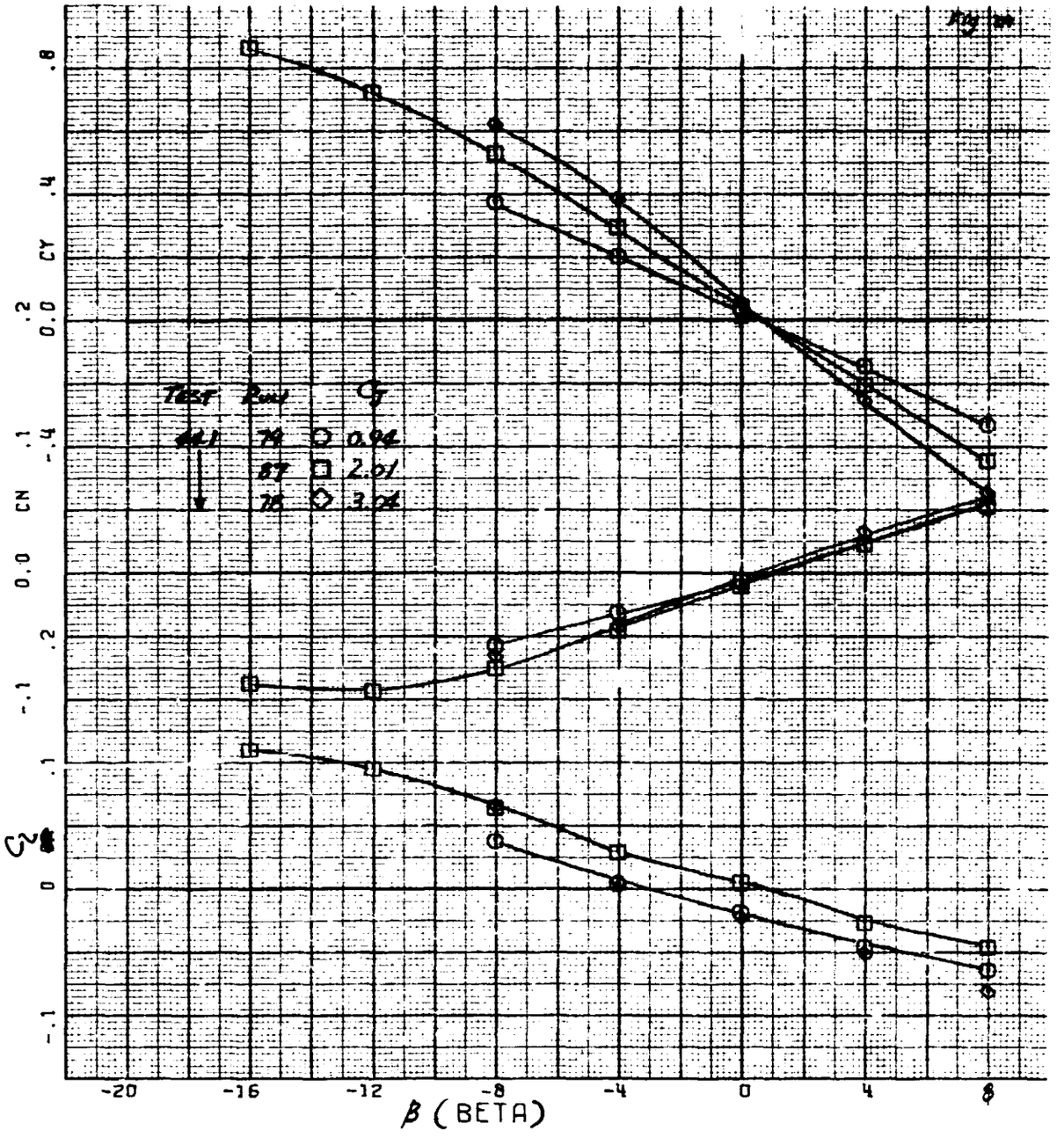


Figure 29.- Variation of side force, yawing-moment, and rolling-moment coefficients with sideslip; $\delta_f = 30°$, $\delta_{ail} = 0°$, $C_{\mu_{LE}} = 0$, $C_{\mu_{NAC}} = 0$, $\alpha_u = 4°$, wing fence off, nacelle vane off, LE configuration 6, tail on.

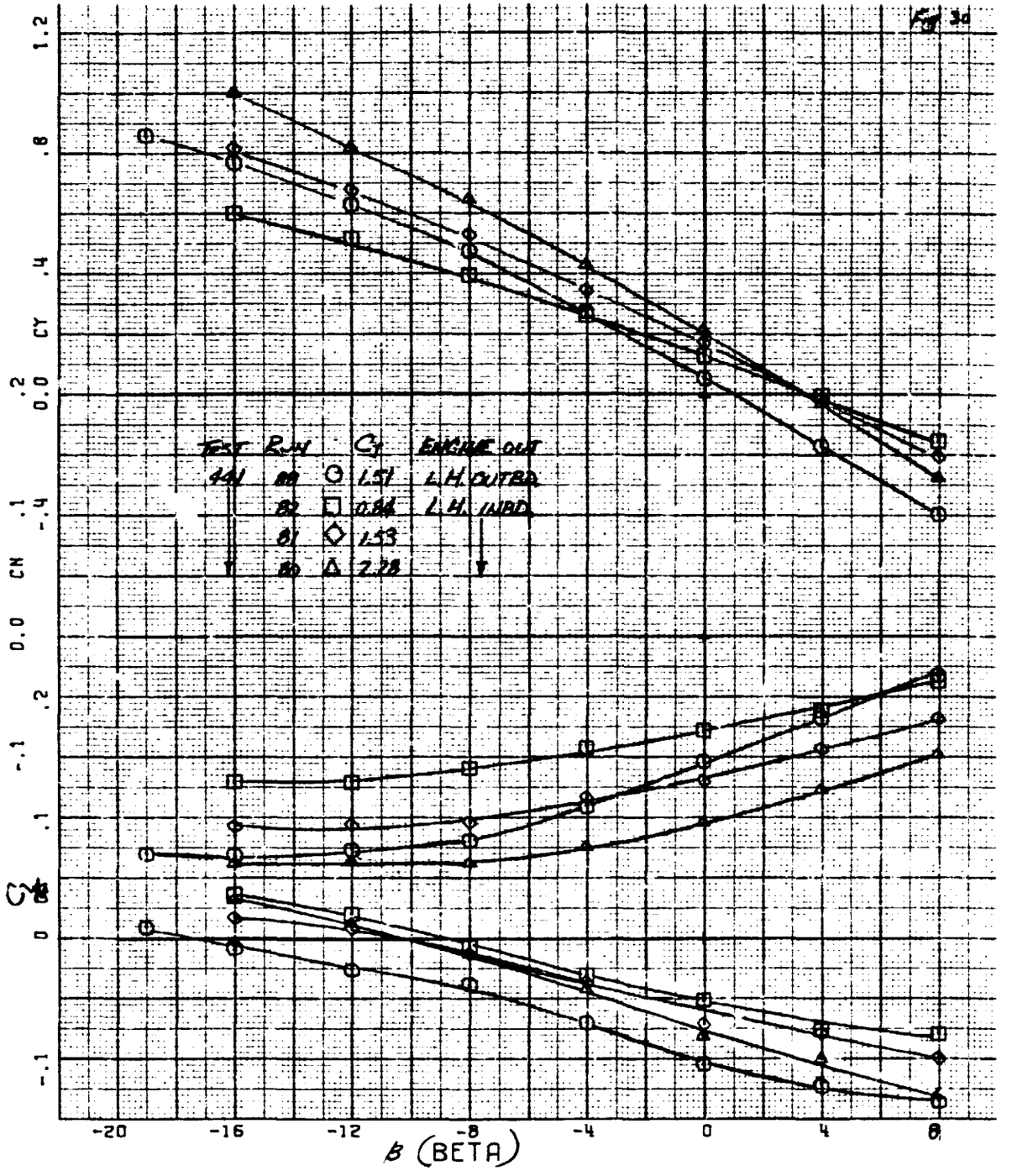


Figure 30.- Variation of side force, yawing-moment, and rolling-moment coefficients with sideslip and with an engine out; $\delta_f = 30°$, $\delta_{ail} = 0$, $C_{\mu_{LE}} = 0$, $C_{\mu_{NAC}} = 0$, $\alpha_u = 4°$, wing fence off, nacelle vane off, LE configuration 6, tail on.

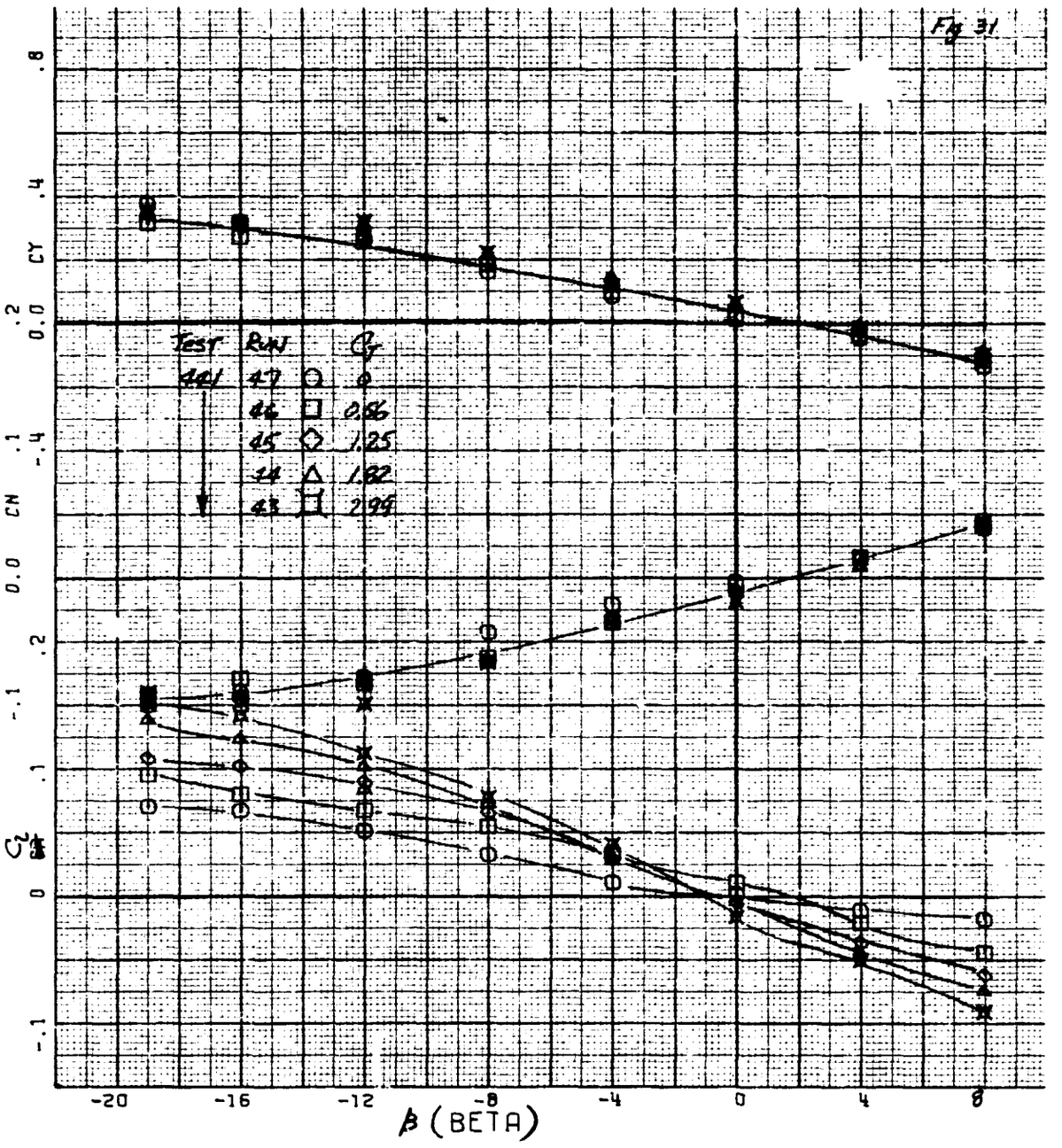


Figure 31.- Variation of side force, yawing-moment, and rolling-moment coefficient with sideslip; $\delta_f = 90°$, $\delta_{ail} = 0°$, $\alpha_u = 4°$, wing fence off, nacelle vane off, LE configuration 5, tail on.

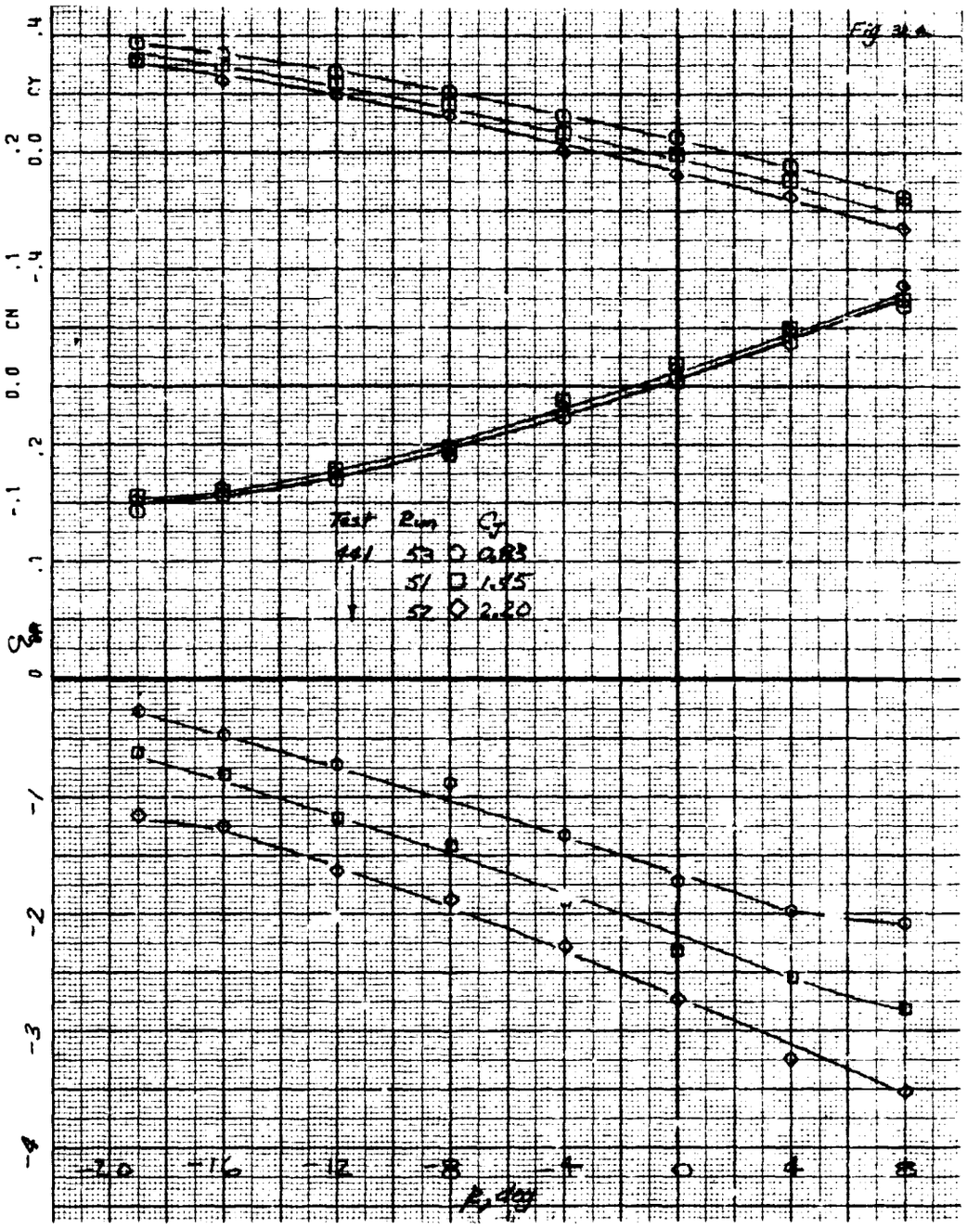


(a) L.H. outboard engine out.

Figure 32.- Variation of side force, yawing-moment, and rolling-moment coefficient with sideslip and with an engine out; $\delta_f = 90°$, $\delta_{ail} = 0°$. $C_{\mu_{LE}} = 0$, $C_{\mu_{NAC}} = 0$, $\alpha_u = 4°$, wing fence off, nacelle vane off, LE configuration 5, tail on.

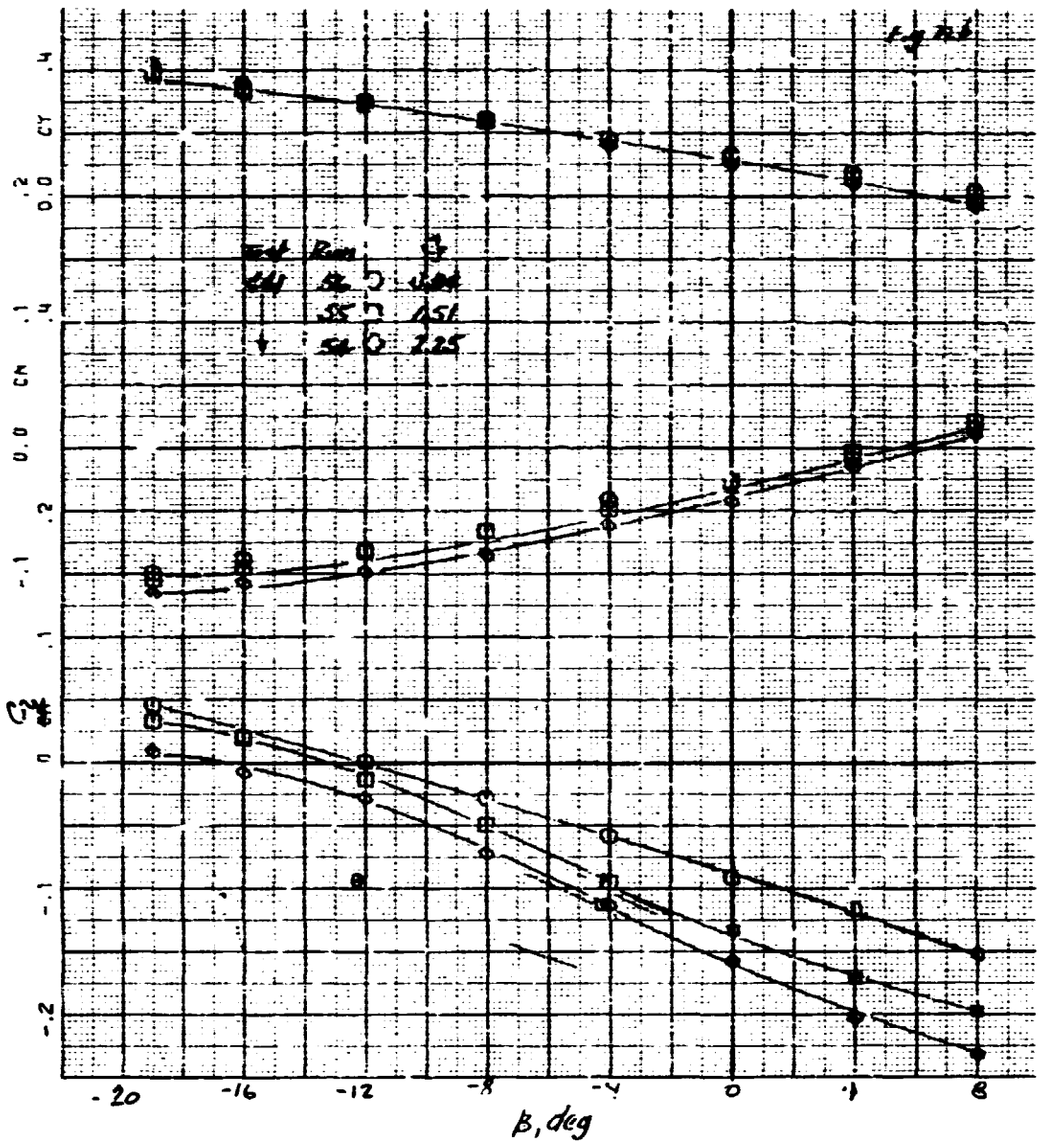


(b) L.H. inboard engine out.

Figure 32.- Concluded.

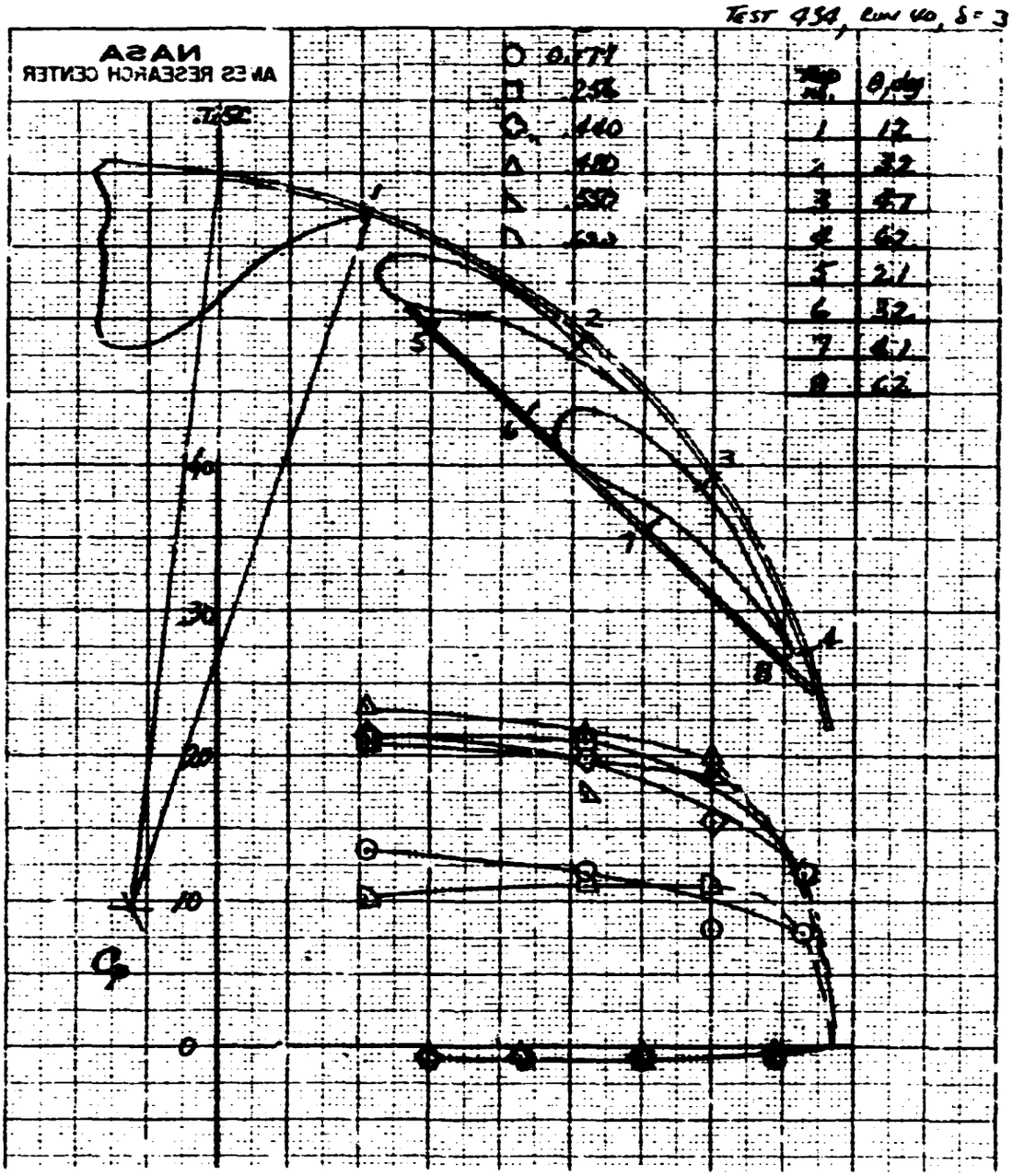


(a) $\alpha_u = 0°$

Figure 33.- Flap surface pressures at several spanwise stations, $\delta_f = 90°$, $C_J = 3.0$, $q = 239.40$ N/m$^2$, avg. exhaust pressure ratio = 1.06.

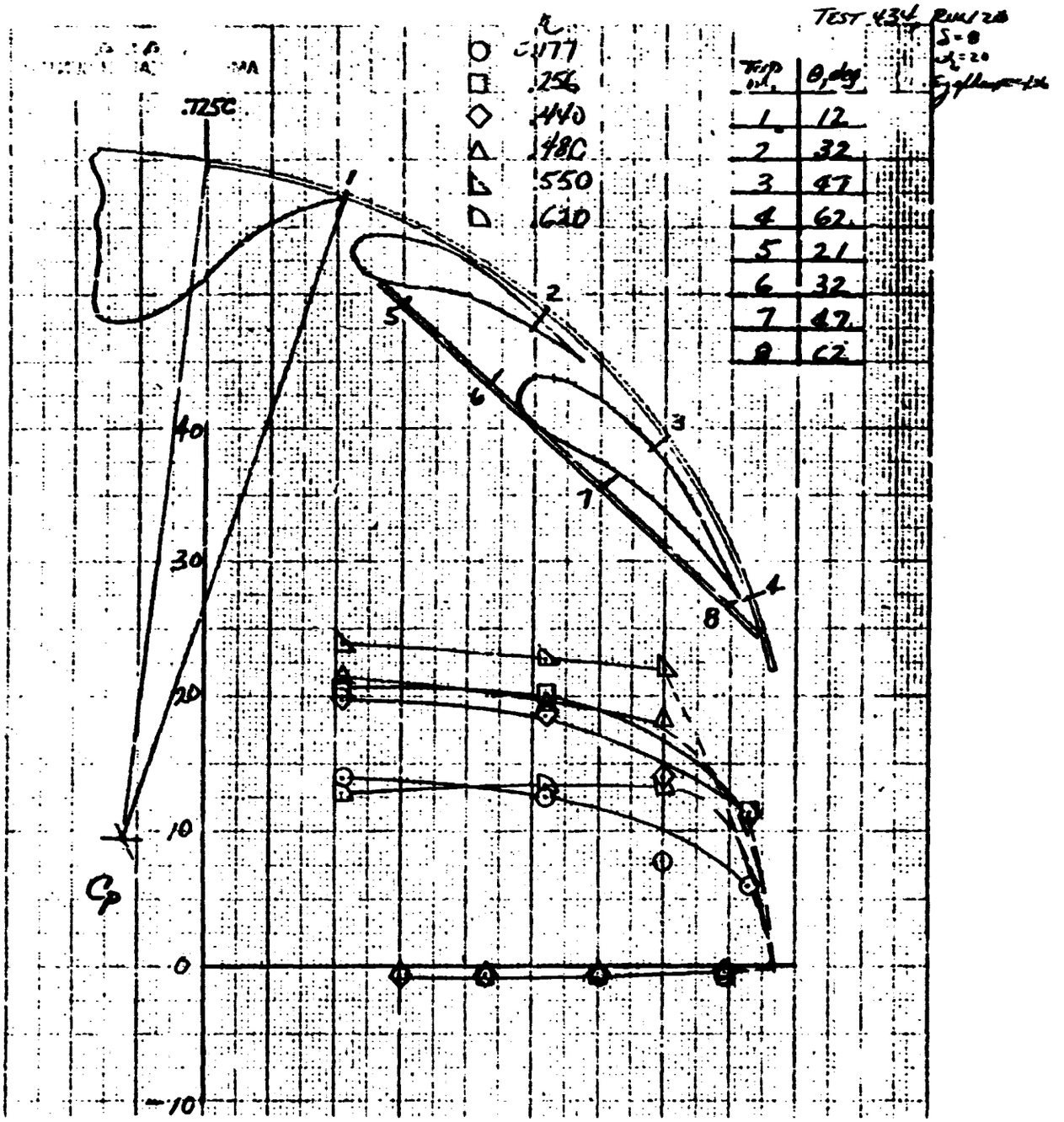


(b) $\alpha_{12} = 20°$.

Figure 33.- Concluded.

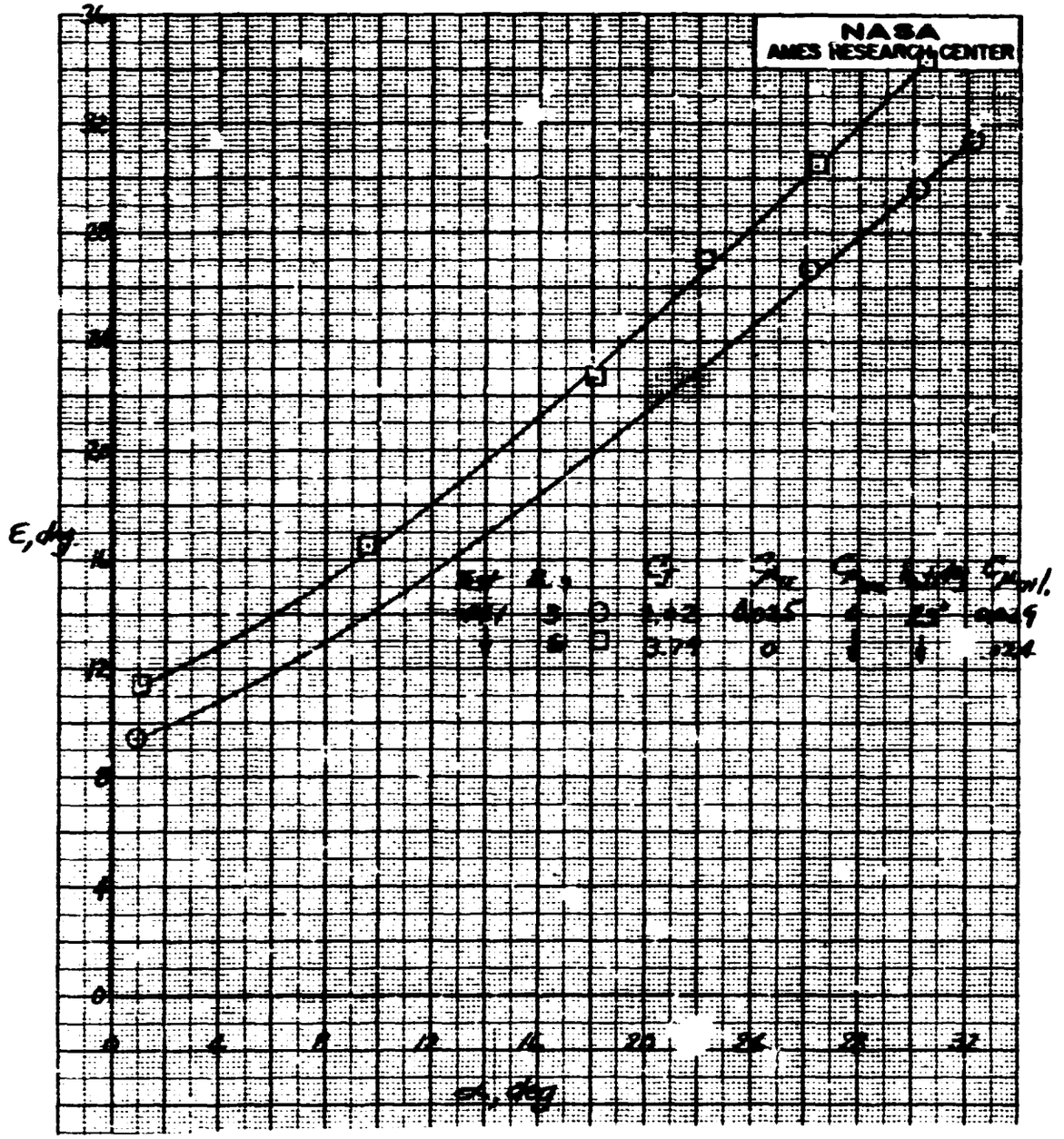


(a) $\delta_f$ = 30°.

Figure 34.- Variation of average downwash angle with angle-of-attack.

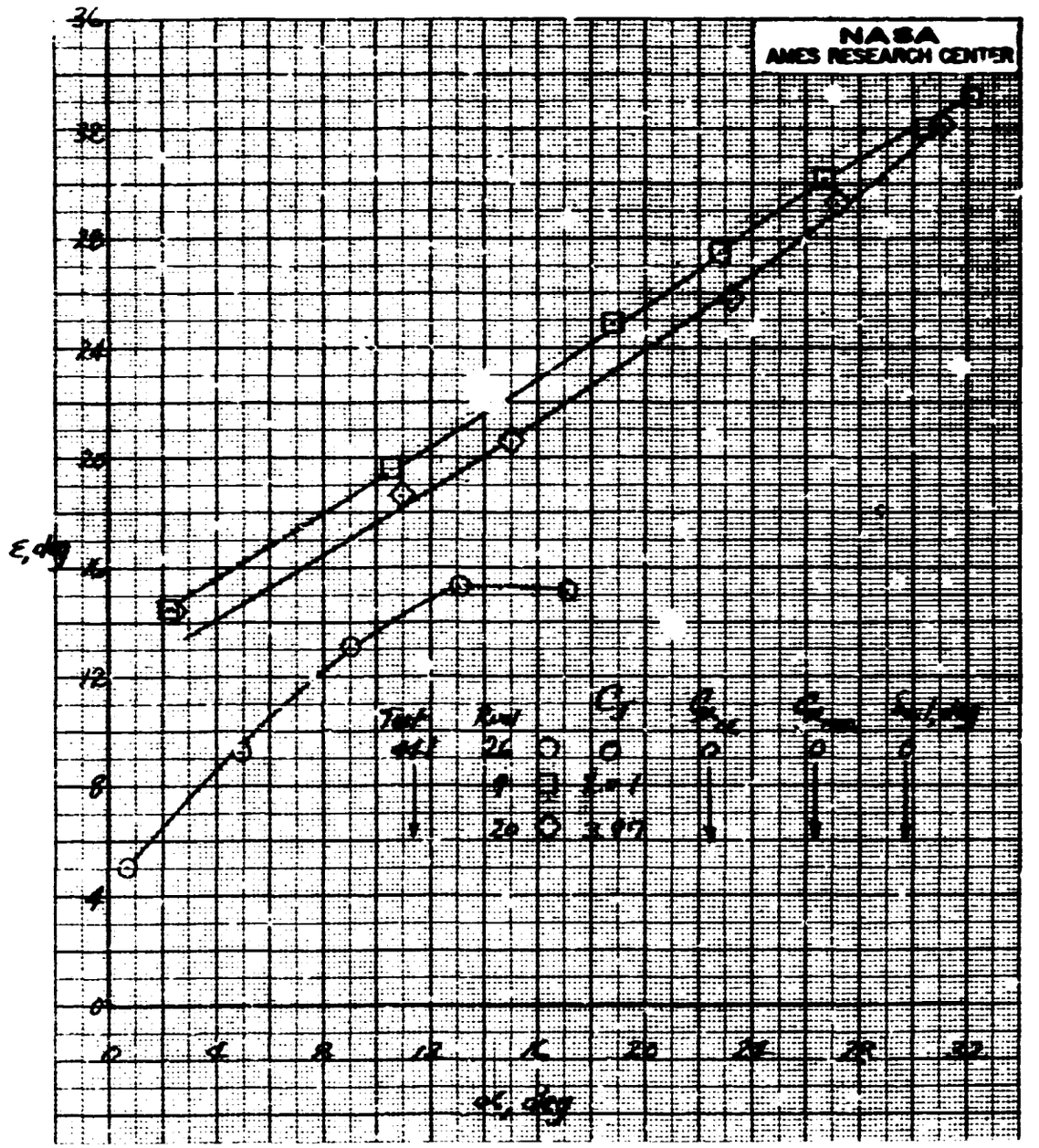


(b) $\delta_f = 90°$.

Figure 34.- Concluded.

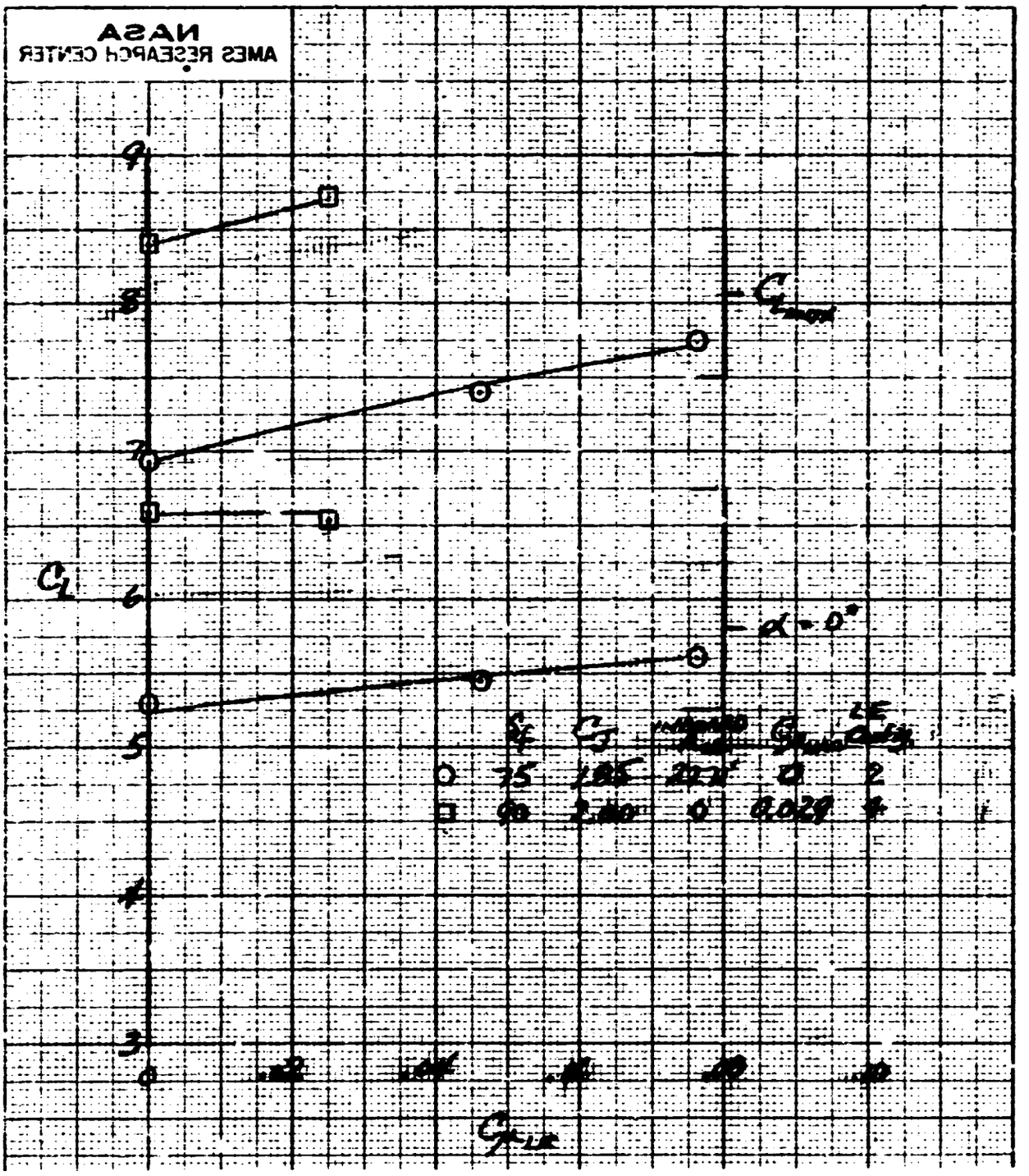


Figure 35.- Variation of $C_L$ with $C_{\mu_{LE}}$ with the swept and unswept inboard leading edge; $\delta_{ail} = 23°$.

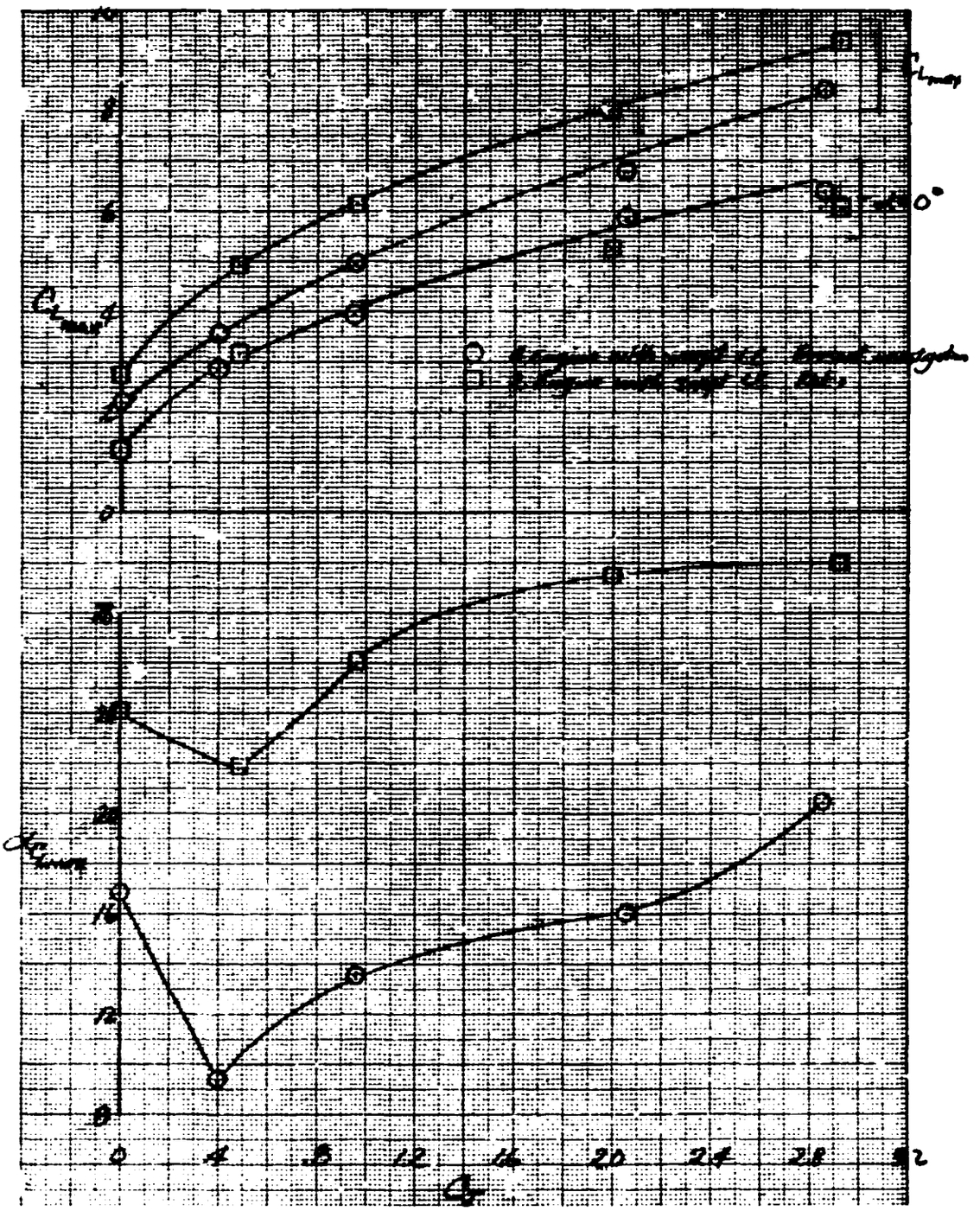

Figure 36.- Comparison of $C_{L_{max}}$ and $\alpha_{C_{Lmax}}$ between the two engine and the four engine US3 model with the leading edge fully swept 27.71°; $i_f$ = 75°.

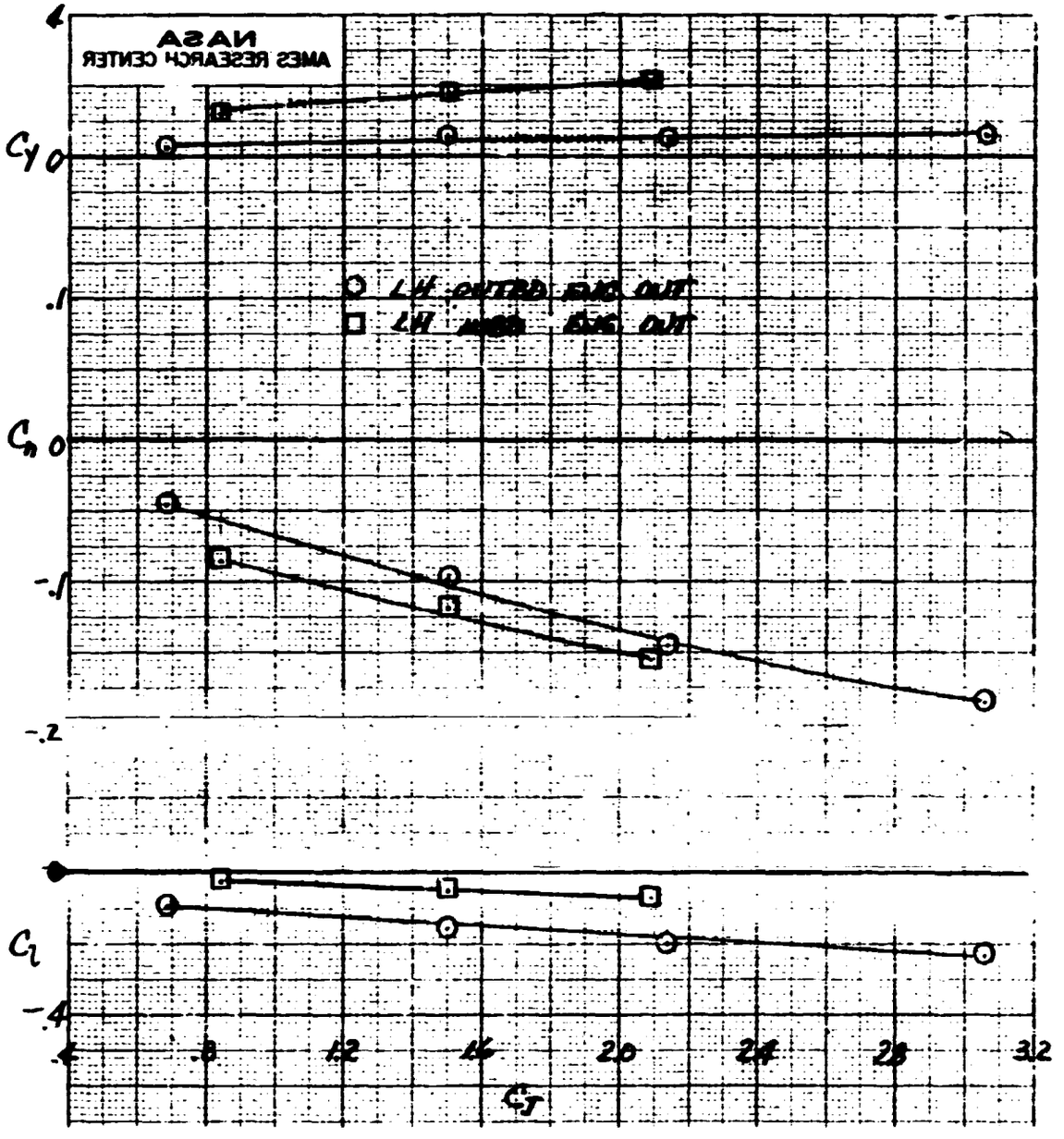


(a) $\delta_f = 30°$.

Figure 37.- Variation of $C_y$, $C_n$, $C_l$ with $C_J$; $\delta_{ail} = 0°$, $\alpha_u = 4°$.

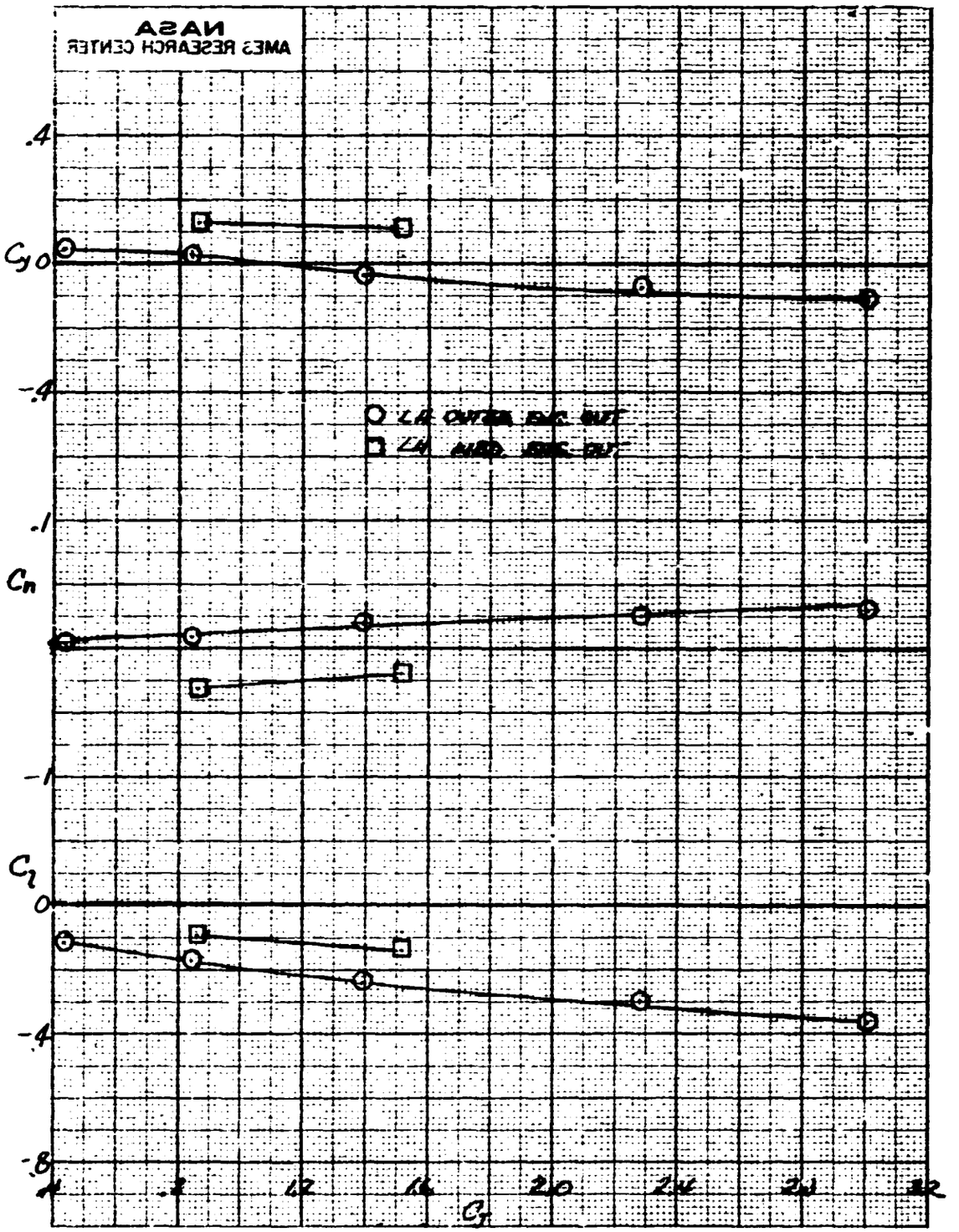


(b) $\delta_f = 90°$.

Figure 37.- Concluded.